POLYVINYLIDENE FLUORIDE AS AN EXOTIC HOST MATRIX MATERIAL FOR DEVELOPING TECHNOLOGICALLY IMPORTANT NANOCOMPOSITES

Thesis Submitted to

COCHIN UNIVERSITY OF SCIENCE AND TECHNOLOGY

In partial fulfillment of the requirements

for the award of the degree of

DOCTOR OF PHILOSOPHY

By

SABIRA.K

DEPARTMENT OF PHYSICS
COCHIN UNIVERSITY OF SCIENCE AND TECHNOLOGY
COCHIN-22

June 2017

Polyvinylidene fluoride as an exotic host matrix material for developing technologically important nanocomposites

Ph.D thesis in the field of material science

Author:

Sabira.K

Division for Research in Advanced Materials
Department of Physics
Cochin University of Science and Technology
Cochin-682022, Kerala, India
Email: sabiran005@gmail.com

Supervisor:

Dr. S. Jayalekshmi

Professor
Division for Research in Advanced Materials
Department of Physics
Cochin University of Science and Technology
Cochin-682022, Kerala, India
Email: jayalekshmi@cusat.ac.in

June 2017

Department of Physics
Cochin University of Science and Technology
Cochin – 682022

Dr. S. Jayalekshmi
Professor

Certificate

Certified that the work presented in the thesis entitled "**Polyvinylidene fluoride as an exotic host matrix material for developing technologically important nanocomposites**" is based on the original work done by Mrs.Sabira.K, under my guidance and supervision at the Department of Physics, Cochin University of Science and Technology, Cochin-22, India and has not been included in any other thesis submitted previously for the award of any degree. All the relevant corrections and modifications suggested by the audience during the pre-synopsis seminar and recommendations by doctoral committee of the candidate have been incorporated in the thesis.

Cochin – 22
02 -06-2017

Prof.S.Jayalekshmi
(Supervising Guide)

Declaration

Certified that the work presented in the proposed thesis entitled **"Polyvinylidene fluoride as an exotic host matrix material for developing technologically important nanocomposites"** is based on the original work done by me under the guidance of Dr.S.Jayalekshmi, Professor, Department of Physics, Cochin University of Science and Technology, Cochin–22, India and it has not been included in any other thesis submitted previously for the award of any degree.

Cochin – 22
02-06-2017

Sabira.K

Acknowledgments

At this moment of towering achievement, I would like to express my heartfelt thanks to all those who have helped me in my efforts. I would like to express my sincere gratitude to my supervising guide, Dr. S. Jayalekshmi, Professor, Department of Physics, CUSAT for instilling in me the motivation, determination and enthusiasm to pursue a research oriented career in Physics. Her experience and boundless knowledge have been of great help to me along the way of the said pursuit. I thank her for giving me the chance to work under her guidance and consider it as a real privilege to have worked alongside such a logical and knowledgeable guide. I have been very fortunate to earn her encouragement, guidance and most importantly her friendship, all through my research career. She is not only a guide, but also a mentor, friend and philosopher for me.

I am grateful to Prof. M. Junaid Bushiri, Head of the Department of Physics, CUSAT and Prof. B. Pradeep, former Physics H.O.D, for letting me access all the necessary facilities and also for their co-operation. I am indebted to Prof. Godfrey Louis, Doctoral committee member of the PhD programme for the consideration he has given me throughout my research period. I take this opportunity to thank sincerely all the faculty members of the Department of Physics, CUSAT, especially Prof. M. K. Jayaraj, for his constant encouragement and limitless support. I would like to thank the office, library and laboratory staff of the Department of Physics for the services they have offered me all through my research career.

I am extremely thankful to Prof. K. P. Mohanan, Department of Electronics, CUSAT, for his assistance to conduct the EMI shielding measurements. I would like to thank Prof. K. Chandrasekharan, Department of Physics, NIT, Kozhikode for the help extended by him to carry out the nonlinear optical studies. I also take this opportunity to express my sincere thanks to Prof. Manoj Namboothiri, IISER, Trivandrum for the help provided to do the PLQY measurements. I acknowledge with thanks the services rendered by STIC, CUSAT. I also consider it a privilege to thank my colleagues in the Division for Research in Advanced Materials laboratory (DREAM lab), - Manoj, Saheeda, Jinisha, Joseph John, Abhilash, Dr. Pradeep, and Ranjini, Department of Physics, CUSAT, for being with me and extending all sorts of help whenever necessary. I express my thanks for the encouragement and co-operation shown by senior research students, Dr.Anand, Dr. Sreekanth, Dr. Sajimol, and Dr.Jeeju of the DREAM lab.

Words are inadequate to thank Anuroop of Solid State Physics laboratory and Anil Kumar of my own DREAM lab, Department of Physics, CUSAT, for the unparalleled help rendered by them throughout my research period.

I extend my heartfelt gratitude to all the research scholars in the Department of Physics, especially to my friends in the Optoelectronic and Nanophotonic Devices, Thin film Photovoltaics, Applied Optics, Solid State Physics, Magnetics and the Nano Functional Materials laboratories. I take this opportunity to thank Hasna, Jasna, Anjana, Subha and Manu of the Optoelectronics lab for helping me with the XRD and Raman measurements, without any hesitation.

I am extremely thankful to Prof. Sivaramakrishnan, Principal, Govt. Arts & Science College, Kozhikode and all the former principals for their blessings and encouragement. I fear that words may be inadequate to express my gratitude to Prof. M. K. Remesh Babu, the Head, Department of Physics, for his constant support throughout my tenure. I also express my thanks to the teaching and non-teaching staff of the Govt. Arts & Science College, Kozhikode and all the members of the Department of Physics, for the help and encouragement extended, throughout my career.

I express my sincere thanks to my friends, Dr. Naseema, Associate Professor, Nehru Arts & Science College, Kanhangad and Dr. Shamaan, Asst. Professor, R.V. College of Engineering, Bangalore for the fruitful discussions I had with them.

I would also like to take this opportunity to thank my students, Mrs. Divyasree and Dr.Siji Narendran of NIT, Kozhikode for the help rendered for the nonlinear optical studies. I also express my gratitude to Miss.Bicy, M.G. University, Kottayam for the help extended to conduct the mechanical strength measurements.

I am also grateful to the University Grants Commission, Government of India for providing the teacher fellowship under the Faculty Development Programme.

I acknowledge with deep affection the support, love and benevolence of my husband, Abdurahiman, my sons - Azhar, Ameen, my daughter Ashikha and my son-in-law, Asharudheen, who have prayed for me and stood by me throughout my

research career. It would not have been possible to bring my efforts to a successful completion, if not, for their overwhelming support. At this occasion, I remember the faces of my grand old parents, without whose sincere prayers, this effort would have been futile. Finally I praise the Almighty for the blessings showered on me in all my endeavours.

Sabira. K

Preface

Materials are of fundamental importance for the development of the technology that adds luxury and amenities to our daily life, the typical examples being laptop computers and digital cell phones. The challenges of creating novel and more useful types of different classes of materials grow with the needs of the society. Recent developments in nanotechnology have revolutionized all walks of human activity with immense benefits not limited to the arenas of science and technology alone, but to those influencing everyday life as well. The size and shape dependent properties of the nanostructured materials have opened up, the possibilities for tuning the properties as desired, over wide ranges of the particle size. Polymer nanocomposites, consisting of host polymers and nanostructured filler materials dispersed within the host polymers, offer unprecedented application possibilities owing to the unique combination of the beneficial characteristics of the component materials.The experimental realization of graphene in 2004 has revolutionized the realm of nanotechnology and given wings to the dreams of achieving unparalleled breakthroughs in materials science and device technology. It is now possible to imagine the design of computers as fast as lightning but small enough to be folded up and carried in pockets and smart phones that can continue working without being recharged for weeks together. The products of advanced nanotechnology, yet to be made accessible in the

coming decades, promise even more innovative applications, far beyond the scope of the current products.

The entire research work included in the thesis is portrayed in different sections as follows**:**

The **first chapter** begins with an overview of the developments in the fields of nanotechnology and polymer nanocomposites, with emphasis on their application prospects. The motivation and the objectives of the present study are also addressed, which form an integral part of this chapter. The impetus for selecting poly(vinylidene fluoride) (PVDF) as the host polymer matrix and its beneficial features are elucidated, followed by a brief description of the nanostructured filler materials chosen, with due emphasis on their technological application prospects.

A brief description of the various experimental techniques employed for the characterization of the polymer nanocomposites developed for the present investigations is given in **chapter 2**. The structural, optical, thermal and electrical characterizations of the samples are carried out using different sophisticated techniques and a comprehensive description of them is included in this chapter.

The detailed analysis of the photoluminescence emission from free-standing and flexible, PVDF/ doped ZnS nanocomposite films, forms the focal theme of **chapter 3**.The semiconductor, ZnS, synthesized to be in the nanostructured form and doped with manganese

(ZnS:Mn) and copper (ZnS:Cu) are used for making nanocomposites with PVDF and flexible, free standing films of PVDF/ZnS:Mn and PVDF/ZnS:Cu are grown using the simple method of solution casting. These ZnS:Mn and ZnS:Cu based nanocomposite films are found to show intense yellow orange emission at 598 nm and blue emission at 432 nm respectively and can be of ample application prospects in developing flexible, luminescent devices. Plenty of scope also exists for realizing white light emitting, flexible devices by mixing the yellow and blue emissions from these nanocomposite films in the appropriate way.

The excellent UV shielding characteristics of the nanocomposite films of the well-known transparent conducting oxide ZnO, with PVDF, obtained as flexible and free standing films of thickness around 20 micrometers along with the observation of the intense photoluminescence emission all through the visible region, giving rise to the appealing white light emission, are comprehensively addressed in **chapter 4**. The simultaneous observation of excellent UV shielding characteristics and white light emission is the novelty of the work on PVDF/ZnO nanocomposite films.The work also extends ample scope for developing white light emitting flexible films, in a cost effective way.

The chapters 3 and 4 constitute the first phase of the work, related to the investigations on PVDF nanocomposite films, using the inorganic semiconductors, ZnS and ZnO as the nanostructured filler materials.The second phase of the work deals with the studies on the nanocomposite

films of PVDF using the carbon based nanostructured materials, reduced graphene oxide (RGO) and graphene as the fillers.

The PVDF/RGO nanocomposite films are grown by solution casting method using the filler material RGO, synthesized from graphite, using the modified Hummer's method. Significant enhancement of the β phase of PVDF, which is the most ordered polymorph form of PVDF, is found to be achieved by the addition of RGO to PVDF. The central theme of the work described in **chapter 5** is focused on assessing the nonlinear optical response of these nanocomposite films using open aperture and closed aperture Z scan technique, employing pulsed Nd:YAG laser of 532 nm wavelength, as the source. The novelty and highlight of the work on PVDF/RGO nanocomposite films is the achievement of normalized transmittance as low as 10% and the low optical threshold power around 7.84 MW/cm^2. These flexible films of PVDF/RGO nanocomposite of thickness around 10 microns offer plenty of scope for realizing efficient optical limiting devices of any shape or size.

The final part of the work is centered on studying the electro-magnetic interference (EMI) shielding properties of the PVDF/graphene nanocomposite films, obtained by solution casting method using commercially available graphene and is the essence of **chapter 6**. The EMI shielding measurements are done using wave guide transmission line technique in a Vector Network Analyser, in the frequency range

4-12 GHz. Convincing evidence for the increase in the β phase of PVDF with the addition of graphene, similar to the one observed upon the addition of RGO to PVDF, has been obtained from the structural characterization of the PVDF/graphene composites using XRD, Raman and FTIR spectroscopic techniques. The FESEM and TEM studies clearly establish the dense dispersion of graphene within the PVDF matrix, the interconnectivity between the graphene flakes and the high extent of crystallinity of the PVDF/graphene films. The high electrical conductivity of these nanocomposite films around 16 S/cm, is a consequence of the good connectivity among the graphene flakes and the high carrier concentration and carrier mobility observed in these nanocomposite films, which is quite significant for effective EMI shielding behaviour. The novelty of these studies is the observation of remarkably high electro-magnetic interference (EMI) shielding effectiveness of about 47 dB, observed in the highly conducting, ordered and flexible films of the PVDF / graphene nanocomposite of thickness around 20 microns, in the X-band frequency range of the microwave spectrum. This impressive EMI shielding effectiveness has been achieved in these films with 15% graphene loading, without adding foaming agents or surfactants. These free standing and flexible films are ideal for EMI shielding applications, without the geometrical constraints of the shape or size of the object. The absorption dominated shielding properties of these flexible nanocomposite films are found to be quite suitable for stealth applications as well.

The salient features of the investigations are summarized and the summary of the research work along with the conclusions drawn from these investigations, form the integral part of **chapter 7**. The highlights and novelty of the results and the scope for further investigations, based on the outcomes of the present studies are also emphasized.

List of Publications

Papers published in International/National peer reviewed Journals related to the work presented in the thesis.

[1] **K.Sabira**, P.Saheeda, E.I.Anila, S.Jayalekshmi **"**Highly luminescent and free standing, PVDF/doped ZnS nanocomposite films for flexible device applications" **Journal of Luminescence 188 (2017) 490 – 496;** doi.org/10.1016/j.jlumin.2017.05.014

[2] **K.Sabira**, P.Saheeda, S.Jayalekshmi "White light emission and excellent UV shielding observed in free standing and flexible films of polyvinylidene fluoride (PVDF)/zinc oxide (ZnO) nanocomposite" **Materials Letters 200 (2017) 125 – 127;** doi.org/10.1016/j.matlet. 2017.04.119

[3] **K.Sabira**, P.Saheeda, S.Jayalekshmi "Blue green fluorescence from free-standing films of PVDF/ZnS:Cu nanocomposites" **Material today proceedings**, 4 (2017) 4380–4388; 10.1016/j.matpr.2017. 04.009

[4] **K.Sabira**, P.Saheeda, M.C.Divyasree, S.Jayalekshmi "Impressive non-linear optical response exhibited by PVDF/ reduced graphene oxide(rGO) nanocomposite films" **Optics &Laser Technology** (Under minor revision)

[5] **K.Sabira**, M.P.Jayakrishnan, P.Saheeda, S.Jayalekshmi "On the absorption dominated EMI shielding effects in free standing films of poly vinylidene fluoride/graphene nanocomposite" **European Polymer Journal** (Under revision)

[6] Saheeda P; **Sabira K**; Jayalekshmi S "Investigation on the pH independent photoluminescence emission from carbon dots impregnated on polymer matrix" **Journal of biological and chemical luminescence** (Accepted)

Papers presented in International/National conferences

1) **K.Sabira**, P.Saheeda, S.Jayalekshmi "Blue green fluorescence from free standing films of PVDF/ZnS:Cu nanocomposites" at International Symposium on Photonics Applications and Nanomaterials **(ISPAN 2015**) at Trivandrum during 28-30 ,Oct 2015.

2) **K.Sabira**, P.Saheeda, S.Jayalekshmi "Enhanced luminescence in PVDF/ chitosan capped ZnS:Mn free standing films" at National seminar **SPAN-2015,** at Govt. Arts& Science College, Kozhikode on 3&4 Dec 2015

3) **K.Sabira**, P.Saheeda, S.Jayalekshmi "Photoluminescence in PVDF/ZnS:Mn nanocomposite films" at International conference on Nano technology,**NANO-15**, at K.S.R.College of technology, Tamil Nadu, India, during Dec 7-10, 2015

4) **K.Sabira**, P.Saheeda, S.Jayalekshmi "Functionalized Graphene – A Promising Filler Material for realizing, Conducting and Flexible Polymer Nanocomposite Films" at International conference on Advances in Polymer Technology (**APT 2016**), at Dept.of Polymer Science &Rubber Technology, CUSAT on 25&26, Feb 2016.

5) **K.Sabira**, P.Saheeda, S.Jayalekshmi "Excellent UV Shielding using free- standing, flexible PVDF/ZnO Nanocomposite Films" at "International Conference on Smart Engineering materials (**ICSEM**)" during 20-22 October 2016, at R.V. College of Engineering, Bangalore

6) **K.Sabira**, P.Saheeda, S.Jayalekshmi "White photo luminescence from free standing, flexible PVDF/ZnO nanocomposite films" at International Conference on Material Sciences (**SCICON' 16)**, during 19-21 December 2016 at Amrita University, Coimbatore, India

7) P.Saheeda, **K.Sabira**, S.Jayalekshmi "Investigations on the Structural and Optical properties of Polypyrrole/ MWCNT Composites Synthesized through a novel approach" at Inter national conference on Nano technology,**NANO-15**, at K.S.R.College of technology, Tamil Nadu, India, during Dec 7-10, 2015

8) P.Saheeda, **K.Sabira**, S.Jayalekshmi "Fluorescent nanocomposite films of Polyvinyl alcohol and functionalized Multiwalled Carbon Nanotubes for Biomedical Applications" at International Symposium on Photonics Applications and Nanomaterials **(ISPAN 2015**) at Trivandrum during 28-30 ,Oct 2015

9) P.Saheeda**, K.Sabira**, S.Jayalekshmi "Polypyrrole/ Multi walled carbon nanotube composite synthesized through liquid/liquid interfacial polymerization" at International conference on Advances in Polymer Technology (**APT 2016**), at Dept.of Polymer Science &Rubber Technology, CUSAT on 25&26,Feb 2016.

10) P.Saheeda, **K.Sabira**, Joseph John, S.Jayalekshmi "Transparent and flexible nanocomposite films of Polyvinyl alcohol/Multi walled carbon nanotube for optical limiting applications" at "International Conference on Smart Engineering materials (**ICSEM**)" during 20-22 October 2016, at R.V. College of Engineering, Bangalore

11) P.Saheeda, **K.Sabira**, Joseph John, S.Jayalekshmi "Fluorescent Multi walled carbon nanotube /Polyvinyl alcohol nanocomposite films synthesised through green routes" at International Conference on Material Sciences (**SCICON' 16)**, during 19-21 December 2016 at Amrita University, Coimbatore, India

Contents

List of Tables

List of Figures

Chapter 1

Chapter 2

Chapter 3

Chapter 4

Chapter 5

Chapter 6

Chapter 1

Introduction

Contents

This chapter serves as a general introduction to the work presented in the thesis. Investigations on the status of poly (vinylidene fluoride) (PVDF) as an exotic host matrix for realizing technologically important nanocomposites form the essence of the thesis. The basic concepts and relevance of nanotechnology with emphasis on polymer nanocomposites and the significance of the host polymer PVDF are discussed. The motivation for carrying out the present study, the importance of the materials chosen as nanostructured filler materials (ZnO, ZnS, reduced graphene oxide and graphene) to form the polymer nanocomposites and the objectives of the present study are also portrayed in this section.

1.1 Motivation of the present study

Laptop computers, digital cell phones and touch screens are examples that add convenience and luxury to our daily life. Since the demands of the society are increasing constantly and new needs emerge day by day, a systematic understanding of the productivity of available materials and the efforts towards the development of novel types of

materials with tunable characteristics must be continued with increasing drive, to meet the current and future requirements. Polymers constitute one of the most successfully exploited classes of materials due to the implausible variety of chemical structures available and their wonderful properties, along with their relatively low cost and applicability as sustainable materials. The area of polymer nanocomposites (PNCs) has grown to represent one of the largest classes within the scope of materials science, offering ample scope in the development of advanced materials for numerous technological applications.

In the search for a suitable polymer matrix for realizing the polymer nanocomposites investigated in the present work, poly (vinylidene fluoride) (PVDF) has been identified as the host polymer matrix, considering the quite impressive and unique features associated with this polymer. It is a semicrystalline fluoropolymer which is nontoxic and is endowed with excellent mechanical strength and is easy to process in the form of films. Its high dielectric permittivity, relatively low dissipation factor and high dielectric strength have made this polymer a very useful capacitor dielectric as well. It exhibits polymorphism and exists in five different forms as α, β, γ, δ and ε. It has a glass transition temperature (T_g) of about −35°C and is structurally 50 – 60% crystalline. It is an attractive material for use in various applications, because of its promising piezoelectric, ferroelectric and pyroelectric properties. It is chemically, thermally and mechanically very stable and is a highly flexible and processable material [1-4]. Because of its excellent film

forming properties, it is ideal as a polymer matrix for obtaining a variety of polymer nanocomposite films. It is unaffected by long-term exposure to sunlight and other sources of ultraviolet radiation and is nontoxic. It is resistant to most acids and alkalis and is valued for its toughness, good thermal and mechanical stability and distinct engineering advantages.

Generally polymer nanocomposites exhibit superior properties compared to those of the component materials. The improvement in the properties depends mainly on the type and size of the nanofiller materials used. Zinc oxide (ZnO) and zinc sulphide (ZnS) are semiconductors of the II-VI group, with wide band gap energy and high exciton binding energy, endowed with quite interesting electrical and optical characteristics. By making composites of nanostructured ZnO with the polymer PVDF, the UV shielding properties of the composite films can be enhanced, since ZnO is a very good absorber of UV radiation. Doped ZnS is a very good phosphor at room temperature and the nanocomposite films of PVDF/doped ZnS can be expected to be of application in the designing of free standing luminescent films for flexible device applications. Reduced graphene oxide (RGO) and graphene are highly sought after, carbon based nanofiller materials, capable of enhancing the electrical conductivity and mechanical strength of the resulting nanocomposite films with PVDF. It is also expected that these nanofiller materials can bring about enhancement in the β phase of the polymer PVDF, which is, structurally the most ordered polymorphic phase of PVDF [5-7].

1.2. Nanoscience and Nanotechnology

Nanoscience is one of the most interesting areas of applied materials science, in which behavior of systems confined to nanoscale dimensions is studied. Nanostructured materials are of vast scientific interest as they act as a bridge between bulk materials and atomic or molecular structures. The properties of bulk materials are not size dependent but for materials with nano-scale dimensions this is often not the case. The most striking features of nanostructured materials, quite different from their bulk counterparts, can be attributed to the sensitive dependence of the material properties on the particle size.

The ideas and concepts behind the development of nanoscience and nanotechnology started with the talk entitled "There's plenty of room at the bottom" by the famous physicist Richard Feynman at an American Physical Society meeting at the California Institute of Technology (CalTech) on December 29, 1959 [8].

Nanoscience deals with the art of manipulating matter at atomic and molecular scales, and generally involves the studies of structures sized at the nanoscale at least in one dimension. Nanostructured materials are gifted with properties quite different from what they exhibit on a macro scale, enabling exclusive applications. Nanotechnology is considered to be the next industrial revolution and is believed to cause huge impacts on the society, economy and life in general in the near future. One of the striking aspects of nanotechnology is the vastly increased surface to volume ratio of the nanostructured materials which makes possible new quantum

mechanical effects, like the “quantum size effects” whereby the material properties of solids are surprisingly altered with reductions in particle size. For the synthesis of nanostructured materials, there are two main approaches, the "bottom-up" approach where materials are built up atom by atom and the "top-down" approach where they are synthesized by removing existing materials from larger entities.

Nanocomposites are multiphase materials, where one or more of the phases have at least one dimension in the nanoscale, with enhanced functionality and a wide range of applications. The phases may be inorganic, organic, or both, with amorphous, semi-crystalline or crystalline phases or combinations of these phases. The driving force behind the creation of novel nanocomposites is to achieve innovative functionalities suitable for many technological applications. The material properties of nanocomposites are in general much superior to those of the component materials.

Depending on the types of the matrices used, nanocomposites can be mainly divided into (1) polymer matrix nanocomposites (2) ceramic matrix nanocomposites and (3) metal matrix nanocomposites [9]. The research work included in the thesis is specifically focused on polymer nanocomposites. They are of considerable interest because they combine the advantages of both polymers and filler components. The size and shape of the filler materials, especially if they are nanostructured, have direct effect on the properties of the resulting nanocomposites. The aspect ratio of the nanofillers, the extent of dispersion of nanofiller

materials in the polymer host matrix, individual properties of the host matrix and the interfacial regions shared by both the components affect the properties of the polymer nanocomposites. Generally, polymer rnanocomposites can be obtained by both in-situ and ex-situ techniques. In in-situ methods, the nanostructured filler particles are generated inside the polymer matrix by decomposition or chemical reduction of a metallic precursor dissolved in the polymer. In the ex-situ approach, the nanofillers are first synthesized by soft chemistry routes and then dispersed in the polymeric matrices.

Among the many highly glorified technological products developed, polymer nanocomposites have shown ubiquitous presence in various fields of applications as illustrated below.

- In food packaging and flexible and rigid drinking water bottles
- As mirror housing materials on various types of vehicles and in door handles, engine covers and belt covers
- As covering materials for portable electronic equipment such as mobile phones and pagers
- As transparent UV shielding materials suitable for applications in UV-sheltering windows, contact lenses and goggles
- As optical switches, optical limiters and other nonlinear optical devices for fast and efficient processing of the information content of data

- In drug delivery, bio sensing, bone tissue engineering and neural network applications
- As electrodes in flexible batteries and high power super capacitors, as solid electrolyte materials and as efficient electromagnetic interference shielding materials

1.3. Materials used in the present work

1.3.1. Poly(vinylidene fluoride) (PVDF) -- an exotic polymer host matrix

Poly (vinylidene fluoride) (**PVDF**) is a non-reactive and non toxic thermoplastic fluoropolymer with high molecular weight, synthesized by the polymerization of vinylidene fluoride. It is a semi crystalline polymer with the repeat unit of CH_2-CF_2 and consists of both amorphous and crystalline phases [1,2]. The chemical structure of PVDF is shown in figure (1) and the photograph of PVDF granules in figure (2).

The glass transition temperature (T_g) of PVDF is about −35 °C and is quite stable and easy to handle at room temperature [10,11].

Dr. Heiji Kawai discovered the piezoelectric properties of PVDF, in 1969 [3]. Furakawa and Johnson confirmed PVDF's piezoelectric nature in 1981 and identified the Curie point of PVDF as 103 ºC.

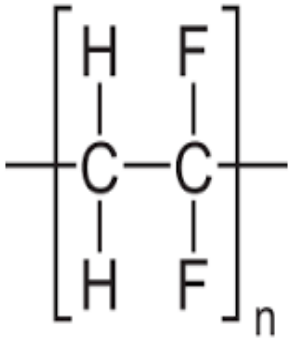

Fig (1) Chemical structure of PVDF **Fig (2)** Photograph of PVDF granules

Since PVDF has a low density of ~1.78 gm/cc and low cost compared with other fluoropolymers, it has been used to make pipes, sheets, films, filaments, plates for various applications and as an insulator material for premium wires. It can be injected, molded or welded and is commonly used in the chemical, semiconductor and medical industries and is also used as a binder in lithium ion cells. This material, with its impressive piezoelectric, ferroelectric and pyroelectric behaviour finds widespread applications in sensors, transducers, energy harvesters, actuators and MEMS [12,13]. The PVDF based fluorocarbon paints have superior weather resistance and their long term reliability allows outdoor use with less maintenance [14,15]. It is well known that PVDF membranes are quite useful for filtering and reverse osmosis applications [16,17]. The important properties of PVDF can be listed as follows

- Excellent film forming property and good flexibility
- Low weight
- Low thermal and electrical conductivity and good insulating properties
- High chemical corrosion resistance.
- Good heat resistance.
- High mechanical strength and toughness.
- High abrasion resistance.
- Resistance to most chemicals and solvents.
- Low permeability to most gases and liquids
- Good biocompatibility
- High piezoelectric coefficient
- Low acoustic and mechanical impedance
- High elasticity
- Unaffected by long term exposure to UV-radiation

For the advanced applications requiring electrostatic dissipation and electromagnetic interference shielding, the high electrical resistivity of PVDF is a limitation. This is usually addressed by making composites with highly conducting carbon nanofillers like graphene and carbon nanotubes [18,19].

Poly (vinylidene fluoride) has several polymorphs including four known chain conformations and a fifth suggested one termed as α, β, γ, δ and ε [20]. The most common crystalline phase is the α phase, which occurs in a Trans-Gauche–Trans-Gauche (TGTG) conformation. The α phase with monoclinic unit cell is generally formed during polymerization and crystallizes from the melt at all temperatures. It is a non-polar phase and does not exhibit piezoelectricity, pyroelectricity and ferroelectricity .

The most popular β-phase which is piezoelectrically and pyroelectrically active, with an orthorhombic unit cell in Trans–Trans (TT) conformation can only be obtained after special processing. In this all trans (TTTT) conformation, fluorine and hydrogen atoms are located on opposite sides of the polymer backbone which gives rise to a net non-zero dipole moment for the polymer. The presence of this dipole moment makes PVDF a good, piezoelectrically and pyroelectrically active polymer. Conversion of α-phased PVDF to β-phased one is done by mechanical drawing at high pressures and poling at high voltages. In its β-phase form, PVDF finds extensive applications in polymer sensors, actuators, transducers, energy harvesters and MEMs. [21,22].

The third phase is the γ-phase which is considered as the intermediate phase between the α and β-forms. This phase is formed due to the crystallization of PVDF at a temperature of 160 °C. The δ-phase is the polar form of α-phase and is generally obtained by polarization of α-form under a strong electric field and it has the same unit-cell dimensions and

chain conformation as the α-phase [23,24]. The fifth hypothetical polymorph is the ε-phase which contains T3GT3G′ conformation similar to the γ-phase but in an anti-polar arrangement.

The good solubility of PVDF in polar solvents such as esters, acetone, Dimethyl formamide (DMF), N-methyl-2-pyrrolidone (NMP) and Tetra hydro furan (THF) is advantageous for film casting from the solutions. The most commonly used copolymers of PVDF in piezoelectric and electrostrictive applications are P(VDF-trifluoroethylene), (PVDF-TrFE) and P(VDF-tetrafluoroethylene) (PVDF-TFE). They improve the piezoelectric response by improving the crystallinity of the material. The polymorphs α, β, γ and δ of PVDF are shown in figure (3) and the important physical properties of PVDF are given in the Table (1).

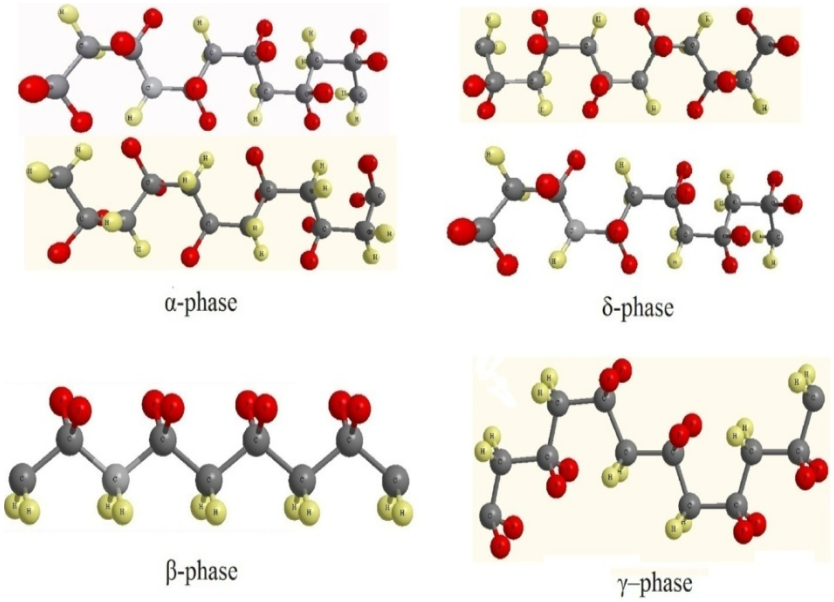

Fig. (3) Polymorphs of PVDF

Table (1): Important material properties of PVDF

Properties	Reported values
Melting point	174 °C
Glass transition temperature	~ -35 °C
Density	1.78 gm/cc
Heat capacity (300K)	1.9 $Jg^{-1}K^{-1}$
Tensile strength	35 -50 MPa
Dielectric constant (1MHz)	8
Dielectric strength	160 kV/mm
Resistivity	10^{14}ohms.cm
Thermal conductivity	0.2 $Wm^{-1}K^{-1}$
Piezoelectric co-efficient	6-7 pC/N
Refractive index	1.42
Co-efficient of linear expansion	14 x10^{-5} K^{-1}

1.3.2. Zinc Oxide (ZnO)

Nanostructured semiconductors are quite important in various types of device applications since their electrical, magnetic and optical properties can be tuned by changing the particle size [25].

Currently, there has been an increasing demand for the development of semiconductor nanostructures for applications in optoelectronic and electronic devices with multifunctionality [26-28]. ZnO is a n-type semiconductor of the II-VI group , with wide direct

bandgap energy of 3.37eV [29,30] and exciton binding energy of 60 meV at room temperature, well known for its room temperature luminescence characteristics. The structural, morphological and luminescence properties of nanostructured ZnO are quite sensitively influenced by the synthesis techniques. Zinc oxide, endowed with high chemical and environmental stability, high electrochemical coupling coefficient, broad range of radiation absorption, optical transparency in the visible range, high electron mobility, high photo-stability and impressive room temperature luminescence characteristics, is a low cost and nontoxic multifunctional material and offers ample opportunities to develop light emitting diodes (LEDs), solar cells and transparent electronic and optoelectronic devices [31-34]. Its UV absorbing property has been utilized in the design of UV shielding films and the synthesis of cosmetic sunscreen lotions. Because of its low toxicity, biocompatibility and biodegradability, ZnO can be used as a material of interest for biomedicine, bio imaging and drug delivery applications. The high third order optical nonlinearity associated with ZnO can be of application in developing efficient optical limiters for protection against high intensity laser radiation [35-37]. Some of the key properties of ZnO are shown in table 2 and important crystal structures of ZnO are shown in figure (4a) and figure (4b).

Table (2) Important characteristics of ZnO

Properties	Values
Band gap energy	3.37 eV
Exciton binding energy	60 meV
Dielectric constant	3.7
Refractive index	2.008
Stable crystal structure	Wurtzite
Lattice parameters	a= 0.325nm and c= 0.521nm
Thermal conductivity	0.6-1.2 $Wcm^{-1}K^{-1}$
Specific heat capacity	$Cp=40.3\ J\ mol^{-1}K^{-1}$
Solubility in water	Insoluble

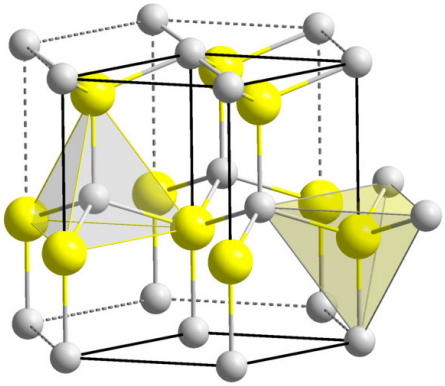

Fig (4a) Wurtzite (hexagonal packing)

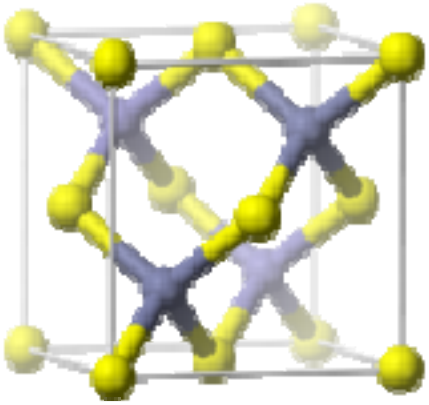

Fig (4b) Zinc blend (cubic packing)

1.3.3. Zinc Sulphide (ZnS)

Zinc sulfide is another important II–VI semiconductor, which has been studied extensively because of its broad spectrum of potential

applications in catalysts, cathode-ray tubes (CRT), field emission displays (FED), electroluminescent devices and photodiodes. Doped nanostructures of ZnS with dimensions below Bohr diameter are specifically suitable for a variety of applications in optoelectronics and nanophotonics [38,39]. It has a large bandgap of 3.72 eV for cubic zinc blend and 3.77 eV for hexagonal wurtzite structures respectively and has been widely used as an important phosphor material for photoluminescence (PL), electroluminescence (EL) and cathodoluminescence (CL) device applications due to its better chemical stability compared to other chalcogenides like ZnSe [40,41]. Its atomic structure and chemical properties are comparable to the more popular and widely known ZnO [42,43].

The nanostructured, manganese doped ZnS, (ZnS:Mn) has been widely investigated since the first report of efficient luminescence emission in the yellow-orange region in ZnS:Mn, by Bhargava et al [44,45]. The nonlinear, multiphoton absorption characteristics of nanostructured ZnS:Mn in the infrared and visible wavelength regions have intensified the research attraction of this material due to the prospects in bioimaging applications. Important properties of ZnS are shown in table 3 and important crystal structures of ZnS are shown in figure (5a) and figure (5b).

Table (3) Important characteristics of ZnS

Properties	Values
Band gap energy	3.7 eV
Exciton binding energy	40 meV
Dielectric constant	8.9
Refractive index	2.356
Stable crystal structure	Zinc blende
Lattice parameter	a= 0.541 nm
Density	4.102 gm/cc
Melting point	1850 °C
Solubility in water	Insoluble

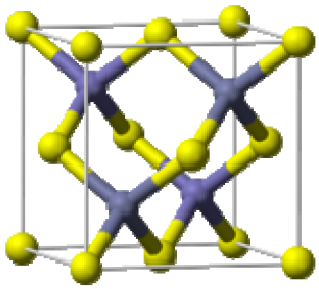

Fig (5a) Zinc blend (cubic)

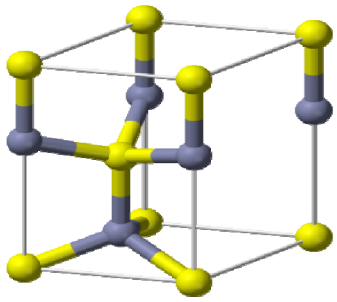

Fig (5b) Wurtzite (hexagonal)

1.3.4. Reduced Graphene Oxide (RGO)

Reduced graphene oxide (RGO) is commonly used as a carbon based nanofiller material for the synthesis of polymer nanocomposites. It is endowed with graphene like properties and can be synthesized in large quantities using easier methods compared to those adopted for

synthesizing single layer graphene or multi layer graphene. For many of the applications involving graphene, RGO can be used as a cost effective substitute. The commonly adopted synthesis approach of RGO starts from the low cost material, graphite. The deep oxidation of graphite using Hummer's method [46,47] results in graphene oxide (GO). The reduction of graphene oxide (GO) to RGO can be achieved through chemical, thermal or electrochemical methods. Each method has its own merits and drawbacks. Some of these drawbacks include the use of toxic substances, longer hours of reaction and the need for maintaining high temperatures and harsh conditions [48].Some reported examples of graphene oxide reduction are given below.

- Treating graphene oxide with the reducing agent, hydrazine hydrate at 100°C for 24 hrs.
- Exposure to hydrogen plasma for several seconds
- Exposure to powerful pulsed light from xenon flashtubes
- Heating the graphene oxide with urea as an expansion-reduction agent
- Direct heating of graphene oxide in a furnace to very high temperatures

The RGO produced by chemical reduction method often has comparatively lower electrical conductivity and surface area. Electrochemical production of RGO would be the preferred commercial

method in future, since it yields a material almost identical in structure to pristine graphene. Generally, RGO resembles graphene, but contains residual oxygen and other hetero atoms as well as structural defects [49]. It is widely used in graphene research, rechargeable batteries, supercapacitors, printable graphene electronics and catalysis. The electrical conductivity of RGO is generally less than that of graphene [50], since the former cannot have the perfect graphene structure and there can be oxygen functional groups attached to the surfaces of RGO. In the present work, RGO is used as the filler material to make nanocomposites with PVDF, as the cost effective substitute for graphene and study the nonlinear optical response of this nanocomposite.

1.3.5. Graphene

The experimental realization of graphene in 2004 has revolutionized the realm of nanotechnology and given wings to the dreams of achieving unprecedented breakthroughs in materials science and device technology. It is now possible to imagine the design of computers as fast as lightning but small enough to be folded up and carried in pockets and smart phones that can continue working without being recharged for weeks together. Graphene, a highly sought after carbon nanostructure in the form of a two-dimensional, atomic-scale, hexagonal packed lattice structure, is endowed with many intriguing

unique properties which include the superior electrical conductivity and thermal conductivity even higher than those of metals, the quantum Hall effect, quite high charge carrier mobility at room temperature, good optical transparency, surprisingly high young's modulus and mechanical strength and excellent flexibility [7].

Graphene is emerging as the most glorious two dimensional material because of its unique combination of superb properties, which has been utilized for applications in a wide spectrum of areas ranging from nano-electronics to nanophotonics, bioimaging, biosensing and targeted drug delivery. The excellent mechanical strength of this material has resulted in the development of various types of graphene-reinforced composites [51-54].

Another promising application of this material includes the development of graphene based polymer nanocomposites. The interfacial effects between graphene flakes and polymer chains are quite interesting to be pursued in depth, but such studies have not been carried out deeply to tap the full potential of graphene based polymer composites in practical applications.

Graphene considerably improves the properties of polymer composites even at a little loading and the very high surface conductivity of graphene facilitates the formation of numerous types of electrically

conducting polymer composites. These conducting polymer / graphene nanocomposites have been widely used in sensors, memory and energy storage devices, antistatic coatings, as EMI shielding materials and as bipolar plates for fuel cells. The discovery of graphene as a filler material for polymer nanocomposites has opened new dimensions for realizing light weight and high performance composite materials for a range of applications in aerospace, automobile, petrochemical and biomedical industries [55-57].

Prior to the synthesis of polymer/graphene nanocomposites, graphene should be made dispersible in or compatible with the chosen polymer matrices. Chemical modification or functionalization of graphene is generally required to effect its homogeneous dispersion in polymer matrices. Earlier reports have established that functionalization can effectively prevent the agglomeration of graphene and improve the interfacial bonding between graphene flakes and polymer chains. In the present work, the PVDF/graphene nanocomposite films, grown as free standing and flexible films with high electrical conductivity and good crystalline order have been studied to assess their suitability as light weight shields against the unwanted electromagnetic interference which can adversely affect the performance of electronic devices.

The important properties of graphene are given in table (4).

Table. (4) Important properties of graphene

Properties	**Values**
Tensile strength	130+- 10GPa
Thermal conductivity	$4.84x10^3$ to $5.3x10^3$ $Wm^{-1}K^{-1}$
Electrical conductivity	10^8 Sm^{-1}
Young's modulus	1TPa
Optical transparency	97.7%
Surface area	2630 m^2g^{-1}
Carrier mobility	10^4 cm^2 V^{-1} s^{-1}
Inter planar spacing	0.335 nm

1.4. Objectives of the present study

The thesis portrays a journey, exploring the versatile roles of the semi-crystalline fluoropolymer, PVDF as an exotic polymer matrix to realize polymer nanocomposite films, using different but intrinsically connected filler materials, with ample prospects for flexible device applications.

- The first category of these nanocomposite films belongs to the films of PVDF/doped ZnS in which, manganese and copper doped samples of nanostructured ZnS act as the filler materials. It is envisaged to realize PVDF /ZnS:Mn and PVDF/ZnS:Cu nanocomposite films by solution casting method, as free standing and flexible films and investigate in detail their photoluminescence

characteristics by varying the concentration of doping. As a sequel to these studies, it is anticipated to assess the prospects of these nanocomposite films in flexible light emitting device applications and in the design of white light emitters.

- The potential of the polymer matrix PVDF for growing flexible films of PVDF / nanostructured ZnO, will be assessed as the next phase of work. The main objectives will be focused on investigating the UV shielding properties and the photo luminescence characteristics of these nanocomposite films and the application prospects.
- Reduced graphene oxide (RGO), generally considered as a cost effective substitute to graphene will be synthesized by Hummers method and will be used as the third type of filler material to realize PVDF/RGO nanocomposite films by solution casting method. Expecting an enhancement in the β phase of PVDF upon the addition of RGO, the structural aspects of the nanocomposite will be investigated in detail. The nonlinear optical response of the PVDF/RGO nanocomposite films will be explored using Z scan technique and the scope of these films in the design of flexible optical limiting devices will be assessed.
- The last phase of the work will be focused on using graphene as the filler material to grow PVDF/graphene nanocomposite films, after the chemical treatment of graphene to facilitate its effective

dispersion in PVDF. Expecting the films to have quite good electrical conductivity, these nanocomposite films will be investigated to evaluate their effectiveness in electromagnetic interference (EMI) shielding applications. The prospects of developing light weight and flexible EMI shields with impressive shielding effectiveness in the broad region of the electromagnetic spectrum, using PVDF/graphene nanocomposite films will be addressed in detail.

References

[1] Hari singh Nalwa; *Ferroelectric Polymers: Chemistry: Physics, and Applications* (1995) CRC Press

[2] Brasure.D.E, Ebnesajjad.S; *Vinyl Fluoride polymers, Encyclopedia of polymer science & Engg* 2; 468-491; Wiley (1998)

[3] Kawai.H. (1969) 'The piezoelectricity of poly (vinylidene fluoride)', *Japanese Journal of Applied Physics*, 8(7), pp. 975; doi. 10.1143/ jjap. 8. 975

[4] R. Gregorio Jr, E. M. Ueno ; Effect of crystalline phase, orientation and temperature on the dielectric properties of poly (vinylidene fluoride) (PVDF); *Journal of Materials Science* 34 (1999) 4489 – 4500, doi: 10.1023/a:1004689205706

[5] A.K. Geim, K.S. Novoselov, The rise of graphene, *Nature, Nat. Mater*. 6 (2007) 183 – 191; http://dx.doi.org/10.1038/ nmat1849

[6] P. Noorunnisa Khanam, Deepalekshmi Ponnamma and M.A. AL-Madeed; *Electrical Properties of Graphene Polymer Nanocomposites;* Springer International Publishing Switzerland 2015, doi 10.1007/978-3-319-13875-6_2

[7] Tapan K. Das and Smita Prusty; Graphene-Based Polymer Composites and Their Applications; *Polymer-Plastics Technology and Engineering*, 52: 319–331, 2013, doi: 10.1080/03602559. 2012.751410

[8] R. P. Feynman, *Philosophical Transactions*, Reinhold, New York, 1961

[9] D. Suneel, D. Nageswra Rao, *J. of Mechanical Engineering*, 1, 75 (2008)

[10] A.K. Chilvery, A.K. Batra, M. Thomas, Investigation on Characteristics of PVDF / ZnO Nanocomposite Films for High-k Capacitors, " *Physical Science International Journal*" 4(5): (2014) 734–741. doi 10.9734/psij/2014/9026

[11] P.I.Devi, K. Ramachandran, Dielectric studies on hybridised PVDF – ZnO nanocomposites*," Journal of Experimental Nanoscience*", vol.6,no.3,June2011.8080 (2015). doi:10.1080/ 17458080.2010. 497947.

[12] B. Jaleh, A. Jabbari, Evaluation of reduced graphene oxide/ZnO effect on properties of PVDF nanocomposite films, "*Appl. Surf. Sci*." 320 (2014) 339–347. doi:10.1016/ j.apsusc.2014.09.030.

[13] H. Yu, T. Huang, M. Lu, M. Mao, Q. Zhang, H. Wang, Enhanced power output of an electrospun PVDF/MWCNTs-based nanogenerator by tuning its conductivity, "*Nanotechnology*" 24 (2013) 405401. doi:10.1088/0957-4484/24/40/405401

[14] Landry.V.,Blanchet. P, Weathering resistance of opaque PVDF acrylic coatings applied on wood substrates,; *Progress in organic coatings*, 75,494-501, (2012)

[15] Hay.T.R, Rose.J.L ; Flexible PVDF comb transducers for excitation of antisymmetric guided waves in pipe,; *Sensors and Actuators A: Physical*, 100,1018-23 (2002)

[16] Prince.J.A., Rana.D., Singh.G., Matsuura.T., Junkai.T., Shanmugha sundaram.T.S, Effect of hydrophobic surface modifying macromolecules on differently produced PVDF membranes direct contact membrane distillation, *Chemical Engg. Journal*, 242,387-396, (2014)

[17] Kang.G, Cao.Y, Application and modification of PVDF membranes, *Journal of Membrane Science*, 463,145-165(2014)

[18] Shailaja Pande , B. P. Singh, R. B. Mathur , T. L. Dhami, P. Saini and S. K. Dhawan "Improved EMI Shielding Properties of MWCNT–PMMA Composites Using Layered Structures"; *Nanoscale. Res. Lett*. (2009) 4:327–334; doi 10.1007/s11671-008-9246-x.

[19] Jiajie Liang, Yan Wang, Yi Huang, Yanfeng Ma, Zunfeng Liu, Jinming Cai, Chendong Zhang, Hongjun Gao, Yongsheng Chen; " EMI shielding of graphene/epoxy Composites"; *Carbon .47* (2009) 922-925 ; doi:10.1016/j.carbon. 2008.12.038

[20] Lovinger. A.J., *Science* 220 ; p 1115,(1983).

[21] Furukawa.T., *Phase transitions* 18; p 143 (1989)

[22] Sencadas.V, Moreira.V.M., Lanceros.S, Pouzada.A.S, Gregorio.R; Alpha to Beta transformation on PVDF films obtained by uniaxial stretch , *Adv.Mat*., vol.514, 872-876 (2006).

[23] Gregorio.R, Cestari.M, Effect of crystallization temperature on the crystalline phase content and morphology of poly(vinylidene fluoride); *J.Poly.Sci, Part.B, Pol.Phy*, 32; p.859 (1994) doi: 10.1002/ polb.1994.090320509

[24] Schwartz.M, *Encyclopedia of Smart Materials*, Wiley (2002)

[25] P. M. Aneesh, K. A.Vanaja, M. K. Jayaraj, Synthesis of ZnO nanoparticles by hydrothermal method; *Proc. of SPIE* Vol. 6639 66390J-1, doi: 10.1117/12.730364

[26] T.-H. Moon, M.-C. Jeong, W. Lee, J.-M. Myoung, Nano-ZnO film preparation at low temperature and the optical indices calculation; *Appl. Surf. Sci*. 240(1–4), 280 (2005)

[27] U. Ozgur, Y.I. Alivov, C. Liu, A. Teke, M.A. Reshchikov, S. Dogan, V.Avrutin, S.J. Cho, H. Morkoc, A comprehensive review of ZnO materials and devices *J. Appl. Phys*. 98(4),41301 (2005); 10.1063/1.1992666.

[28] S.J. Pearton, C.R. Abernathy, M.E. Overberg, G.T. Thaler, D.P.Norton, N. Theodoropoulou, A.F. Hebard, Y.D. Park, F. Ren, J. Kim, *J. Appl. Phys*. 93(1), 1 (2003)

[29] Y. Abdollahi, A. H. Abdullah , Z. Zainal , N. A. Yusof, Synthesis and Characterization of Manganese Doped ZnO Nanoparticles*; International Journal of Basic & Applied Sciences* IJBAS-IJENS Vol: 11 No: 04; 118104-7373 .

[30] B.K. Meyer, H. Alves, D.M. Hofmann, W. Kriegseis, D. Forster, F.Bertram, J. Christen, A. Hoffmann, M. Straburg, M. Dworzak, U.Haboeck, A.V. Rodina, *;* *Physica Status Solidi (b*) 241(2), 231 (2004))

[31] Agnieszka Kołodziejczak-Radzimska and Teofil Jesionowski; Zinc Oxide—From Synthesis to Application: A Review; *Materials* 2014, *7*, 2833-2881; doi:10.3390/ma7042833

[32] Hamid Reza Ghorbani, Ferdos Parsa Mehr, Hossein Pazoki and Behrad Mosavar Rahmani; Synthesis of ZnO Nanoparticles by Precipitation Method**;** *Orient. J. Chem.,* Vol. **31**(2), 1219-1221 (2015)

[33] P.P. Jeeju , S. Jayalekshmi , K. Chandrasekharan , P. Sudheesh; Enhanced linear and nonlinear optical properties of thermally stable ZnO/poly(styrene)–poly(methyl methacrylate) nanocomposite films, *Thin Solid Films* 531 (2013) 378–384, http://dx.doi.org/10.1016/ j.tsf.2012.12.043

[34] K. Omri , J. El Ghoul , O.M. Lemine , M. Bououdina , B. Zhang, L. El Mir, Magnetic and optical properties of manganese doped ZnO nanoparticles synthesized by sol–gel technique; *Superlattices and Microstructures* 60 (2013) 139–147

[35] Huan-Ming Xiong, *Advanced material letters*; Volume 25, Issue 37 October 4, 2013; DOI 10.1002/adma.201301732

[36] Chennupati Jagadish and Stephen Pearton," Zinc Oxide- Bulk, Thin films and Nano structures-Processing, Properties and Applications", Elsevier Ltd. UK (2006) Volume 2014, http://dx.doi.org/10.1155/ 2014/371720

[37] Satyanarayana Talam, Srinivasa Rao Karumuri and Nagarjuna Gunnam, Synthesis, Characterization, and Spectroscopic Properties of ZnO Nanoparticles**,** International Scholarly Research Network; *ISRN Nanotechnology*;Volume 2012, Article ID 372505, doi: 10.5402/2012/372505

[38] Xiaosheng Fang , Tianyou Zhai , Ujjal K. Gautam , Liang Li , Limin Wua, Yoshio Bando, Dmitri Golberg, ZnS nanostructures: From synthesis to applications, *Progress in Materials Science* 56 (2011) 175–287

[39] V. Ramasamy , K. Praba, G. Murugadoss , Synthesis and study of optical properties of transition metals doped ZnS nanoparticles, *Spectrochimica Acta Part A: Molecular and Biomolecular Spectroscopy* 96 (2012) 963–971

[40] A. K. Kole , P. Kumbhakar, Effect of manganese doping on the photoluminescence characteristics of chemically synthesized zinc sulfide nanoparticles, *Appl Nanosci* (2012) 2:15–23; doi 10.1007/ s13204-011-0036-x

[41] RajneeshK.Srivastava , NitinPandey , SheoK.Mishra, Effect of Cu concentration on the photoconductivity properties of ZnS nanoparticles synthesized by co-precipitation method , *Materials Science in Semiconductor Processing* 16(2013) 1659–1664

[42] M. Bangal, S. Ashtaputre, S. Marathe, A. Ethiraj, N. Hebalkar, S. W. Gosavi, J. Urban and S. K. Kulkarni, Semiconductor Nanoparticles, *Hyperfine Interactions (*2005) 160:81–94 doi 10.1007/s10751-005-9151-y

[43] Iftikhar M.Ali, Raad M.Al-Haddad, Khalid T. Al-Rasoul, Structural and Optical Properties of Synthesized Manganese doped ZnS Quantum Dots**,** IJISET - *International Journal of Innovative Science, Engineering & Technology*, Vol. 1 Issue 10, December 2014.

[44] R. N. Bhargava, D. Gallagher, X. Hong and A. Nurmikko, *Phys. Rev. Lett*. 72 416 (1994)

[45] R.N.Bhargava, D.Gallagher, T.Welker, Doped nanocrystals of semiconductors- a new class of luminescent materials, *Journal of Luminescence* (1994) 275-280

[46] Hummers, W.S. and Offeman, R.E., Preparation of Graphitic Oxide, *J. Am. Chem. Soc.*, 1958, vol. 80, no. 6, pp. 1339–1339.

[47] Kovtyukhova, N. I.; Ollivier, P. J.; Martin, B. R.; Mallouk, T. E.; Chizhik, S. A.; Buzaneva, E. V.; Gorchinskiy, A. D; Layer-by-Layer Assembly of Ultrathin Composite Films from Micro-Sized Graphite Oxide Sheets and Polycations, *Chem. Mater*. 1999, 11, 771−778

[48] S. V. Tkachev, E. Yu. Buslaeva, A. V. Naumkin, S. L. Kotova, I. V. Laure, and S. P. Gubin, Reduced Graphene Oxide ; ISSN 0020-1685, *Inorganic Materials*, 2012, Vol. 48, No. 8, pp. 796–802

[49] T. Szabo, O. Berkesi, P. Forgo, K. Josepovits, Y. Sanakis, D. Petridis, et al., Evolution of surface functional groups in a series of progressively oxidized graphite oxides, *Chemistry of Materials* 18 (2006) 2740–2749.

[50] H. A. Becerril, *et al*., "Evaluation of Solution-Processed Reduced Graphene Oxide Films as Transparent Conductors"; *ACS Nano*, Vol. 2, No. 3, 2008, pp. 463-470. doi:10.1021/ nn700375n

[51] Tapas Kuilla, Sambhu Bhadra , Dahu Yao, Nam Hoon Kim, Saswata Bose , Joong Hee Lee Recent advances in graphene based polymer composites; *Progress in Polymer Science* 35 (2010) 1350–1375;

[52] Rama K Layek, Arun K Nandi; A review on synthesis and properties of polymer functionalized graphene; *Polymer;* Volume 54, Issue 19,2013, 5087 – 5103

[53] Horacio J. Salavagione, Gerardo Martínez and Gary Ellis; Graphene-Based Polymer Nanocomposites; www.intech open.com

[54] Dilini Galpaya, Mingchao Wang, Meinan Liu, Nunzio Motta, Eric Waclawik, Cheng Yan; Recent Advances in Fabrication and Characterization of Graphene-Polymer Nanocomposites; *Graphene,* 2012, 1, 30-49; http://dx.doi.org/10.4236/ graphene. 2012.12005;

[55] Balandin A A, Ghosh S, Bao W Z, Calizo I, Teweldebrhan D, Miao F and Lau C N, 2008 Superior thermal conductivity of single-layer graphene ; *Nano Lett*. 8 902–7

[56] Jiwu Shang , Yihe Zhang , Li Yu , Bo Shen , Fengzhu Lv , Paul K. Chu; Fabrication and dielectric properties of oriented polyvinylidene fluoride nanocomposites incorporated with graphene nanosheets, *Materials Chemistry and Physics* 134 (2012) 867 - 874; doi:10.1016/j.matchemphys.2012.03.082

[57] Jianchuan Wang, Jieli Wu, Wei Xu, Qin Zhang, Qiang Fu; Preparation of poly(vinylidene fluoride) films with excellent electric property, improved dielectric property and dominant polar crystalline forms by adding a quaternary phosphorus salt functionalized graphene; *Composites Science and Technology* 91 (2014) 1–7 ; doi.10.1016/ j.compscitech. 2013.11.002.

Chapter 2

Characterization Techniques

Contents

This chapter portrays the brief description of the experimental techniques used for the characterization of the different types of samples used for the present studies. The structural, optical and thermal characterizations of the synthesized samples are carried out using different sophisticated instruments and a comprehensive description of the tools utilized is addressed in this chapter.

2.1. Introduction

It is mandatory to determine the particle size and analyse the structural and morphological details of the different types of the nanocomposite samples used in the present work. A variety of techniques can be used for this purpose, and the details are given in the following sections. The sophisticated techniques used for the structural and

morphological characterization of the samples investigated in the present study include, X-ray diffraction (XRD), Raman spectroscopy, Fourier transform infrared (FTIR) spectroscopy, transmission electron microscopy (TEM) and field emission scanning electron microscopy (FESEM). The thermal studies were carried out using thermo gravimetric analysis (TGA) and differential scanning calorimetry (DSC). The UV-visible –NIR absorption spectroscopy and the photoluminescence (PL) spectroscopy techniques were used for the optical characterization of the various nanocomposite film samples. The thickness of the films was measured using the stylus profiler.

2.2. X-Ray Diffraction (XRD)

X-ray diffraction can be used to study the crystallographic properties of polycrystalline, powder and thin film samples and also for the compositional analysis of nanocomposites. The given sample generates a characteristic X-ray diffraction pattern, whether it is present in the pure state or as one of the constituents of a mixture of substances. This fact is the basis for the diffraction method of chemical analysis. The diffraction methods are much faster and they require only very small amounts of sample and are non-destructive. X-ray diffraction data can provide information about the crystal structure, atomic spacing, lattice parameters, phase composition and grain size of the samples studied.

The average grain size 'd' of the sample can be calculated using the Scherrer's formula, $d = 0.9 \lambda / \beta \cos \theta$

where, λ is the wavelength of the X-rays used, β, the full width at half maximum intensity of the diffraction peaks and θ is the glancing angle in radians.

It is a non-destructive analytical technique which can yield the unique fingerprint of Bragg reflections associated with a crystal structure. The wavelength of X-rays is typically the same order of magnitude (1–100 angstroms) as the spacing between the crystal planes [1 – 3]. In the present work, XRD studies were carried out using Rigaku model D max 2500 X-ray diffractometer.

Fig. (1) X-ray diffractometer

2.3. Fourier Transform Infrared Spectroscopy (FTIR)

Fourier Transform Infrared Spectroscopy is the analytical technique based on the interaction of infrared radiation with matter as a function of photon frequency, which provides specific information about

the vibrational and rotational states of the chemical bonding and molecular structures, making it quite useful for analyzing the structural aspects of materials. An infrared spectrum represents a fingerprint of a sample with absorption peaks corresponding to the frequencies of vibrations between the bonds of the atoms making up the material. The advantages of infrared spectroscopy include wide applicability, nondestructiveness, measurement options under ambient atmosphere and the capability of providing detailed structural information [4 – 6].

Attenuated Total Reflectance (ATR) is the most widely used FTIR spectroscopic sampling tool. This technique generally allows qualitative or quantitative analysis of samples with little or no sample preparation formalities, which increases the speed of sample analysis. The main benefit of ATR sampling comes from the very thin sampling path length or depth of penetration of the IR beam into the sample. This is in contrast to the traditional FTIR spectroscopic sampling by transmission, where the sample must be diluted with IR transparent salt and pressed into a pellet or pressed to a thin film, prior to analysis, to prevent totally absorbing bands in the infrared spectrum. The ATR technique is an easy way to identify the presence of certain functional groups in a molecule or to detect the presence of specific impurities and is a leading FTIR spectroscopic sampling tool due to its ease-of-use and speed of analysis [7,8]. In the present study, Fourier transform infrared spectra of the samples were taken using Shimadzu FTIR spectrophotometer, having a resolution of 4 cm^{-1} in the range 400 – 4000 cm^{-1}.

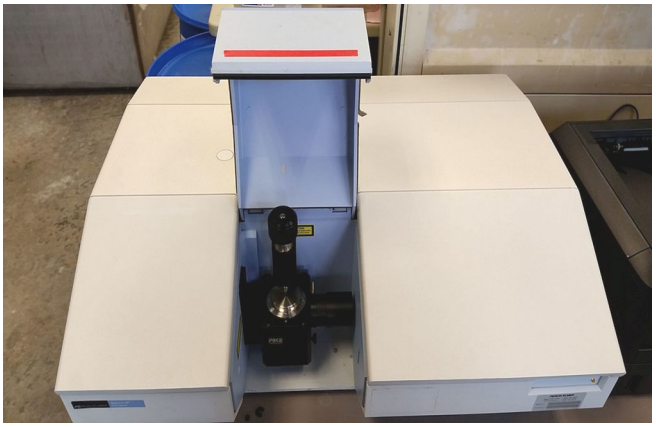

Fig. (2) FTIR (ATR) spectrophotometer

2.4. Raman Spectroscopy

Raman spectroscopy, based on the Raman effect is a powerful technique, commonly used to study the vibrational, rotational, and other low-frequency modes in materials. The energy of the laser photons increases or decreases when the laser light interacts with molecular vibrations, phonons or other excitations in the material under study. The shift in energy gives information about the phonon modes in the system. Raman spectroscopy named after Sir C.V.Raman is used to analyze the vibrational states of materials and also to obtain information about the structure and phase purity of materials and the phonon confinement in them. It is commonly used to provide a fingerprint of materials by which different molecules can be identified [9,10]. In the present work, Raman spectroscopic studies were carried out, using a Micro Raman spectrometer, HORIBA JOBIN YVON using a He-Ne laser (633nm) as the excitation source.

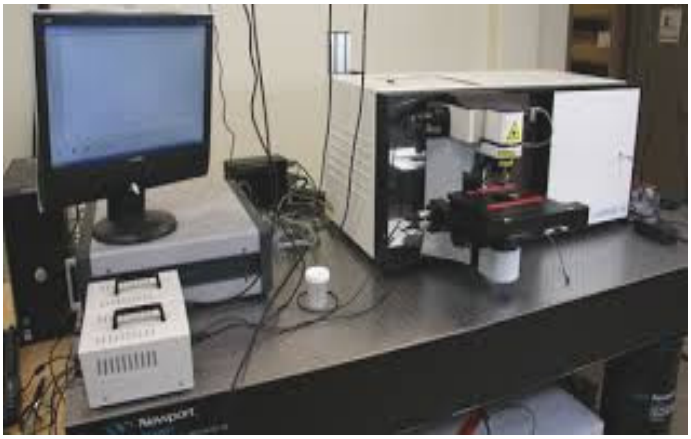

Fig. (3) Raman spectrometer

2.5. Transmission Electron Microscopy (TEM)

Transmission electron microscopy (TEM), used for the microstructural characterization of materials, specifically nanostructured materials, is an imaging technique in which, a beam of electrons is focused onto the specimen under study, causing an enlarged version to appear on a photographic film or fluorescent screen or to be detected by a CCD camera. Using TEM images, the particle size of the nanostructured materials can be determined and it is also possible to identify the orientation of the crystal planes in the material. Selective area electron diffraction (SAED) is the map of the reciprocal lattice, which also gives the signatures of various planes in the material. Depending on the crystalline nature of the material, the SAED patterns will be orderly arranged spots, distinguishable rings or fused rings. It is a microscopy technique in which a beam of electrons is transmitted through an ultra-thin specimen and the electron beam interacts with the

specimen as it passes through. Electron microscopes have higher resolving power, compared to optical microscopes and can reveal the structure of lower dimensional objects. The transmission electron microscopes can achieve resolutions better than 50 pm and magnifications up to about 10^7 x, whereas most optical microscopes are limited to about 200 nm resolution and magnifications below 2000 x. In the transmission electron microscopes, electromagnetic lenses are used to focus the electrons into a very thin beam whereas in optical microscopes, glass lenses are used to focus the light [11–13]. The TEM images of the samples in the present work were obtained using TEM, JEOL 2100 machine, operating at an accelerating voltage of 200 kV.

Fig. (4) Transmission Electron Microscope

2.6. Field Emission Scanning Electron Microscopy (FESEM)

Field Emission Scanning Electron Microscope (FESEM) is an electron microscope with a wide range of applications in materials science and engineering. The electrons, liberated by a field emission source interact with the atoms that make up the sample, producing signals that contain information about the sample's surface topography, composition, and surface roughness. The electrons liberated from the field emission source are accelerated in a high electrical field gradient. The main difference between the Scanning Electron Microscope (SEM) and the Field Emission Scanning Electron Microscope (FESEM) is regarding the type of the electron emitter used. The FESEM gives 3 to 6 times better resolution than the conventional SEM and produces a clean image of the sample with less electrostatic distortions and good spatial resolution and provides specific information about the topography, crystallography, surface features and specimen composition [12,14,15]. The FESEM images of the samples in the present work were obtained using Carl-Zeiss Sigma, field emission scanning electron microscope.

Fig. (5) FESEM experimental setup

2.7. Thermo Gravimetric Analysis (TGA)

Thermo gravimetric analysis (TGA) is a method of thermal analysis in which mass of the sample is measured as a function of increasing temperature (with constant heating rate) or time. The experimental atmosphere may be purged with an inert gas to prevent sample oxidation or other undesired reactions. The technique of TGA can be utilized for the determination of the degradation temperatures and absorbed moisture content of materials, the concentration of inorganic and organic components in materials, the decomposition points of explosives, and the presence of solvent residues. Materials analyzed by TGA include polymers, plastics, composites, laminates, adhesives, food, coatings, pharmaceuticals, organic materials, rubber, petroleum, chemicals, explosives and samples. In the present work, TGA is used primarily for

determining the thermal stability of polymers and polymer nanocomposite films [16,17]. A derivative weight loss curve (DTG curve) can identify the point where weight loss is most apparent. The thermo gravimetric measurements in the present study were done using Perkin Elmer, Diamond TG/DTA instrument at a heating rate of 10 °C /min in nitrogen atmosphere.

Fig. (6) TGA experimental setup

2.8. Differential Scanning Calorimetry (DSC)

Differential Scanning Calorimetry (DSC) is the technique used to measure the temperature and heat flow associated with transitions in materials in controlled atmosphere. These measurements provide quantitative and qualitative information about the physical and chemical changes that involve endothermic or exothermic processes, or changes in

heat capacity. Using this technique, it is possible to calculate the melting temperature (T_m), the crystallization temperature (T_c), the glass transition temperature (T_g) and the percentage of crystallinity of the samples under study [18,19]. In the present work, the differential scanning calorimetry (DSC) experiment was done on a Mettler Toledo DSC 822e instrument.

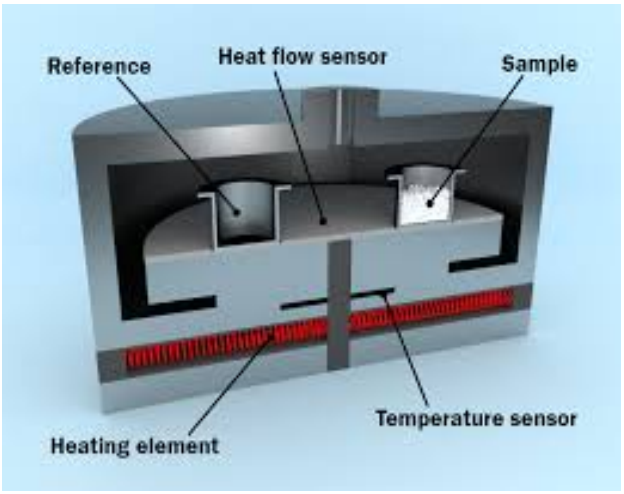

Fig. (7) Inner side of the DSC setup

2.9. UV-visible absorption spectroscopy

Absorption spectroscopy refers to spectroscopic techniques that measure the absorption of radiation, as a function of frequency or wavelength, due to its interaction with matter. The UV-visible spectrophotometry uses radiation in the UV and visible parts of the electromagnetic spectrum as the source. The radiation in this wavelength range can excite the electrons from the ground state to higher energy levels, giving rise to absorbance at wavelengths specific to the samples under

study. The absorption ability of a material is measured by its absorption coefficient α, where α is related to the intensity of the transmitted radiation I as, $I = I_0 \exp(-\alpha t)$ where, I_0 is the intensity of the incident radiation and t, the thickness of the sample. The band gap energy of samples can be determined by extrapolating the linear portion in the $(\alpha h\upsilon)^2$ versus $(h\upsilon)$ plot to the abscissa in the case of direct allowed transitions [20,21]. In the present study, the optical absorption of the samples was recorded using JASCO V-570 spectrophotometer, having a deuterium lamp (190-350 nm) and a halogen lamp (330-2500 nm) as sources.

Fig. (8) UV-visible spectrophotometer

2.10. Photoluminescence Spectroscopy

Photoluminescence (PL) spectroscopy is a non-contact and non-destructive method of probing the luminescence emission characteristics of materials under the excitation by photons. When photons are absorbed

by a sample, photo-excitation causes the electrons to jump to higher energy states. The excited electrons then release the energy (photons), as they relax and return to lower energy states. The radiative transitions to lower energy states result in the emission of light and this process is known as photoluminescence. The photoluminescence (PL) spectrum provides information on the spectral distribution of the light emitted by a sample for a given excitation wavelength [22]. In the present work, the excitation and emission spectra of the samples were recorded using Fluoromax-4 spectrofluorometer, **c**onsisting of 150W Xenon arc lamp, monochromator and a detector.

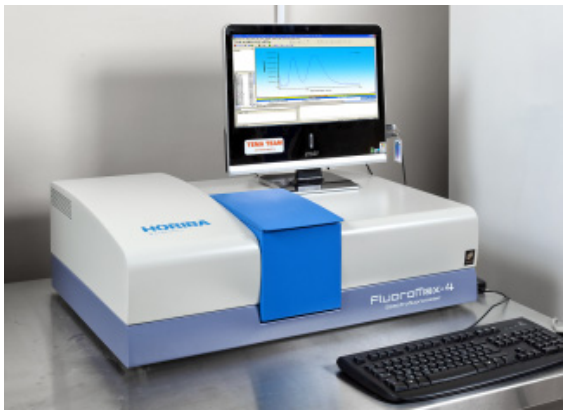

Fig. (9) Spectrofluorometer

2.11. Stylus Profiler for film thickness measurement

Thickness plays an important role in the film properties and it is the most important thin film parameter to be accurately determined. The thickness of the film samples investigated in the present work was measured using the Veeco Dektak 6M stylus profiler.

In the stylus profiler, the measurements are taken by moving the sample electromechanically beneath a diamond tipped stylus. The high precision stage moves the sample according to a user defined scan length, speed and stylus force. The stylus is mechanically coupled to the core of a linear variable differential transformer (LVDT) and the stylus moves over the sample surface. Surface variations cause the stylus to be translated vertically. Electrical signals corresponding to the stylus movements are produced as the core positions of the LVDT change. The LVDT scales an ac reference signal proportional to the position changes, which in turn is conditioned and converted to a digital format through a high precision, integrating, analog-to-digital converter [23]. The film whose thickness is to be measured is deposited on a substrate with a region masked. This creates a step on the sample surface. The thickness of the sample can be determined accurately by measuring the vertical motion of the stylus over the step. The photograph of Dektak 6M stylus profiler is given below.

Fig. (10) Dektak 6M stylus profiler.

References

[1] B.D. Cullity and S.R. Stock," Elements of X-Ray Diffraction", Third edition, New Jersey, Prentice Hall (2001)

[2] M.J. Buerger, "X-Ray Crystallography", John Wiley and sons, NewYork(1962).

[3] C. Kittel, "Introduction to Solid State Physics", Seventh edn, Wiley Eastern Limited, USA (1996)

[4] White, Robert, 'Chromatography/Fourier transform infrared spectroscopy and its applications", published by Marcel Dekker, New York, 1990; ISBN 0824781910.

[5] J. B. Pendry; " Low Energy Electron Diffraction", Academic press, New York, 1974

[6] E.S.Halberstadt , H.K. Henish ; J.Crystal Growth, 3 (1968) 363

[7] M.V.Hobden ; J.Appl.Phys., 38 (1967) 4365

[8] N.Kaneko, M. Kaneko, H. Takanashi ; Spectrochim. Acta Part A, 40 (1984) 33

[9] C.N.Banwell; E.M.McCash, (1994). "Fundamentals of Molecular Spectroscopy", (4th edn). McGraw-Hill. ISBN 0-07-707976-0.

[10] D.J.Gardiner, (1989). "Practical Raman spectroscopy" Springer-Verlag. ISBN 978-0387502540).

[11] M. V. Heimendahl, "Electron Microscopy of Materials", Academic Press, New York, 1980

[12] D. K. Schroder, "Materials and Device Characterization", Wiley Interscience, New York, 1998.

[13] E.R. Lippincott, R.Schroeder; J.Chem.Phys., 23 (1955) 1099

[14] P. E. J. Flewitt and R. K. Wild, "Physical methods for materials characterization", IOP Publishing Ltd, London (2003)

[15] G.I.Goldstein, D.E. Newbury, P. Echlin, D.C. Joy, C. Fiori, E.Lifshin, (1981). "Scanning electron microscopy and x-ray microanalysis", New York: Plenum Press. ISBN 030640768X.

[16] M.E. Brown, "Introduction to Thermal Analysis", Kluwer Academic Publisher, London, 2001.

[17] B.Wunderlich, (1990) "Thermal Analysis" New York: Academic Press. pp. 137–140 ISBN 0127656057.

[18] M. J. O'Neill (1964). "The Analysis of a Temperature-Controlled Scanning Calorimeter.". Anal. Chem. 36: 1238–1245.

[19] B. Wunderlich, "Thermal Analysis", Academic Press, NewYork, 1990, pp. 417-431

[20] D.R.Viji, "Luminescence of solids", Plenum Press, New York (1998)

[21] A.L. Fahrenbruch and R.H.Bube, "Fundamentals of solar cells", Academic Press, NewYork (1983)

[22] T .H. Gfroerer, "Photoluminescence in Analysis of Surfaces and Interfaces", JohnWiley & Sons Ltd, Chichester (2000)

[23] M. Ohring; Materials Science of Thin Films: Deposition and Structure. Academic Press, New York (2001)

Chapter 3

Highly luminescent and free-standing, PVDF/doped ZnS nanocomposite films for flexible device applications

Contents

The search for developing freestanding, flexible and thermally stable films endowed with the excellent luminescent characteristics of doped zinc sulphide (ZnS) is the motivation behind the research work presented in this chapter. The detailed studies on the photoluminescence emission in poly(vinylidene fluoride) /doped ZnS nanocomposite films grown by solution casting method form the focal theme of this chapter. Nanostructured zinc sulphide is doped with manganese and copper for different doping concentrations. When PVDF/ doped ZnS nanocomposite films are subjected to UV excitation, bright yellow orange luminescence is observed for the manganese doped film and blue luminescence, for the copper doped film. These nanocomposite films offer high prospects of wide range of applications in field emission displays, plasma displays and electroluminescent devices. By combining the yellow orange emission of manganese doped ZnS and the blue emission of copper doped ZnS in the required optimised ratio, it is possible to develop white light emitting, freestanding, stable and flexible nanocomposite films of PVDF/doped ZnS.

K.Sabira et al
Journal of Luminescence 188 (2017) 490–496
"Highly luminescent and free-standing, PVDF/doped ZnS nanocomposite films for flexible device applications"

3.1. Introduction

Poly(vinylidene fluoride) (PVDF) is a semi crystalline polymer with the repeat unit of CH_2-CF_2. It is a highly sought after material because of its promising piezoelectric, ferroelectric and pyro- electric behaviour and finds widespread applications in sensors, infra-red detectors, transducers, energy harvesters, actuators, super capacitors and MEMS [1-3]. The advantageous properties of PVDF can be attributed to its crystalline structures for which five different polymorphs have been observed and are referred to as α, β, γ, ε and δ phases or forms. The first two are the most common crystalline structures observed in PVDF [4,5]. It is chemically, thermally and mechanically very stable and is a highly flexible and processable material. Because of its excellent film forming properties, it is ideal as a polymer matrix for growing a variety of polymer nanocomposite films. Due to its excellent piezoelectric and ferroelectric properties, PVDF and its copolymers have been extensively investigated by many research groups and are considered to be promising materials for making low cost sensors for applications in a variety of fields [6].

Semiconductor quantum dots (QDs) have potential applications in biological labeling, light emitting diodes (LEDs), solar cells and various types of display devices. Zinc sulphide (ZnS), is one of the most important semiconducting optical materials of II–VI group with a wide band gap of 3.7eV, which has promising application prospects as

photochemical catalyst, gas sensor, lasers and infrared detector and material for solar cells, nonlinear optical devices, display devices and waveguides [7]. The doping of ZnS with transition metals such as Mn, Cu, Ni and Fe is interesting to researchers because of the intriguing effects of dopants on the photoluminescence properties of the semiconductor**.** Quantum dots of ZnS, doped with transition metal ions are the most popular materials for research in semiconductor quantum dots and these doped quantum dots generally have high yield of luminescence [8]. Due to their excellent luminescence properties, manganese doped and copper doped zinc sulphide quantum dots have potential applications in displays, sensors, lasers and biomedical labeling [9,10].

Nanocomposite materials are multiphase solids where one of the phases has dimensions in the nanoscale regime. The development of polymer/inorganic nanocomposite materials is a rapidly expanding multidisciplinary research area with profound industrial application prospects [11-13]. Recently, incorporation of inorganic nanoparticles into polymer matrices has attracted much attention, because the combination of inorganic nanoparticles and polymers provides a simple route to design, stable and processable composite materials by integrating the promising properties of both components. Composite materials consisting of zinc sulphide and polymers exhibit the merits of blending the advantageous properties of zinc sulphide with the processability and flexibility of polymers. Polymers like poly(methyl methacrylate) (PMMA), poly(styrene) (PS), poly(vinyl alcohol) (PVA), polyimide (PI) and poly(vinyl

pyrrolidone) (PVP) have been used as matrices for synthesizing polymer nanocomposites [14-18]. The optical characterization of these materials provide rich information of various optical and electronic phenomena, vital for various device fabrication technologies. It is reported that PVA and PVP can be used as suitable capping agents in the synthesis of nanostructured ZnS and doped ZnS in order to reduce the particle size and thereby modify the optical characteristics [19,20]. There are no reports related to using PVDF as the matrix for synthesizing nanocomposites of ZnS and doped ZnS, especially in the form of flexible and free standing films. On comparing the reported luminous intensity of the yellow orange peak of various ZnS:Mn nanocomposites and the blue peak of various ZnS:Cu nanocomposites, it is seen that, the peak intensity reported in the present work is much higher [11,14,15]. Composite materials involving soluble polymers with excellent mechanical properties and easy film forming properties can be of profound applications in realizing large area flat panel displays and efficient polymer light emitting diodes [21,22].

In the present work, chemical co-precipitation method was used to synthesize nanostructured, Mn/Cu doped ZnS. The nanocomposite of doped ZnS with PVDF was obtained by solution mixing and the corresponding nanocomposite films were grown in a petri-dish using solution casting. Detailed studies were carried out on the structural, thermal and luminescent properties of the free standing, nanocomposite films of PVDF/doped ZnS and the application prospects of these films in display devices and solid state lighting technology were assessed.

3.2. Experimental Details

3.2.1. Materials and methods

In the present work, zinc acetate [$Zn(CH_3COO)_2.2H_2O$] (purity>98%), manganese acetate, [$Mn(CH_3COO)_2.4H_2O$] (purity >99.5%), copper acetate [$Cu(CH_3COO)_2$] (purity >99.5%) and sodium sulphide [$Na_2S.9H_2O$] (purity >98%) were purchased from Merck Specialities Private Limited, Mumbai. Poly vinylidene fluoride, [$(CH_2\text{-}CF_2)_n$] granules (product code RM 4439) were obtained from Hi Media Laboratories, Private Limited, Mumbai and N,N-Dimethyl formamide (DMF) was purchased from Spectrochem Private Limited, Mumbai.

3.2.2. Sample preparation

3.2.2.1. Synthesis of manganese/copper doped ZnS

Manganese doped, nanostructured ZnS, (ZnS:Mn) was synthesized using the simple technique of chemical co-precipitation method. Freshly prepared, aqueous solutions of zinc acetate, manganese acetate and sodium sulphide were used for the synthesis. In a typical reaction, 50 ml of 1 M solution of zinc acetate was mixed with 50 ml of 0.01 M solution of manganese acetate in a conical flask. To this solution, 50 ml of 1 M sodium sulphide solution was added drop by drop, from a burette, with vigorous stirring for 2 hrs at 60 ^{0}C. The precipitate was washed several times with distilled water and methanol and dried in an oven at 50 ^{0}C and thoroughly ground in a mortar [22,23]. The experiment was repeated

with 0.02 M, 0.04 M and 0.06 M manganese acetate solution without varying the molarity of zinc acetate or sodium sulphide. Similar procedures were adopted for synthesizing copper doped, nanostructured ZnS, (ZnS:Cu), using copper acetate instead of manganese acetate.

3.2.2.2. Casting of PVDF/ ZnS:Mn and PVDF/ ZnS:Cu nanocomposite films

In the solution mixing technique, 1 gm of PVDF granules was dissolved in 10 ml of DMF, by heating at 60 ^{0}C, on a magnetic stirrer for two hours under stirring. To this solution, the well sonicated, homogeneous dispersion of 5% of 0.01 M ZnS:Mn in DMF was added and stirred vigorously for 6 hrs. This solution was poured into a petri-dish and kept in an oven at 100 ^{0}C for 2 hrs. It was found that the nanocomposite film formed could be easily peeled off from the petri-dish to get freestanding films of thickness around 20 micrometers [2]. These freestanding films were used for all further characterizations. Adopting similar routes, the corresponding PVDF/ZnS:Cu nanocomposite films were also grown in the petri-dish, which could be peeled off to get free standing films. The only difference was that, copper acetate was used instead of manganese acetate for synthesizing copper doped ZnS [24].

3.3. Results and Discussion

3.3.1. X-Ray Diffraction (XRD) analysis

The structure of the doped nanocomposite samples was determined by XRD technique, using a Rigaku model D max 2500 X-ray diffractometer. The analysis was carried out using Cu-Kα radiation (λ= 1.54 Å) at 30 kV and 20 mA with a scanning rate of 5° per minute from 10° to 70°. The XRD patterns of ZnS:Mn powder sample and PVDF/ZnS:Mn film are shown in figures 1(a) and 1(b) respectively. The observed diffraction peaks correspond well with the standard powder diffraction data of cubic ZnS. The XRD pattern shows three prominent peaks at 29.37°, 48° and 57.56° corresponding to (111), (220) and (311) lattice planes of the zinc blend structure of ZnS (JCPDS No. 050566) [25]. There is an obvious broadening of the XRD peaks which indicates the formation of nanosized ZnS:Mn. The XRD plot corresponds to the radiation reflected from the planes, where the periodic arrangement of the atoms is perfect and continuous. As the dopant Mn^{2+} ions do not significantly disturb the planes, due to the low concentration of the dopant, no change in XRD pattern was obtained upon manganese doping [26]. The average particle size of the nanostructured ZnS:Mn was found to be in the range of 2 to 4 nm from Scherrer equation. Since the crystallite size is comparable to exciton Bohr radius of ZnS (2.5 nm), the resulting quantum confinement effects facilitate the formation of ZnS quantum dots.

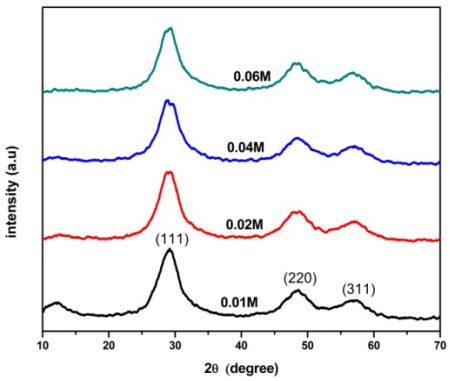

Fig. (1a) XRD patterns of ZnS:Mn powder

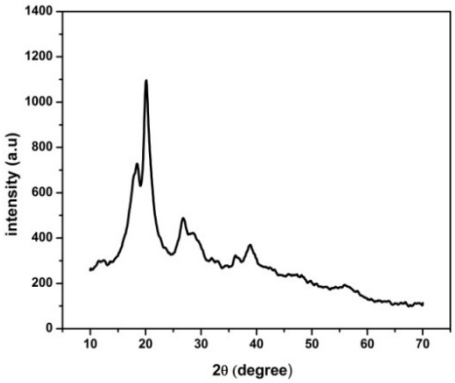

Fig. (1b) XRD pattern of PVDF/ ZnS:Mn film

Additional peaks are observed around 18.39°, 20.28°, 26.86° and 38.82° for the PVDF/ ZnS:Mn nanocomposite film. These peaks correspond to (020), (110), (120) and (200) planes respectively of α PVDF [2]. In the XRD pattern of the nanocomposite film, the presence of the peak at 29.3°, corresponding to the prominent diffraction peak of ZnS:Mn, confirms its presence in the nanocomposite.

3.3.2. UV-visible absorption spectroscopic studies

The optical absorption of the samples was recorded using JASCO V 570 spectrophotometer over the range 200 nm-700 nm and the absorption spectra of nano-structured ZnS:Mn and PVDF/ZnS :Mn films are given respectively in figures (2a) and (2b). The absorption peak for nano-structured ZnS:Mn appears around 314 nm which is fairly blue shifted from that of the bulk (340 nm)[7][10][27]. The band-gap energy is found to increase from 3.88 eV to 3.96 eV which is an indication of strong quantum confinement effects.

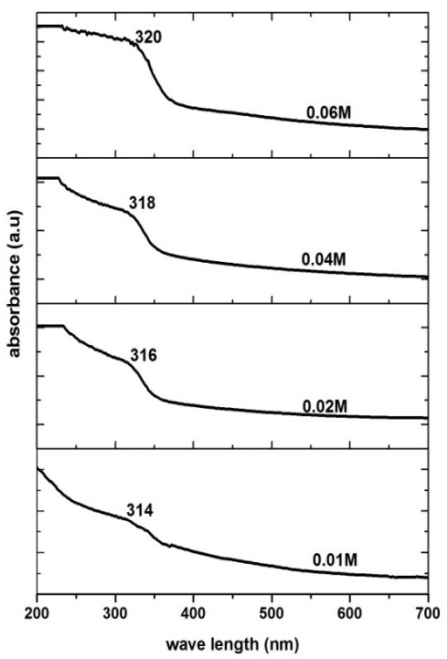

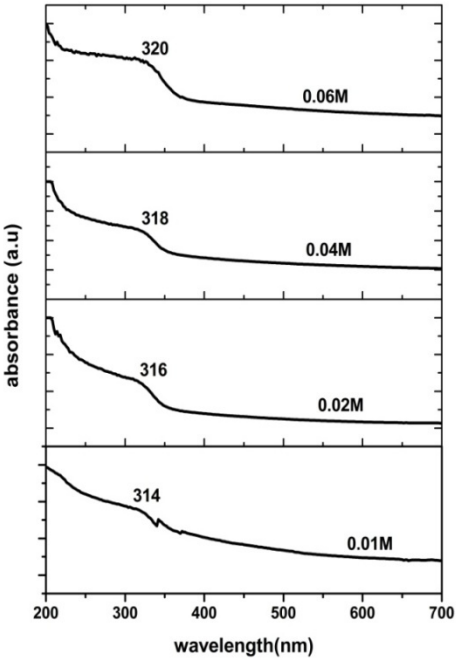

Fig. (2a) Absorption spectra of ZnS:Mn

Fig. (2b) Absorption spectra of PVDF/ZnS:Mn films

From the absorption spectrum of ZnS: Mn, it is seen that there is a red shift in the absorption peak, when the molarity of ZnS :Mn is increased from 0.01 M to 0.06 M [10],[22]. The same red shift in the absorption peak is observed in the case of PVDF/ZnS:Mn nanocomposite films also, which confirms the good dispersion of ZnS:Mn in the polymer matrix.

3.3.3. Fourier Transform Infrared (FTIR) spectroscopic studies

Fourier Transform infrared spectra of the samples synthesized in the present investigations were recorded using a FTIR spectrophotometer (Shimadzu) with a resolution of 4 cm^{-1} in the range of 400 cm^{-1} to

2500 cm^{-1} and the FTIR spectra for PVDF and PVDF/ZnS:Mn films are shown in figures (3a) & (3b). The peaks of α-phase PVDF appear at 556, 676, 880, 1077, 1526, 1691 and 2312 cm^{-1}, and the absorption band at 840 cm^{-1} is characteristic of β-phase [2]. The peak at 466 cm^{-1} corresponds to asymmetric bending and those at 601 cm^{-1} and 764 cm^{-1} to stretching vibrations in ZnS. Bands around 1100 and 1200 cm^{-1} are due to the characteristic vibrations of inorganic ions. Weak additional bands observed around 975 cm^{-1} indicate the presence of resonance interaction between vibrational modes of sulphide ions in ZnS [27,28]. Since there is no shift or change in intensity for the FTIR peaks of ZnS, after getting dispersed in the PVDF matrix, there is no possibility for any bond formation between PVDF and ZnS:Mn in the nanocomposite. This can be of application while investigating the photoluminescence properties of PVDF/ZnS:Mn films.

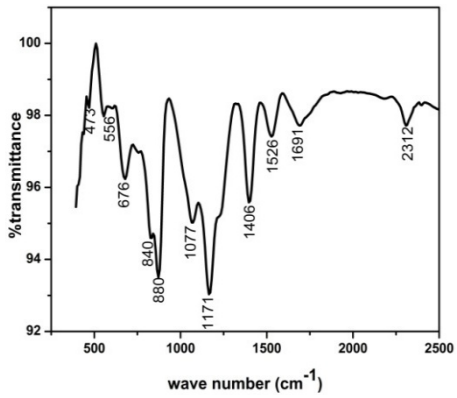

Fig. (3a) FTIR spectrum of PVDF film

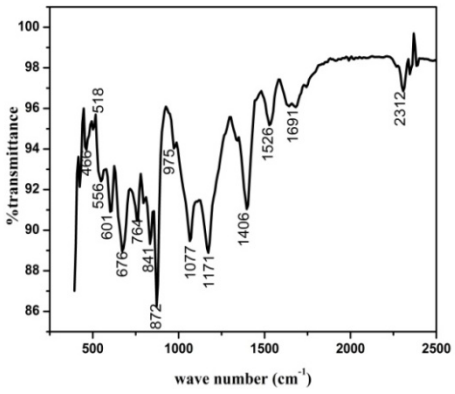

Fig. (3b) FTIR spectrum of PVDF/ZnS:Mn film

3.3.4. Thermal studies

3.3.4.1. Thermo Gravimetric Analysis

Thermo gravimetric analysis (TGA) is a useful technique to study the thermal characteristics of materials. In the present work, the thermal studies of the samples were carried out on a Perkin Elmer, Diamond TG/DTA instrument. Samples were heated to 700 °C at a scan rate of 10°C per minute in nitrogen atmosphere. The polymer matrix, PVDF, is thermally stable upto 420 °C in an inert atmosphere, and upto 400 °C in the presence of oxygen. The thermo gravimetric analysis (TGA) curves of PVDF film and PVDF/ZnS:Mn nanocomposite film examined under the inert atmosphere of nitrogen gas are shown in figure(4). The degradation onset temperature of PVDF/ZnS:Mn nanocomposite film, measured as the temperature required for percentage degradation, is slightly higher than that of PVDF film. The thermal stability of PVDF film and PVDF/ZnS:Mn film is almost the same, when 5% mass loss is compared. The decline of the TGA curve of PVDF/ZnS:Mn film (curve 2) before the decomposition temperature can be due to the release of trapped DMF, around 5%. By increasing the concentration of ZnS:Mn in the nanocomposite film, it may be possible to enhance the thermal stability still further. [21].

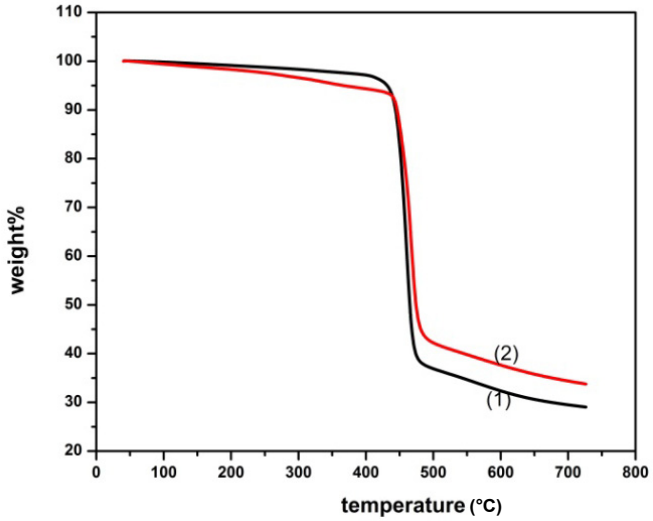

Fig. (4) TGA curves of PVDF and PVDF/ZnS:Mn films

3.3.4.2. Differential Scanning Calorimetry studies

Differential Scanning Calorimetry (DSC) measurements were carried out in Mettler Toledo DSC 822E instrument containing thermal analysis software for data interpretation, to investigate the changes in the thermal properties. The samples taken in sealed standard pans were ramped from -50 °C to 200 °C at a heating rate of 10 °C per minute in three cycles – initially heating from 30 °C to 200 °C and then cooling from 200°C to -50°C and finally heating from -50°C to 200°C. To avoid oxidative degradation, the sample and reference pans were purged with nitrogen at a constant flow rate. The DSC curves of PVDF film and PVDF/ZnS:Mn film are given in figures (5a) and (5b) respectively and the data is given in Table 1.

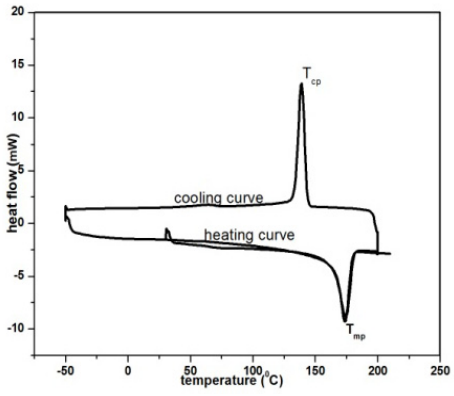

Fig. (5a) DSC curve of PVDF film

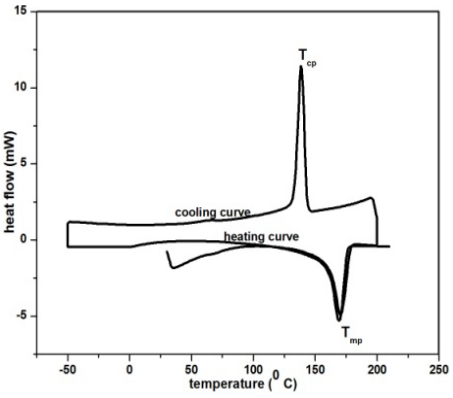

Fig. (5b) DSC curve of PVDF/ZnS:Mn film

From the DSC curves, the values of temperature corresponding to melting peak (T_{mp}) and crystallization peak (T_{cp}) are obtained. There is not much difference between the T_{mp} and T_{cp} values in the two samples. The value of glass transition temperature (T_g), cannot be determined from the plots, since the steps in DSC are not clear.

The percentage crystallinity was calculated from the equation,

$$\% \text{ crystallinity} = (H_m/H_m^0) \times 100$$

where, H_m is the heat of melting evaluated by integrating the area under the melting peak and H_m^0 is the heat of melting of the theoretically 100% crystalline sample, which is reported to be 104.6 Jg^{-1} for PVDF [29].

Table. (1) DSC data of PVDF film and PVDF/ZnS:Mn film

Sample	T_{mp} (°C)	T_{cp} (°C)	H_m (J/g)	% crystallinity
PVDF film	174	140	55.4	52.97
PVDF/ZnS:Mn film	169.8	139.7	49.1	46.97

From the data given in Table 1, one can see that the thermal data is almost similar for PVDF film and the PVDF/ZnS:Mn nanocomposite film.

3.3.5. Photoluminescence (PL) studies

The photoluminescence (PL) spectra of nanostructured ZnS:Mn and PVDF/ZnS:Mn films were recorded using spectro fluorometer –Fluoromax 4, at the excitation wavelength of 325 nm, for different concentrations of the dopant manganese. From the PL spectra depicted in figures (6a) and (6b), one can see that manganese doped ZnS has intense emission in the yellow orange region corresponding to 598 nm, as reported in earlier studies [23]. For the nanocomposite films, the emission is retained at the same wavelength with comparatively less intensity. The emission from the freestanding and flexible films of PVDF/ZnS:Mn is visible even for the naked eye and its photograph is shown in the inset of figure (6b). It is also observed that the intensity of the PL emission peak increases with the increase in manganese concentration which supports the inference that in manganese doped ZnS, the emission in the yellow orange region is determined mainly by the transition between the electronic states of manganese. The polymer PVDF serves as a stable and flexible matrix for the homogeneous assembling of ZnS:Mn molecules, retaining its exquisite luminescence characteristics.

The PL peak observed at 598 nm for Mn doped ZnS can be interpreted as due to an indirect excitation, initially into the states of the host matrix ZnS, followed by an energy transfer from the host to the

Mn^{2+} ions and the subsequent de-excitation, leading to luminescence [23]. According to Bhargava, [30] when Mn^{2+} ions substitute Zn^{2+}cation sites in ZnS lattice, the mixing of s-p electrons of host ZnS with 3d electrons of Mn^{2+} causes strong hybridization and makes the forbidden transition of $^4T_1$ -- $^6A_1$ partially allowed, giving rise to yellow orange emission at 598 nm. In doped semiconductor nanostructures one can expect efficient energy transfer of the electron hole pairs to the dopant impurity and it should depend on the particle size of the doped semiconductor. In nanostructured, manganese doped ZnS ,below the exciton Bohr diameter (typically ~ 5-10nm), the electron orbitals of the host ZnS, hybridize (mix) with Mn electron orbitals due to quantum confinement. The electronic confinement experienced by the s-p host states and the corresponding increase of the overlap of their spatial wavefunctions with the localized 'd' electron states of manganese, promote the process of hybridization. An immediate benefit of the mixing is, an enhanced energy transfer rate to the 'd' electron levels. This will lead to fast trapping, resulting in an instant capture of the electrons by the activator, manganese. The captured electron must recombine at the impurity to yield appropriate emission spectra. The sp-d mixing (hybridization) can change the forbidden transitions to allowed transitions [31-33].

It is interesting to observe that in the PL emission spectra of both the ZnS:Mn powder samples and the PVDF/ZnS:Mn film samples, the emission is entirely confined to yellow orange region and the emission

due to defect states observed generally in the blue region is almost quenched. In the ZnS:Mn powder sample, the much enhanced emission intensity in the yellow orange region brings about the almost vanishing of the defect related emission peaks in the blue region. The same effect is observed in the PVDF/ZnS:Mn films also. But the decrease in the intensity of the yellow orange emission peak in the nanocomposite films compared to that of the yellow orange emission in the nanostructured ZnS:Mn powder sample can be due to the surface passivation effects of the polymer matrix PVDF. One of the highlights of the present work is the identification of the free-standing films of PVDF/ZnS:Mn as thermally, mechanically and environmentally stable, highly luminescent, flexible films with excellent application prospects in high contrast and flexible types of display devices.

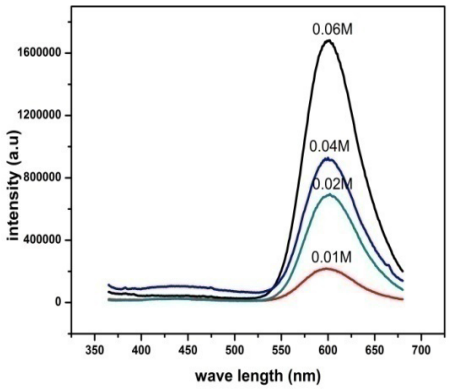

Fig. (6a) PL spectra of ZnS:Mn

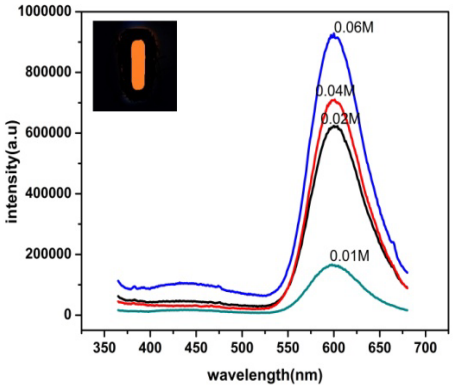

Fig. (6b) PL spectra of PVDF/ZnS:Mn films

For the nanocomposite films of copper doped ZnS with PVDF, the XRD and FTIR plots are similar to those of the nanocomposite films of Mn doped ZnS with PVDF. The particle size of ZnS:Cu could be estimated from the XRD peaks and it comes to about 3 nm. The thermal stability of the PVDF/ZnS:Cu nanocomposite films is found to be comparable to that of PVDF/ZnS:Mn films, from the TGA studies. The PL studies comprise the most significant part of the work carried out on PVDF/ZnS:Cu films. From the earlier studies, ZnS:Cu is found to show intense PL emission around 430 nm [9].The PVDF/ZnS:Cu nanocomposite films of the present work are found to be freestanding, thermally and mechanically stable and flexible, similar to PVDF/ZnS:Mn films.

The PL emission spectra of PVDF/ZnS:Cu films for the different concentrations of the dopant Cu in ZnS:Cu are shown in figure (7).It is observed that the emission peak is confined to the blue region. The photograph of the intense blue emission from the freestanding, flexible films of PVDF/ZnS:Cu is shown in the inset of figure (7). Both the dopants, Mn and Cu are transition metals and hence the PL emission from the copper doped ZnS can be theoretically explained on similar footing to that of manganese doped ZnS [23]. It is observed that the PL intensity increases when the concentration of Cu in the ZnS:Cu increases from 0.01 M to 0.03 M and gradually decreases when the concentration is increased to 0.05 M and above. This is due to the formation of copper sulfide resulting in a decrease in the amount of Cu^{2+} ions which may otherwise serve as optically active luminescence centers in ZnS

[9][24][34-36]. Such a behaviour is however not observed in the PL spectra of PVDF/ZnS:Mn films, where emission intensity increases with the increase in the concentration of manganese.

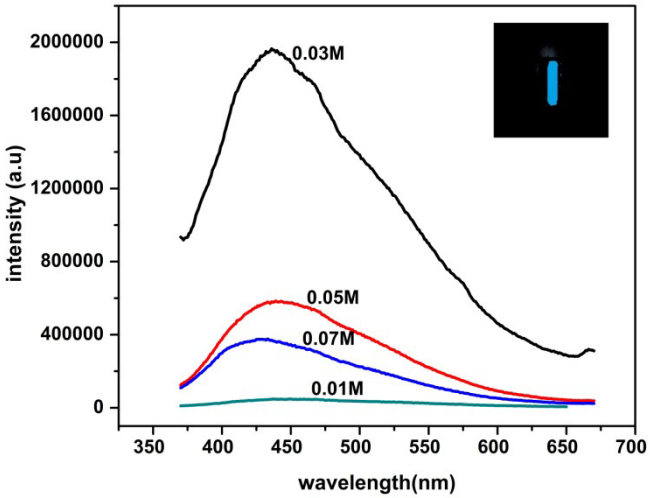

Fig. (7) PL spectra of PVDF/ZnS:Cu films

The chromaticity diagrams of PVDF/ZnS:Mn and PVDF/ZnS:Cu films are shown in figures (8a) and (8b) respectively. These diagrams agree quite well with the orange red emissin for the former and blue emission for the latter.

Another highlight of the present work is the possibility of realizing white light emitting, stable and flexible films of PVDF/doped ZnS nanocomposite, where the dopants refer to manganese and copper, since the blue emission from ZnS:Cu and the yellow orange emission from ZnS:Mn can be suitably combined to produce white emission.

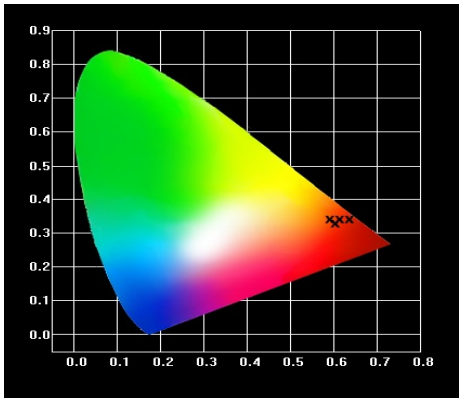

Fig. (8a) Chromaticity diagram of PVDF/ZnS:Mn film

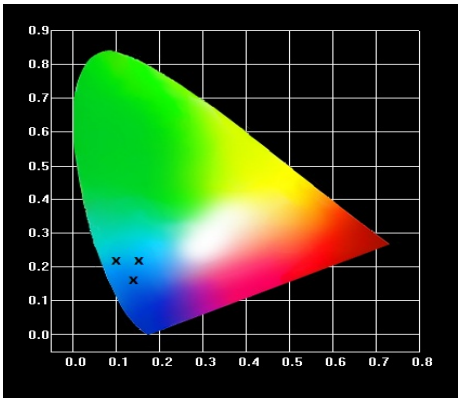

Fig. (8b) Chromaticity diagram of PVDF/ZnS:Cu film

By suitably optimizing the concentrations of manganese and copper, while synthesizing the doped samples of ZnS, there exist high prospects for achieving white emission from the flexible, nanocomposite films of PVDF in which the Mn doped and Cu doped ZnS are embedded in the required proportions. If suitably developed,these white light emitting, freestanding, flexible and stable nanocomposite films can emerge as efficient, cost effective and eco-friendly components of the contemporary solid state lighting technology.

3.3.6. Photoluminescence Quantum Yield (PLQY) measurement

Photoluminescence quantum yield of the nanocomposite films was measured using HORIBA JOBIN YVON NANOLOG spectrofluorimeter in combination with QUANTA-PHI integrating sphere, coated with $BaSO_4$. The photo luminescence quantum yield is the ratio of the number of

photons emitted through luminescence to the number of photons absorbed. It is a measure of the probability of the deactivation of the excited states by radiative mechanisms like fluorescence, rather than by other non- radiative processes [37]. The measured PLQY values are given in Table 2. In the given data, PZMn and PZCu refer to PVDF/ZnS:Mn and PVDF/ZnS:Cu respectively and the numbers refer to the molarity of the dopant used.

Table (2). PLQY data of PVDF/doped ZnS films

SAMPLE	PZMn 0.01	PZMn 0.02	PZMn 0.04	PZMn 0.06	PZCu 0.03	PZCu 0.05
PLQY (%)	1.89	4.78	7.78	8.15	1.6	0.95

From the table it is observed that PLQY of manganese doped film samples increases with increase in manganese doping concentration. For the copper doped samples, it was possible to measure the PLQY only for two doping concentrations. The PLQY of 0.01 M and 0.07 M copper doped samples is almost zero. This observation agrees with the PL spectral result that the intensity of blue emission in the copper doped film samples decreases with increase in the dopant concentration above 0.03 molarity. The PLQY data is quite consistent with the photoluminescence spectral data of both the PVDF/ZnS:Mn and PVDF/ZnS:Cu nanocomposite film samples.

3.4. Conclusions

In the present work, attempts have been made to develop, luminescent, freestanding, flexible and stable nano-composite films of

manganese and copper doped ZnS in PVDF matrix. These films are found to show intense emission in the yellow orange and blue regions respectively, when excited at 325nm. The PLQY measurements carried out on both the PVDF/ZnS:Mn and PVDF/ZnS:Cu nanocomposite films are quite consistent with the photo luminescence spectral data. The present results offer ample scope for developing white light emitting, freestanding nanocomposite films based on PVDF and suitably doped ZnS. The present work is novel, since the luminescent characteristics of the nanocomposite films of doped ZnS in PVDF matrix have not been reported earlier. The highly luminescent, freestanding, flexible, stable and eco-friendly signatures constitute the most advantageous aspects of these nanocomposite films of thickness around 20 micrometers. The highlight of the present investigations is the development of these luminescent, stable and freestanding nanocomposite films for the first time, with high application potentials in the present day display device technology and the day by day progressing solid state lighting technology.

References

[1] A.K. Chilvery, A.K. Batra, M. Thomas, Investigation on characteristics of PVDF / ZnO Nanocomposite Films for High-k Capacitors, *Phys. Sci. Int. J.*4(5): (2014) 734–741. doi 10.9734/ PSIJ/2014/9026

[2] P.I. Devi, K. Ramachandran, Dielectric studies on hybridised PVDF – ZnO nanocomposites, *J. Exp.Nanosci.* ,vol.6,no.3, June 2011. 8080 (2015). doi:10.1080/17458080.2010.497947.

[3] B. Jaleh, A. Jabbari, Evaluation of reduced graphene oxide/ZnO effect on properties of PVDF nanocomposite films, *Appl. Surf. Sci.* 320 (2014) 339–347. doi:10.1016/ j.apsusc.2014.09.030.

[4] H. Yu, T. Huang, M. Lu, M. Mao, Q. Zhang, H. Wang, Enhanced power output of an electrospun PVDF/MWCNTs-based nanogenerator by tuning its conductivity, *Nanotechnology* 24 (2013) 405401. doi:10.1088/0957-4484/24/40/405401.

[5] A.P. Indolia, M.S. Gaur, Optical properties of solution grown PVDF-ZnO nanocomposite thin films, *J. Polym. Res.* 20 (2013) 43. doi:10.1007/s10965-012-004y.

[6] J. Fang, X. Wang, T. Lin, Electrical power generator from randomly oriented electrospun poly(vinylidene fluoride) nanofibre membranes, *J. Mater. Chem* 21 (2011) 11088. doi:10.1039/ c1jm11445j.

[7] A.K.K.P. Kumbhakar, Effect of manganese doping on the photoluminescence characteristics of chemically synthesized zinc sulfide nanoparticles, *Appl. Nanosci.* (2012) 15–23. doi:10.1007/ s13204-011-0036-x.

[8] N. Karar, F.Singh, B.R.Mehta, Structure and photoluminescence studies on ZnS:Mn nanoparticles, *J. Appl. Phys*. 95 (2004) 656. doi:10.1063/1.1633347.

[9] R.K. Srivastava, N. Pandey, S.K. Mishra, Effect of Cu concentration on the photoconductivity properties of ZnS nanoparticles synthesized by co-precipitation method, *Mater. Sci. Semicond. Process.* 16 (2013) 1659–1664. doi:10.1016/ j.mssp.2013.06.009.

[10] I.M. Ali, R.M. Al-haddad, K.T. Al-rasoul, Structural and Optical Properties of Synthesized Manganese doped ZnS Quantum Dots, 1 (2014) 104–114. *Int. J.Innov. Sci.Eng. Technol.*, Vol. 1 Issue 10, 2014 ISSN 2348 – 7968

[11] K. Matras , M. Bredol , A. Szatkowski , O. Sakhno , J. Stumpe & D. Bogdal, Composites from Luminescent Nanosized ZnS and Optical Polymer, *Mol. Cryst. Liq. Cryst.*, Vol. 485, pp.776-779, 2008 doi.org/10.1080/15421400801918062

[12] M. Sajimol Augustine, P.P.Jeeju, V.G.Sreevalsa, S.Jayalekshmi, Excellent UV absorption in spin-coated thin films of oleic acid modified zinc oxide nanorods embedded in Polyvinyl alcohol, *J. Phys. Chem. Solids*, vol. 73 (2012) 396–401 doi:10.1016/ j.jpcs. 2011.11.004

[13] P.P. Jeeju, S. Jayalekshmi; On the Interesting Optical Properties of Highly Transparent , Thermally Stable , Spin-Coated Polystyrene / Zinc Oxide Nanocomposite Films; *Jou.Appl.Pol.Sci,* 120, 1361-1366 (2010). doi:10.1002/app.

[14] H. Althues, R. Palkovits, A. Rumplecker, P. Simon, W. Sigle,| M. Bredol, U. Kynast and S. Kaskel, Synthesis and Characterization of Transparent Luminescent ZnS:Mn/ PMMA Nanocomposites**,** *Chem. Mater,* 2006,vol**.** 18*,* 1068- 1072 doi/abs/10.1021/cm0477422

[15] Sreeja K. V, Irom Nonibala Devi, Ramesh R, Savitha V, Jayasudha S and Priya L, Photoluminescent Polystyrene/ ZnS: Mn nanocomposites, *Adv. Appl. Sci. Res.*, 2014, 5(5):194-202.

[16] U. Baishya and D. Sarkar, Structural and optical properties of zinc sulphide–polyvinyl alcohol (ZnS–PVA) nanocomposite thin films: effect of Zn sourceconcentration, *Bull. Mater. Sci.* , Vol. 34, No. 7, December 2011 , pp. 1285–1288.

[17] Xiaodan Lu , Na Lu , Junfang Gao, Xin Jin and Changli Lu, Synthesis and properties of ZnS/polyimide nanocomposite films, *Polym Int* ,vol.**56** , 601–605 (2007)

[18] Quanyuan Zhang, Eunice Shing Mei Goh, Roger Beuerman, Zaher Judeh, Mary B. Chan-Park, Tupei Chen, Rong Xu" , Development of Optically Transparent ZnS/Poly (vinylpyrrolidone) Nanocomposite Films with High Refractive Indices and High Abbe Numbers, *J. Appl. Polym. Sci. 2*013, doi: 10.1002/App.38883

[19] Murugadoss, B. Rajamannan, V. Ramasamy, Synthesis And Photoluminescence Study of PVA Capped ZnS:Mn^{2+} Nanoparticles**,** *Dig. J. Nanomater. Biostruct.,* Vol. 5, No 2, April 2010, p. 339 – 345

[20] Thi Tran Minh, Ben Pham Van , Thai Dang Van , Hien Nguyen Thi, The optical properties and energy transition process in nanocomposite of Poly vinyl-pyrrolidone polymer and Mn-doped ZnS, *Opt. Quant. Electron* (2013), vol. 45:147–159 .

[21] P.P. Jeeju, S. Jayalekshmi, K. Chandrasekharan, P. Sudheesh, Enhanced linear and nonlinear optical properties of thermally stable ZnO/poly(styrene)-poly(methyl methacrylate) nanocomposite films, *Thin Solid Films* 531 (2013) 378–384. doi:10.1016/j.tsf.2012.12.043.

[22] M. Sajimol Augustine, P.P. Manzur Ali, K. Sapna, K.K. Elyas, S. Jayalekshmi, Size-dependent optical properties of bio-compatible ZnS:Mn nanocrystals and their application in the immobilisation of trypsin, *Spectrochim. Acta ,Part A, Mol. Biomol. Spectrosc* 108 (2013) 223–228. doi:10.1016/ j.saa.2013.01.066.

[23] R. Kripal, A.K. Gupta, S.K. Mishra, R.K. Srivastava, A.C. Pandey, S.G. Prakash; Photoluminescence and photoconductivity of ZnS : Mn^{2+} nanoparticles synthesized via co-precipitation method; *Spectrochim. Acta Part A Mol. Biomol. Spectrosc* 76 (2010) 523–530. doi:10.1016/ j.saa.2010.04.018.

[24] W.Q. Peng, G.W. Cong, S.C. Qu, Z.G. Wang, Synthesis and photoluminescence of ZnS:Cu nanoparticles, *Opt. Mater*. (Amst). 29 (2006) 313–317. doi:10.1016/ j.optmat.2005.10.003.

[25] Z. Dehghani, S. Nazerdeylami, E. Saievar-Iranizad, M.H. Majles Ara, Synthesis and investigation of nonlinear optical properties of semiconductor ZnS nanoparticles, *J. Phys. Chem. Solids.* 72 (2011) 1008–1010. doi:10.1016/ j.jpcs.2011.05.005.

[26] V.D. Mote, Y. Purushotham, B.N. Dole, Structural, morphological and optical properties of Mn doped ZnS nanocrystals., *Ceram.* (Sao Paulo, Brazil). 59 (2013) 395–400. doi:10.1590/S0366-69132013000300008.

[27] R.Viswanath, H. S.B. Naik, Y.K.G.Somalanaik, P.K.P.Neelanjeneallu, K.N.Harish and M.C. Prabhakara, Studies on Characterization, Optical Absorption and Photoluminescence of Yttrium Doped ZnS Nanoparticles, *J. Nanotechnol.* Volume 2014, Article ID 924797, http://dx.doi. org/10.1155/2014/924797.

[28] R. Sharma, Structural and optical characterization of ZnS nanoparticles, *Int. Multidiscip. Res. J.* 2011,. 1 (2011) 8–11.

[29] Ajay Pal Indolia , M. S. Gaur, Investigation of structural and thermal characteristics of PVDF/ZnO nanocomposites, *J. Therm. Anal Calorim* (2013) 113:821–830; doi 10.1007/s10973-012-2834-0

[30] R.N. Bhargava, Doped nanocrystalline materials-Physics and applications, *J. Lumin.* 70 (1996) 85-94

[31] R. N. Bhargava, The role of impurity in doped nanocrystals, *J. Lumin.* 72-74 (1997) SOO22-2313(96)00162-7

[32] R. N. Bhargavaa, D. Gallagher, and T. Welkerb, Doped nanocrystals of semiconductors-A new class of Luminescent materials, *J. Lumin.,* vol. 61, pp. 275–280, 1994. SSDI 0022-2313(94)

[33] R.N.Bhargava, D.Gallagher, Optical Properties of Manganese-Doped nanocrystals of ZnS, *Phys. Rev. Lett.,* vol. 72, no. 3, pp. 1–4, 1994. 0031-9007/94/72(3)/416(4)

[34] Sakshi Sahare , Meera Ramrakhiani, Photoluminescence of ZnS:Cu nanoparticles in PVA matrix, *Int. J. Lumin. Appl.*, Vol. 4(II), 04/04/2014, ISSN 2277 – 6362.

[35] K. Jayanthi, S. Chawla, H. Chander and D. Haranath, Structural, optical and photoluminescence properties of ZnS: Cu nanoparticle thin films as a function ofdopant concentration and quantum confinement effect, *Cryst. Res. Technol.* 42, No. 10, 976 – 982 (2007) / doi 10.1002/ crat.200710950.

[36] Paulina Ziolczyk, Ewa Miller, Malgorzata Przybyt, ZnS Cu-doped quantum dots**,** *Biotechnol. Food Sci* ,2014, 78 (1), 53-69.

[37] Lars Olof Palsson, Andy Monkman, Measurements of solid state PLQY of films using a Fluorimeter, *Adv.Mater,* 2002, 14, No.10, May 17.

Chapter 4

White light emission and excellent UV shielding observed in freestanding and flexible films of PVDF/Zinc Oxide (ZnO) nanocomposite

Contents

The excellent UV shielding properties and white light emission observed in freestanding and flexible films of poly (vinylidene fluoride) /zinc oxide (PVDF/ZnO) nanocomposite, obtained by simple solution casting method, form the central theme of this chapter. From the UV-visible absorption spectral studies of these nanocomposite films, with varying ZnO concentrations, it is seen that, a UV absorption window appears in the range 240 nm – 370 nm, and the intensity of UV absorption increases sharply with the increase of ZnO content in the composite. For all the nanocomposite film samples, the transmittance in the UV region eventually becomes zero. These freestanding nanocomposite films hence offer ample scope for excellent UV shielding applications. These films show intense white light emission when excited at 320 nm and can be of profound application in solid state lighting. Simultaneous observation of UV shielding effects and white light emission in freestanding films of PVDF/ZnO nanocomposite are the highlights of the present work.

K.Sabira et al
Materials Letters 200 (2017) 125–127
"White light emission and excellent UV shielding observed in freestanding and flexible films of poly(vinylidene fluoride) /zinc oxide nanocomposite"

4.1. Introduction

The design and synthesis of novel polymer nanocomposites are of significant technological relevance and the past decades have witnessed remarkable progress in the practical realization of devices based on these composites [1,2]. A variety of polymer/inorganic filler nanocomposites that offer attractive mechanical, thermal, optical and electrical properties has been investigated extensively. As a filler material to realize polymer nanocomposites, the much renowned semiconducting material, zinc oxide, has a host of possibilities to offer [3,4]. As explained in the previous chapters, poly(vinylidene fluoride) (PVDF) is a semi-crystalline fluoropolymer, obtained by the polymerization of vinylidene fluoride and is one of the best-known examples of an active polymer noted for its excellent film forming properties, which makes it ideal as a polymer matrix for obtaining a variety of polymer nanocomposite films [5-8].

Zinc oxide is a technologically important semiconducting material, noted for its intense luminescence emission in the visible region and ultraviolet (UV) laser action at room temperature [9,10]. It is comparatively cost effective, non toxic, with high optical transparency in the visible spectral region and is one of the best bio-friendly inorganic absorber of UV radiation. It is extensively used in photonic applications, owing to its intense light emission all through the visible spectrum. Because of its hardness, rigidity and piezoelectric properties, it is an important material in the ceramics industry, while its non toxic nature,

biocompatibility and biodegradability make it a material of interest for biomedical research [11-14].

The incorporation of inorganic metal oxides like ZnO ,TiO_2, SiO_2, CeO_2 and SnO_2 can endow the resulting nanocomposites with excellent electrical, optical and mechanical properties. Inorganic polymer nanocomposites, which exhibit an ensemble of properties of both inorganic nanofillers and polymers, are excellent candidates for UV-shielding and light emitting applications. Such composites benefit from the physical flexibility and the ease of processing, which are the typical characteristics of polymers and the excellent optical properties of inorganic metal oxides [15,16]. Over-exposure to UV radiation can cause sunburn and some forms of skin cancer and may lead to direct DNA damage. Because of the changes in atmospheric composition and the thinning of the ozone layer during the past decades, it is important to ensure adequate protection against the adverse effects of UV exposure. Zinc oxide is one of the best nano-fillers for UV shielding applications, since it is a strong UV absorber and is also a nontoxic and biocompatible material [17].

The UV shielding properties of polymer nanocomposite films have already been subjected to detailed studies by different groups. However, there are no reports on the simultaneous observation of UV shielding effects and white light emission in freestanding and flexible films of polymer nanocomposites obtained by simple processing

methods, compared to the expensive techniques like electro-spinning and spin coating, reported earlier [18,19]. M.Sajimol Augustine and co-workers have investigated the excellent UV absorption in spin-coated films of oleic acid modified zinc oxide nanorods, embedded in poly vinyl alcohol (PVA) [16]. Yao Tu and colleagues have developed transparent and flexible films of polystyrene/zinc oxide nanocomposite and studied the UV-shielding applications. P.P.Jeeju and co-workers have reported excellent UV absorption and shielding properties in spin-coated polystyrene/zinc oxide nanocomposite films, which are found to be highly transparent throughout the visible region and the optical absorption in the UV region is quite high [19]. Yewei Zhang's group has fabricated the visible light traversing and ultraviolet (UV) shielding, PMMA/ZnO nanocomposite films by incorporating suitable UV absorbing ZnO quantum dots into a transparent PMMA matrix [20]. These transparent nanocomposite films can almost completely absorb the UV radiation of wavelengths less than 340 nm and thus can be directly applied as UV-shielding organic glasses. X. M. Sui, C. L. Shao and Y. C. Liu reported the white light emission from PVA/ZnO hybrid nanofibers obtained by electro-spinning technique [18]. The excellent UV shielding properties and white light emission observed in flexible, free standing and thermally stable films of PVDF/ZnO nanocomposite of the present work, obtained by simple solution casting method, are being reported for the first time.

4.2. Experimental Details

4.2.1. Materials and methods

All the chemicals used in the present work were of analytical grade. Zinc acetate [$Zn(CH_3COO)_2.2H_2O$] (purity>98%), potassium hydroxide (purity >99.5%) and methanol (purity >98%) were purchased from Merck Specialities Private Limited, Mumbai. Poly(vinylidene fluoride) granules (product code RM 4439) were obtained from Hi Media Laboratories Private Limited, Mumbai and N,N-Dimethyl formamide (DMF) was purchased from Spectrochem Private Limited, Mumbai.

4.2.2. Synthesis of nanostructured ZnO

Wet chemical method was used to synthesize nanostructured ZnO. In a typical reaction, 0.1 M zinc acetate solution in methanol was taken in a conical flask and was kept at 60 ^oC, to which, 0.1 M potassium hydroxide solution in methanol was added drop by drop from a burette. The mixed solution was stirred well for 3 hours. After stirring, the solution was cooled to room temperature, filtered and the filtrate was washed well with de-ionised water and methanol. It was then dried in an oven at 60 ^oC for five hours [9]. The white powder obtained was identified to be nanosized ZnO and was used to grow the PVDF/ZnO nanocomposite films.

4.2.3. Growth of PVDF/ZnO nanocomposite films

Initially, 1 gm of PVDF was dissolved in10 ml of DMF, by heating at 60 ^{o}C for 2 hours on a magnetic stirrer. Sonicated solution of ZnO in DMF, was added to this solution, followed by stirring for 5 hours. The final solution was poured into a petri-dish and was kept in an oven at 60 ^{o}C. Upon evaporation of the solvent, free standing films could be peeled off from the petri-dish which were used for all further studies[1]. Films with four different weight percentages of ZnO (5 %, 10%, 20 % and 30 %) were obtained. For reference, pure PVDF films were also grown as free standing films. Thickness of the films was measured using stylus profiler.

4.2.4. Characterization techniques

The X- ray diffraction (XRD) patterns were obtained using a Rigaku X-ray diffractometer with Cu-Kα (1.5418 A^{0}) radiation operating at 30 kV and 20 mA. Fourier transform infrared (FTIR) spectra of the samples were recorded using a Shimadzu spectrophotometer in the wave number range 400–2500 cm^{-1} with a resolution of 4 cm^{-1}.The particle size and the structural details of ZnO and the PVDF/ZnO nanocomposite films were obtained from TEM and FESEM studies. Thermo gravimetric analysis (TGA) of the nanocomposite films was carried out on a Perkin Elmer, Diamond TG/DTA instrument. UV-visible absorption spectra were obtained using a Jasco V 570 spectrophotometer in the wavelength range 190–700 nm. The photoluminescence (PL) emission spectra of the

samples were recorded with Fluoromax-4 spectrofluorometer using Xenon lamp as the excitation source, under an excitation at 320 nm.

4.3. Results and Discussion

4.3.1. X-Ray Diffraction (XRD) analysis

The X-ray diffraction pattern of nano-structured ZnO and those of PVDF/ZnO nanocomposite films (5 %,10 %, 20 % and 30 % ZnO) are shown in figure(1a) & figure(1b) respectively.

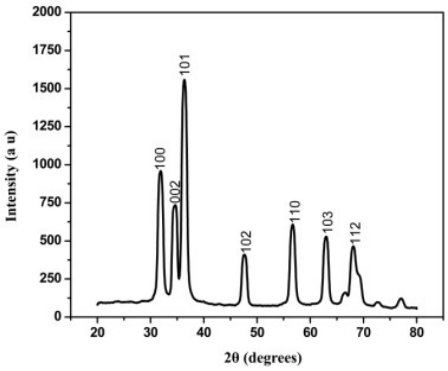

Fig. (1a) XRD pattern of nano structured ZnO

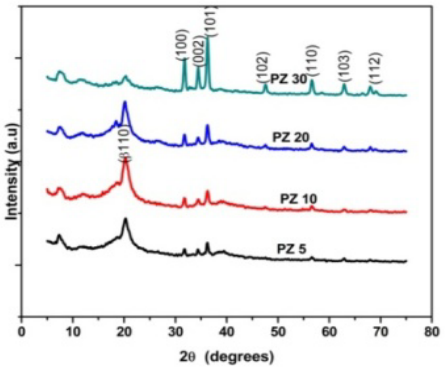

Fig. (1b) XRD patterns of PVDF/ ZnO films

The diffraction peaks located at 31.9°, 34.5°, 36.3°, 47.8°, 56.7°, 62.9° and 68.2° correspond to the planes of ZnO and can be indexed to match the standard diffraction pattern of wurtzite ZnO (JCPDS card no. 36-1451). The diffraction peaks corresponding to (100), (002), (101), (102), (110), (103) and (112) planes indicate the hexagonal structure of zinc oxide [19,20]. Using the Scherrer formula, the particle size of the nanostructured ZnO was estimated as 17 nm. The peaks of ZnO are seen

in addition to those of PVDF at 18° and 20° in the XRD patterns of the nanocomposite films shown in figure (1b), which confirms the dispersion of ZnO in the PVDF matrix [21].

4.3.2. Fourier Transform Infra red (FTIR) spectroscopic studies

The FTIR spectra of PVDF film and PVDF/ZnO nanocomposite films are shown in figure (2a) and figure (2b) respectively.

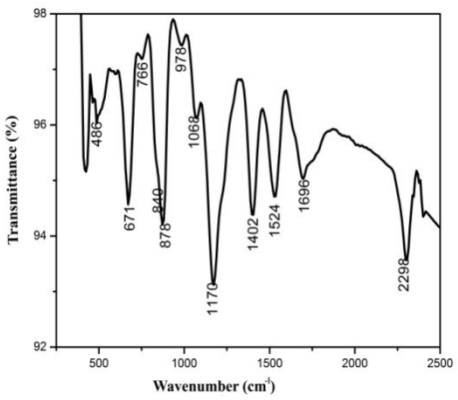

Fig. (2a) FTIR spectrum of PVDF film

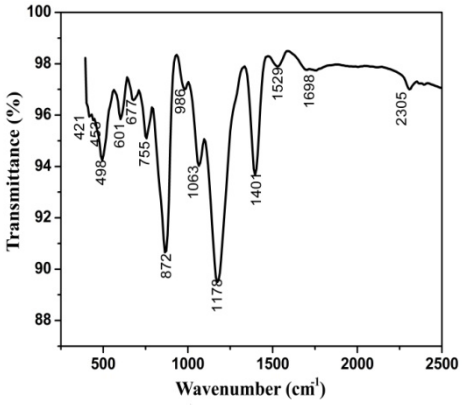

Fig. (2b) FTIR spectrum of PVDF/ ZnO film

In figure (2b), the bands observed at 421, 453 and 601 cm^{-1} are assigned to Zn-O vibrations. In figures (2a) and (2b), the bands at 671 cm^{-1}, 766 $cm^{-1}$and 986 cm^{-1} correspond to the α form of PVDF. The absorption peak at 878 cm^{-1}corresponds to the vibration of the C-C bond and the one at 1178 cm^{-1} is assigned to CF_2 stretching vibrations of PVDF, which are common to all the polymorphs of PVDF. The peak at 1401 cm^{-1} is attributed to the CH_2 deformation in PVDF [6,14,16,21]. The presence of the characteristic bands of both PVDF and ZnO in the

spectrum of PVDF/ZnO nanocomposite, gives additional proof for the dispersion of ZnO in the PVDF matrix.

4.3.3. Morphological studies

The structural and morphological aspects of the nanostructured ZnO and the PVDF/ZnO nanocomposite films were investigated using TEM and FESEM studies. The FESEM images were obtained using ZEISS Sigma field emission scanning electron microscope with an accelerating voltage of 20 kV and the TEM image of the nanostructured ZnO, using transmission electron microscope (TEM), model JEM 2100 of JEOL Ltd, Japan.

The FESEM images of PVDF film and PVDF/ZnO nanocomposite film are shown in figures (3a),(3b) and (3c) and the TEM image of ZnO, in figure (3d). The particle size of ZnO estimated from the TEM image is 20 nm, which is found to be close to that obtained from XRD studies using Scherrer formula. The hexagonal structure of ZnO is confirmed from the TEM image.

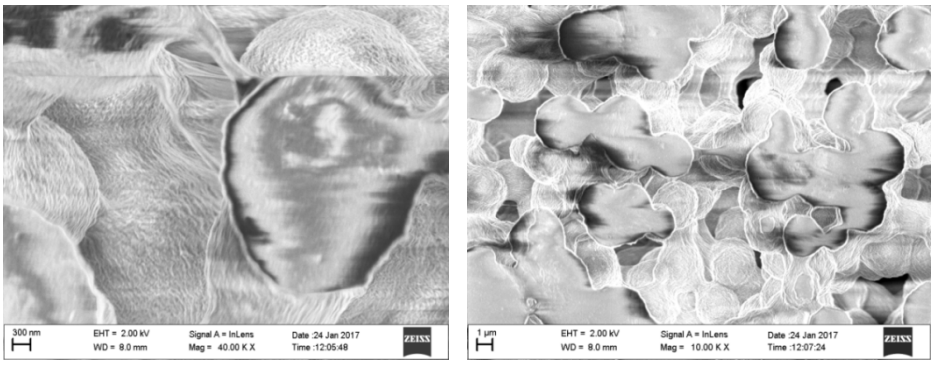

Fig. (3a) & (3b) FESEM images of PVDF film at different magnifications

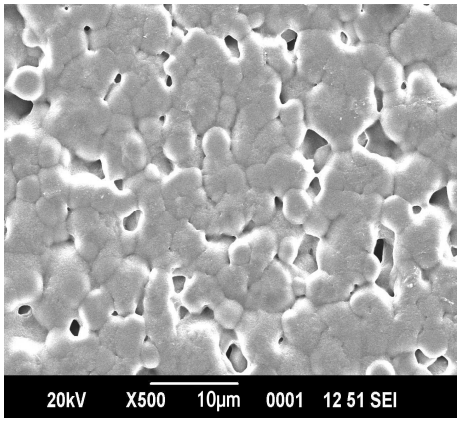

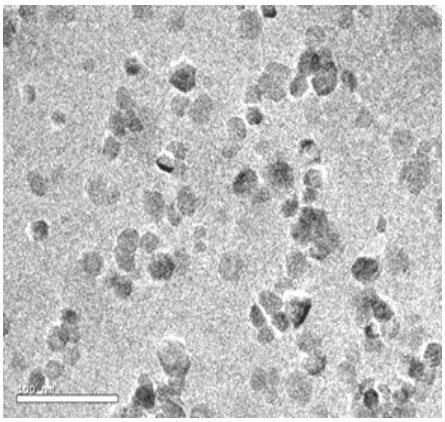

Fig. (3c) FESEM image of PVDF/ZnO film

Fig. (3d) TEM image of ZnO

The spherulitic structure of PVDF is clearly seen in figures (3a) and (3b). Spherulites are composed of highly ordered lamellae which can be observed in figure (3a). The PVDF crystallizes from the melt into spherulitic structures and the size of the spherulites and pores depends on the crystallization conditions, especially, the temperature. When nanostructured ZnO is added to the PVDF matrix, size of the pores is reduced and the size of the spherulites is increased. The uniformity of the distribution of ZnO in the PVDF matrix is quite clear from the FESEM image of PVDF/ZnO nanocomposite film. It is also observed that fine spherulites are arranged in well-defined fashion.

4.3.4. UV visible absorption spectroscopic studies

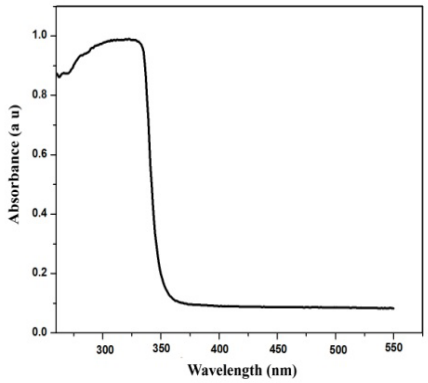

Fig. (4a) UV-visible spectrum of ZnO

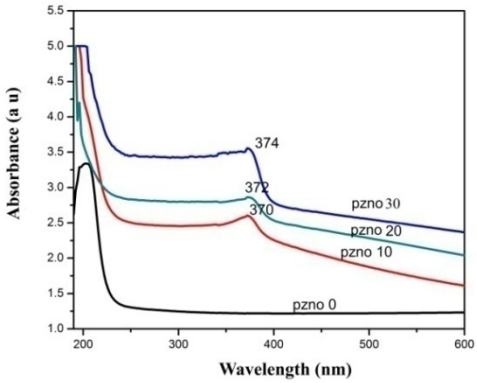

Fig. (4b) UV-visible spectra of PVDF/ZnO films

The optical absorption spectra of the samples were recorded using Jasco V570 spectrophotometer over the range 200 nm – 800 nm and the absorption spectra of nano-structured ZnO and PVDF/ZnO films are given respectively in figures (4a) and (4b). It is clear from figure (4a) that ZnO is nanostructured, since the absorption peak is blue shifted and the band-gap energy is increased to 3.48eV, from 3.31 eV of the bulk ZnO. The UV- visible absorption spectra of PVDF/ZnO nanocomposite films depicted in figure (4b), exhibit some interesting features, where the symbols, PZnO 10, PZnO 20 and PZnO 30 refer to 10%, 20% and 30% of ZnO, respectively in the nanocomposite films. For these films, there is substantial increase in the UV absorption intensity compared to PVDF film, as the concentration of ZnO in the nanocomposite increases from 5% to 20%. For the nanocomposite films, an absorption window is found in the UV range 240 nm – 370nm.

The range of UV wavelengths is often subdivided into UV-A (400–315 nm), UV-B (315–290 nm) and UV-C (290–200 nm). Protection against UV-C radiation is generally not a major concern, in contrast to the dangers posed by UV-A and UV-B radiations. The UV-B radiation is the principal cause of sunburn reactions and it is greatly effective in stimulating the tanning reaction in the skin. The UV-A radiation can also cause sunburns, but less compared to the UV-B radiation. It is observed from figure (4b), that UV absorption is quite enhanced in the region 200 nm - 370 nm, for these PVDF/ZnO nanocomposite films. These films hence offer ample scope as efficient and flexible UV radiation protectors in the entire UV-B region. This shielding efficiency is due to the UV absorption capability of nanostructured ZnO in the composite and PVDF serves the purpose of acting as a suitable host matrix for ZnO and facilitates the formation of flexible nanocomposite films.

From the transmittance plots shown in figure (5a), it is clear that, the PVDF film shows 40% transmittance in the visible region and the transmittance becomes zero only at 200 nm. In the case of the nanocomposite films, shown in figures (5a) and (5b), the transmittance becomes almost close to zero in the UV region itself, below 370 nm and becomes zero around 210 nm [7,17,19]. The symbols, PZ 1, PZ 2, PZ 3 and PZ 5 in figure (5b) refer to 1%, 2%, 3% and 5% of ZnO in the nanocomposite films. In the present work, PVDF/ZnO nanocomposite films of 20 μm thickness, are found to show about 99 % UV absorption

in the wavelength range from 200 nm to 370 nm with 5 % of ZnO loading in the composite.

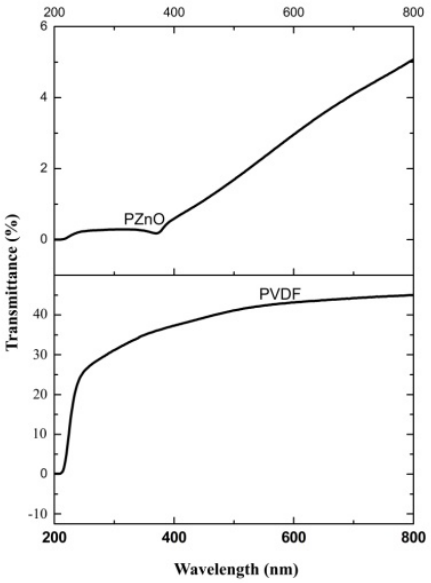

Fig. (5a) Transmittance curves

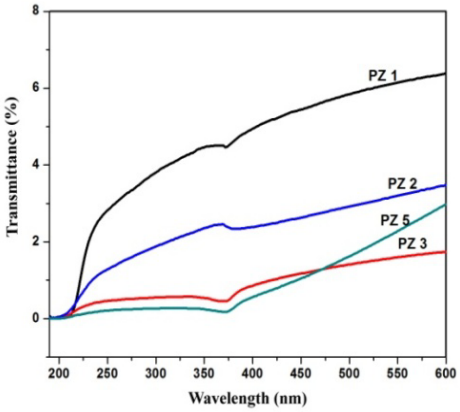

Fig. (5b) Transmittance curves of PVDF/ ZnO films

4.3.5. Themo Gravimetric Analysis (TGA)

Thermo gravimetric analysis (TGA) of the PVDF and PVDF/ZnO nanocomposite films was carried out on a Perkin Elmer, Diamond TG/DTA instrument. The samples were heated to 700 °C at a scan rate of 10 °C per minute in nitrogen atmosphere**.** Thermo gravimetric analysis (TGA) determines the weight changes of a sample upon heating. The TGA curves of PVDF and PVDF/ZnO films are shown in figure (6) and the TGA data is summarized in Table (1). From figure (6), it is seen that the degradation temperature of PVDF/ZnO film is greater

than that of PVDF film. The degradation onset temperature of PVDF/ZnO nanocomposite film measured as the temperature required for % degradation is higher than that of pure PVDF film. In table(1), shown below, $T_{0.1}$, $T_{0.3}$, $T_{0.5}$ and $T_{0.7}$ denote the temperatures for 10 %, 30 %, 50 % and 70 % degradation in weight respectively. From the table it is clear that, PVDF/ZnO film is more thermally stable than PVDF film [3,19]. The PVDF/ZnO nanocomposite films are stable up to 470 ^{o}C and can be used in high temperature applications.

Table. (1) TGA data of PVDF and PVDF/ZnO nanocomposite films

Sample	$T_{0.1}$ (^{o}C)	$T_{0.3}$ (^{o}C)	$T_{0.5}$ (^{o}C)	$T_{0.7}$ (^{o}C)
PVDF film	458	476	488	560
PVDF/ZnO film	473	492	505	585

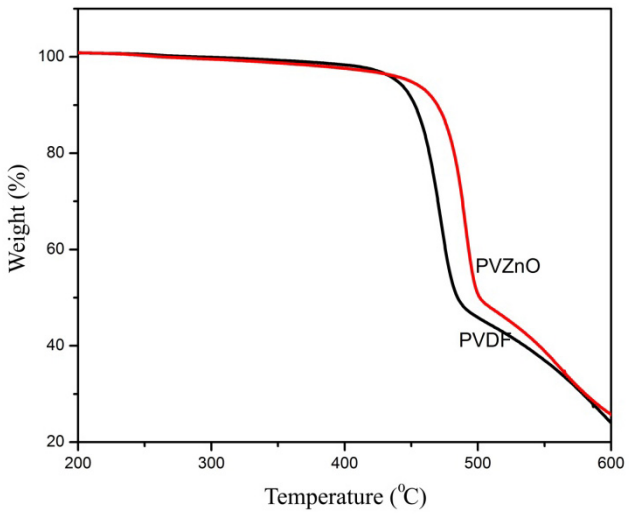

Fig. (6) TGA curves of PVDF and PVDF/ZnO films

4.3.6. Photoluminescence (PL) studies

In the PL spectrum of ZnO shown in figure (7a), intense emission peaks are observed in the visible region and a less intense peak is observed in the UV region [12]. The PL spectra of PVDF/ZnO nanocomposite films shown in figure (7b) consist of intense broad bands covering the visible region and the emission peak of ZnO in the UV region is found to be quenched. The symbols PZ 10, PZ 20 and PZ 30 in figure (7b) refer to 10%, 20% and 30% of ZnO in the nanocomposite films. The combined effect of intense emission all through the visible region gives rise to the white light emission observed from these films. The photograph of the observed white luminescence is shown as the inset of figure (7b) and the corresponding chromaticity diagram is given in figure (8).The chromaticity (CIE) coordinates for the samples PZ 10, PZ 20 and PZ 30 are marked as (1), (2) and (3) in the chromaticity diagram. The chromaticity diagram matches quite well with the PL emission spectra.

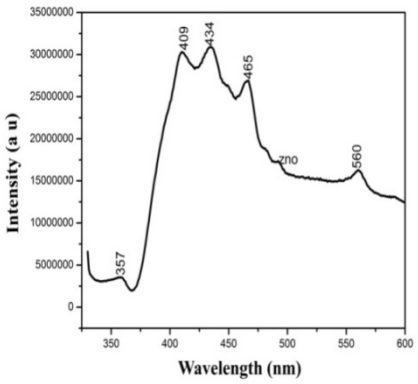

Fig. (7a) PL spectrum of ZnO

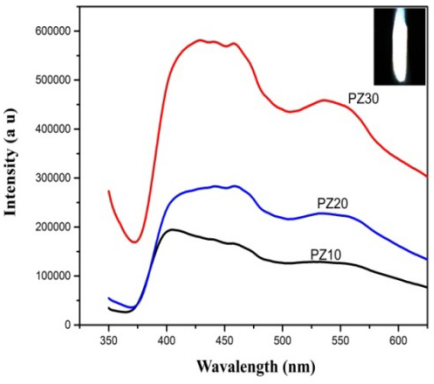

Fig. (7b) PL spectra of PVDF/ZnO films

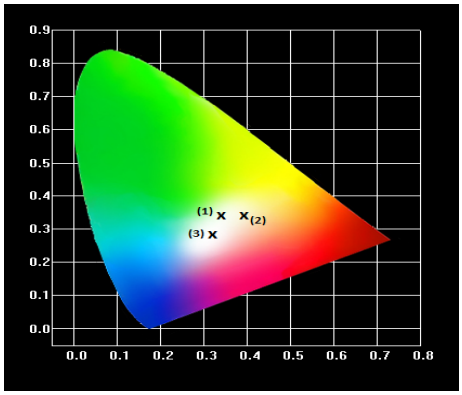

Fig. (8) Chromaticity diagram of PVDF/ZnO films

The UV band edge emission generally observed in ZnO is due to excitonic transitions. The emission peaks observed in the visible region are generally related to defects and dopants. Various intrinsic defects such as V_o (oxygen vacancy),V_{Zn} (zinc vacancy), Zn_i (interstitial zinc) and O_i (interstitial oxygen) contribute towards the visible emissions observed in ZnO. The band edge emission in nanostructured ZnO of the present work is observed at 357 nm as shown in figure (8a). Violet emissions at 409 nm &434 nm are due to the transitions from the conduction band of ZnO to the zinc vacancies which can trap holes. The blue emission at 465 nm is attributed to the direct recombination of conduction band electron in the Zn_{3d} band and hole in the O_{2p} valence band. The green luminescence at 560 nm is assigned to the oxygen vacancies V_o or oxygen antisites (oxygen anti-sites refer to oxygen atoms sitting at the wrong lattice positions). The PL spectra shown in figures (7a) and (7b) are recorded for the UV excitation at 320 nm and hence the plots are shown in the wavelength range 350 nm to 600 nm.

The yellow, orange and red emissions can be observed upon increasing the excitation wavelength to 370 nm. The yellow and orange emissions in ZnO can be attributed to transitions related to oxygen interstitials and the red emission, to transitions associated with zinc interstitials. Most of the visible emission in ZnO originates from the defect centres at the surface, which can be suitably modified to tune the emission to the required spectral region[18][22-27].

It is observed that PVDF film does not give any emission in the visible region. Comparing figures (7a) and (7b), it is observed that the luminescence of ZnO in the UV region is quenched in the PL spectra of the nanocomposite films [28]. The intense broad band emission observed in the nanocomposite films, extending all through the visible region, results in the intense white light emission.

4.4. Conclusions

The PVDF/ZnO nanocomposite films of the present work are obtained by the cost effective and simple method of solution processing, compared to the already reported expensive techniques of electro-spinning and spin coating. The XRD patterns and FESEM images of PVDF/ZnO nanocomposite films confirm the homogenous dispersion of ZnO within the PVDF matrix. These free-standing, flexible and thermally stable films can be of profound applications as excellent UV shielding materials and also as white light emitting films for realizing solid state lighting devices.

References

[1] R. V. Kumar, R. Elgamiel, Y. Diamant, and A. Gedanken, Sonochemical Preparation and Characterization of Nanocrystalline Copper Oxide Embedded in Poly(vinyl alcohol) and Its Effect on Crystal Growth of Copper Oxide; *Langmuir* 17 (2001) 1406-1410; doi: 10.1021/la001331s

[2] G. Kickelbick, Concepts for the incorporation of inorganic building blocks into organic polymers on a nanoscale; *Prog. Polym. Sci.* 28 (2003) 83–114

[3] Y.Kojima, A.Usuki, M. Kawasumi, A. Okada, Y. Fukushima, T. Kurauchi and O.Kamigaito; Polymer/ silicate Interaction in Nylon 6-Clay Hybrid Studied by Temperature Programmed Pyrolysis Techniques; *J. Mater. Res*. 8 (1993) 1185–9

[4] J. Zhu , F.M. Uhl , A.B. Morgan and C.A.Wilkie , Studies on the mechanism by which the formation of nanocomposites enhances thermal stability; *Chem.Mater*. 13 (2001) 4649– 4654

[5] P.Indra Devi, K.Ramachandran; Dielectric studies on hybridised PVDF–ZnO nanocomposites ; *J. Exp. Nanosci.* Vol.6, No.3, (2011) 281–293. doi:10.1080/ 17458080. 2010.497947.

[6] A.P. Indolia, M.S. Gaur; Investigation of structural and thermal characteristics of PVDF/ZnO nanocomposites; *J. Therm. Anal. Calorim*. 113 (2012) 821–830. doi:10.1007/ s10973-012-2834-0.

[7] R. Gregorio; Determination of the α,β and γ Crystalline Phases of Poly (vinylidene fluoride) Films Prepared at Different Conditions; *Journal of Appl. Pol. Sci.*, Vol. 100, 3272–3279 (2006) doi:10.1002/app.23137.

[8] K.S. Tan, W.C. Gan, T.S. Velayutham, W.H.A. Majid; Pyroelectricity enhancement of PVDF nanocomposite thin films doped with ZnO nanoparticles; *Smart Mater. Struct.* 23 (2014) 125006. doi:10.1088/0964-1726/23/12/125006.

[9] P.P. Jeeju, S. Jayalekshmi, K. Chandrasekharan, P. Sudheesh; Enhanced linear and nonlinear optical properties of thermally stable ZnO/poly(styrene)-poly(methyl methacrylate) nanocomposite films; *Thin Solid Films.* 531 (2013) 378–384. doi:10.1016/ j.tsf.2012.12.043.

[10] A. Kołodziejczak-radzimska, T. Jesionowski; Zinc Oxide-From Synthesis to Application: A Review; *Materials (*2014), 7,2833–2881. doi:10.3390/ma7042833.

[11] Z.L. Wang; Zinc oxide nanostructures: growth , properties and applications; *Jou.Phy.Cond.Matter,* 16 (2004) 829–858. doi:10.1088/ 0953-8984/16/25/R01.

[12] S.S. Kumar, P. Venkateswarlu, V.R. Rao, G.N. Rao,; Synthesis, characterization and optical properties of zinc oxide nanoparticles; *Int.Nat.Nano.Lett*. (2013) 1–6.

[13] T. L. Tan, C. W.Lai, S.B.A. Hami; Tunable Band Gap Energy of Mn-Doped ZnO Nanoparticle Using the Coprecipitation Technique**;** *Jou. of Nanomat*.(2014), 371720 doi.org/ 10.1155/2014/371720

[14] Y. Hao, S. Lou, S. Zhou, R. Yuan, G. Zhu, N. Li; Structural , optical, and magnetic studies of manganese-doped zinc oxide hierarchical microspheres by self-assembly of nanoparticles; *Nano scale Res.Lett.* (2012) 19–21.

[15] P.P. Jeeju, S. Jayalekshmi, K. Chandrasekharan, P. Sudheesh; Size dependent nonlinear optical properties of spin coated zinc oxide-polystyrene nanocomposite films; *Opt. Commun.* 285 (2012) 5433–5439. doi:10.1016/j.optcom.2012.07.078.

[16] M. Sajimol Augustine, P.P. Jeeju, V.G. Sreevalsa, S. Jayalekshmi; Excellent UV absorption in spin-coated thin films of oleic acid modified zinc oxide nanorods embedded in Polyvinyl alcohol; *J. Phys. Chem. Solids.* 73 (2012) 396–401. doi:10.1016/j.jpcs. 2011.11.004.

[17] Y. Tu, L. Zhou, Y.Z. Jin, C. Gao, Z.Z. Ye, Y.F. Yang, Q.L. Wang; Transparent and flexible thin films of ZnO-polystyrene nanocomposite for UV-shielding applications; *J.Mater.Chem,* (2010) 1594–1599. doi:10.1039/b914156a.

[18] X.M. Sui, C.L. Shao, Y.C. Liu; White-light emission of polyvinyl alcohol / ZnO hybrid nanofibers prepared by electrospinning; *Appl.Phy.Lett.* 87, 113115 (2005). doi:10.1063/1.2048808.

[19] P.P. Jeeju, S. Jayalekshmi; On the Interesting Optical Properties of Highly Transparent , Thermally Stable , Spin-Coated Polystyrene / Zinc Oxide Nanocomposite Films; *J.Appl.Pol.Sci,* 120, 1361-1366 (2010). doi:10.1002/app.

[20] S. Talam, S.R. Karumuri, N. Gunnam; Synthesis , Characterization , and Spectroscopic Properties of ZnO Nanoparticles; *ISRN Nanotechnology,* (2012). doi:10.5402/ 2012/372505.

[21] P. Martins, A.C. Lopes, S. Lanceros-Mendez; Electroactive phases of poly(vinylidene fluoride): Determination, processing and applications; *Prog. Polym. Sci.* 39 (2014) 683–706. doi:10.1016/j.progpolymsci. 2013.07.006.

[22] D. Li, Y.H. Leung, A.B. Djuriši, Z.T. Liu, M.H. Xie, S.L. Shi, S.J. Xu; Different origins of visible luminescence in ZnO nanostructures fabricated by the chemical and evaporation methods; *Appl.Phy.Lett*. 85 (2004) 1601–1603. doi:10.1063/1.1786375.

[23] Q.X. Zhao, P. Klason, M. Willander, H.M. Zhong, W. Lu, J.H. Yang; Deep-level emissions influenced by O and Zn implantations in ZnO; *Appl.Phy.Lett.*87, 211912 (2005) 18–21. doi:10.1063/ 1.2135880.

[24] A.K. Bhunia, P.K. Samanta, S. Saha, T. Kamilya, ZnO nanoparticle-protein interaction: Corona formation with associated unfolding ; *Appl.Phy.Lett*.103, 143701 (2013). doi:10.1063/1.4824021.

[25] T.M. Børseth, B.G. Svensson, A.Y. Kuznetsov, P. Klason, Q.X. Zhao, M. Willander, Identification of oxygen and zinc vacancy optical signals in ZnO; *Appl.Phy.Lett.*89, 262112 (2006) 1–4. doi:10.1063/1.2424641.

[26] Y. Lin, H. Faber, S. Rossbauer, T.D. Anthopoulos, Y. Lin, H. Faber, S. Rossbauer, T.D. Anthopoulos; photochemical conversion process Solution-processed ZnO nanoparticle-based transistors via a room-temperature photochemical conversion process; *Appl.Phy.Lett.* 102, 193516 (2013). doi:10.1063/1.4804434.

[27] C.Ton-that, M.R. Phillips, M. Foley, S.J. Moody, A.P.J. Stampfl, Surface electronic properties of ZnO nanoparticles; *Appl.Phy.Lett.* 92 261916 (2008) . doi:10.1063/1.2952955.

[28] B.Kulyk, V.Kapustianyk, O.Krupka, B.Sahraoul ;Optical absorption and photoluminescence properties of ZnO / PMMA nanocomposite films; *Jou.Phy. con.series;* 289 (2011). doi:10.1088/1742-6596/289/1/012003.

Chapter 5

Impressive nonlinear optical response exhibited by PVDF/ Reduced Graphene Oxide(RGO) nanocomposite films

Contents

This chapter begins with a brief introduction to the materials showing nonlinear optical behavior and their prospective applications in optical communication and optical data storage and evolves into addressing the nonlinear optical characteristics of free standing films of Poly (vinylidene fluoride)(PVDF) /Reduced Graphene Oxide(RGO) nanocomposite, to assess their suitability as efficient optical limiters. The PVDF/RGO nanocomposite films of the present work have been grown by mixing different concentrations of RGO as the filler, with PVDF, using solution casting method. The open aperture and closed aperture Z-scan technique under nanosecond excitation (532 nm,7 ns) has been used to investigate the nonlinear optical characteristics of the PVDF/RGO nanocomposite filmsThe highlight of the present work is the observation of quite low values of normalized transmittance and low optical limiting threshold power in free standing films of PVDF/RGO nanocomposite. These flexible, free standing and stable nanocomposite films offer high application prospects in the design of efficient optical limiting devices of any desired size or shape.

5.1. Introduction

The past two decades have witnessed fabulous initiatives to identify novel organic materials with remarkable nonlinear optical (NLO) characteristics owing to their prospective applications in optical communications, optical signal processing, optical switching and optical limiting. It is possible to optimize the nonlinear optical response of many organic materials by adopting rational design criteria at the molecular level, without compromising their inherent thermal, mechanical and chemical stability. In this context, nanostructured organic materials, especially, polymer based nanocomposites offer ample scope as NLO materials and many of them are endowed with fast nonlinear optical response and large optical nonlinearity suitable for applications in optical communications and optical data storage.

Poly(vinylidene flouride)(PVDF) is a highly non-reactive, semi-crystalline, fluoro polymer having high molecular weight, well-known by its interesting properties like ease of processability, good mechanical strength, thermal stability and chemical resistance. It shows quite impressive ferroelectric, pyroelectric and piezoelectric properties as well. Among the five different crystal forms α, β, γ, δ and ε, β phase is primarily responsible for the piezoelectric properties of PVDF. Its supreme film forming properties facilitate its application as an excellent polymer matrix, for realizing a variety of polymer nanocomposite films with prospective applications in sensors, actuators and transducers [1-6].

The area of polymer nanocomposites, with conventional polymers as hosts and conductive carbonaceous materials as the fillers, has drawn much attention as a route to obtain new materials with superior structural and functional properties. Polymer-graphene nanocomposites are being extensively investigated owing to the superior optical, electrical, mechanical and thermal properties of graphene. Graphene is quite expensive and generally it is difficult to disperse it in polymer solutions. Hence in the present work, reduced graphene oxide (RGO) is used as the nano-filler material, synthesized in our laboratory by modified Hummers method. The properties of RGO are very much similar to those of graphene [7-9].

Recently, much work has been done to explore the nonlinear optical properties of different types of materials, to assess their application prospects in various nonlinear optical devices. Both graphene and RGO exhibit remarkable nonlinear optical (NLO) properties which make them potential materials for various applications in optical communication, data storage and optical limiting (OL). It is known that RGO shows impressive optical nonlinearity with ultrafast response times and a broadband spectral range. At higher optical frequencies, one can expect enhanced optical nonlinearity in RGO because of its graphene like band structure. The phenomenon of optical power limiting, a nonlinear optical effect, has attracted much attention due to its application for the protection of eyes and sensitive optical devices from high power laser pulses [10-13].The nonlinear optical properties of free standing polymer nanocomposite films endowed with efficient optical limiting characteristics have not been

pursued in depth. In the present work, the open aperture and closed aperture Z-scan technique under nanosecond excitation (532 nm,7 ns) has been used to investigate the nonlinear optical characteristics of the PVDF/RGO nanocomposite films. The novelty of the present work is the observation of remarkable optical limiting efficiency, due to the high value of the nonlinear absorption co-efficient, in free standing films of PVDF/RGO nanocomposite. These freestanding films are highly flexible and offer ample scope for realizing optical limiting devices of any desired size or shape.

5.2. Experimental Techniques

5.2.1. Materials and methods

For the synthesis of the nanocomposite films, PVDF granules were purchased from Hi Media Laboratories, Private Limited, Mumbai and N-N Dimethyl formamide (DMF), from Spectro-chem Private Limited, Mumbai. The filler material, RGO was synthesized by modified Hummers method using hydrazine hydrate as the reducing agent [4][14].

Synthesis of graphene oxide (GO)

Graphene oxide was synthesized by modified Hummer's method from graphite in the present work. Graphite (3 g) and $NaNO_3$ (1.5 g) were first mixed together in a conical flask and then 100 ml, H_2SO_4 (95%) was added to the flask, which was kept under stirring in an ice bath. Potassium permanganate (8 g) was then added to the suspension little by little to avoid overheating. The mixture was brought to room temperature and

stirred for 2 hrs. The color of the suspension then turned to bright brown, to which 90 ml of distilled water was added. The temperature of the suspension was found to rise quickly to about 90 °C and the color changed to yellow. The diluted suspension was stirred at 98 °C for 12 hrs and 30 ml of H_2O_2 was added to the mixture. For purification, the mixture was washed by rinsing with HCl (50 ml) and then distilled water for several times. The suspension was then centrifuged at 4000 rpm for 6 minutes. After filtration and drying in a vacuum oven, graphene oxide was obtained in the form of a black powder.

Synthesis of reduced graphene oxide (RGO)

Graphene oxide (1 g) was first dispersed in 50 ml distilled water and sonicated for 30 minutes. Then the suspension was heated to 100 °C and 5 ml hydrazine hydrate was added to the suspension and sonicated for 30 minutes. The suspension was then kept at 98 °C for 48 h in Ar atmosphere. The resulting product was collected by filtration in the form of a black powder. The obtained material was then washed using distilled water for several times to remove the excessive hydrazine hydrate and was transferred into water for sonication. The suspension was then centrifuged at 4000 rpm for 3 minutes to remove bulk graphite. The final product was collected after vacuum filtration and drying in a vacuum oven.

Synthesis of PVDF/RGO nanocomposite films

The PVDF/RGO nanocomposite films were synthesized by solution casting method. Initially, PVDF was dissolved in N-N Di methyl formamide (DMF) and various amounts of RGO (0.1%, 0.25%,

0.5% and 1% of PVDF), were sonicated well in DMF. The DMF dispersions of RGO were mixed with the PVDF solution and stirred well. These solutions were used for making films on glass slides by solution casting method. Because of the excellent film forming property of PVDF, these films can be peeled off the glass substrates to yield free standing films of thickness around 10 μm[15].

5.2.2 Sample characterization

The PVDF/RGO nanocomposite films were characterized by X-ray diffraction technique employing the Rigaku X-ray diffractometer, UV-visible absorption spectroscopy, using JASCO V-570 UV visible NIR spectro photometer, Raman spectroscopy by high resolution Raman spectrometer (Horiba JY), FTIR spectroscopy using Shimadzu IR affinity FTIR spectrophotometer and FESEM imaging by ZEISS Sigma field emission scanning electron microscope. The nonlinear optical properties of PVDF film and PVDF/RGO nanocomposite films were studied using open and closed aperture Z- scan technique.

5.3. Results and Discussion

5.3.1. Structural and morphological analysis

5.3.1.1. X-Ray Diffraction (XRD) analysis

The XRD patterns of RGO and PVDF/RGO nanocomposite films are shown in figures (1a) & (1b) respectively. The particle size of the RGO calculated from XRD data is around 12 nm. The inset of figure (1a) shows the photograph of the free standing, flexible and transparent film of

PVDF/RGO. In figure (1b), the symbols PRGO1, PRGO2 and PRGO3 correspond to 0.1%, 0.25%, and 0.5% of RGO in the nanocomposite samples. The peaks at 18.21° and 26.5° are attributed to the α phase and that at 20.26° to the β phase of PVDF. It can be seen that the intensity of the β peaks increases and that of α peaks decreases, when the concentration of RGO in the nanocomposite increases. The increase in the intensity of β peaks shows that RGO is well dispersed in the PVDF matrix [16-18].

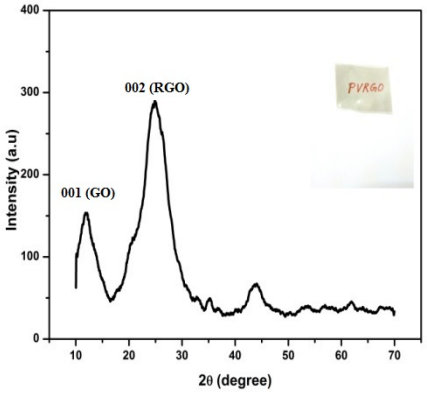

Fig. (1a) XRD pattern of RGO

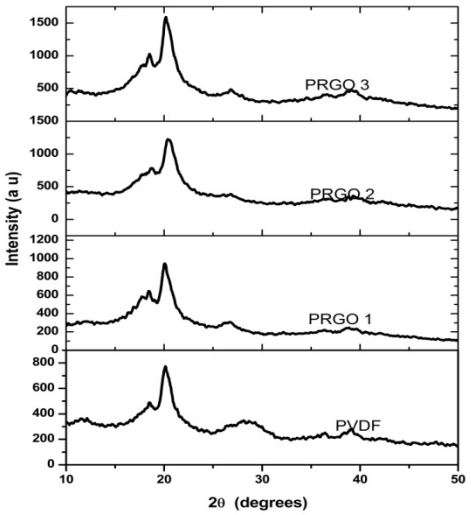

Fig. (1b) XRD patterns of PVDF/RGO films

5.3.1.2. Fourier Transform Infrared (FTIR) spectroscopic studies

The FTIR spectra in the ATR mode for PVDF film and PVDF/RGO film are shown in figures (2a) & (2b) respectively. The peaks at 766 and 976 cm^{-1} are due to the α phase of PVDF. The peak at 878 cm^{-1} corresponds to C-C bond vibration and that at 1170 cm^{-1} to the stretching

mode of CF_2 bond in PVDF. The intensity of the characteristic absorption band at 840 cm^{-1} corresponding to CH_2 rocking of the β phase is found to increase in the PVDF/RGO film. The peaks at 766 cm^{-1} and 976 cm^{-1} attributed to the α phase (in plane bending or rocking) are clearly seen in the spectrum of pristine PVDF film, but are absent in the spectrum of the nanocomposite sample. Hence it is clear that the addition of RGO suppresses the α phase of the PVDF and enhances the β phase [4][16] .

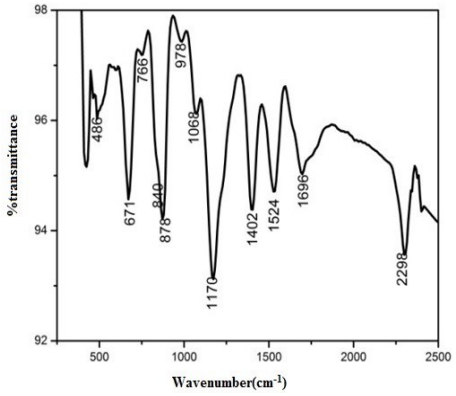

Fig. (2a) FTIR spectrum of PVDF film

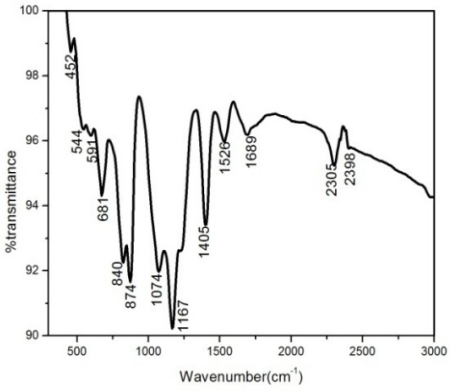

Fig. (2b) FTIR spectrum of PVDF/ RGO film

5.3.1.3 Field Emission Scanning Electron Microscopy (FESEM) studies

The FESEM image of RGO shown in figure (3a) confirms the flake like structure of RGO, quite similar to that of graphene. From the FESEM image of the PVDF/RGO film shown in figure (3b) it is obvious that RGO is well dispersed in the PVDF matrix.

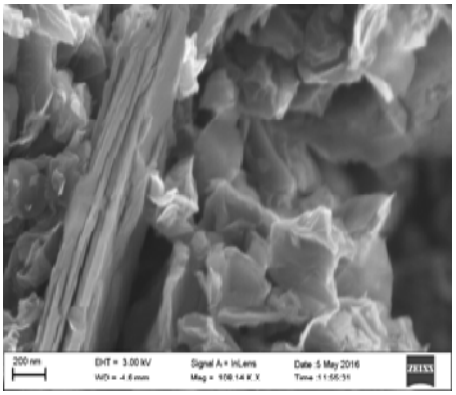

Fig. (3a) FESEM image of RGO

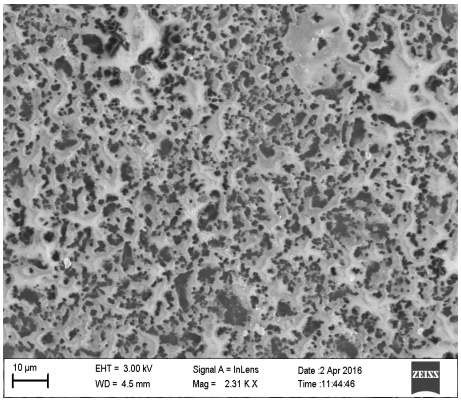

Fig. (3b) FESEM image of PVDF/ RGO film

5.3.2. Optical studies

5.3.2.1. UV-visible absorption spectroscopic studies

The absorption spectra of PVDF film and PVDF/RGO nanocomposite films in the wavelength range 100 nm to 800 nm are given in figure (4), with the absorption peak in the inset. It can be observed that an additional absorption peak is seen in the nanocomposite film at 260 nm, other than that of PVDF at 196 nm. The origin of this peak can be attributed to the π-π^* transition in C= C aromatic rings of RGO and it ascertains the presence of almost completely reduced graphene oxide with re-established π conjugated network of RGO in the nanocomposite [19,20]. For very small concentrations of RGO, this absorption peak is not observable and hence not shown in the figure.

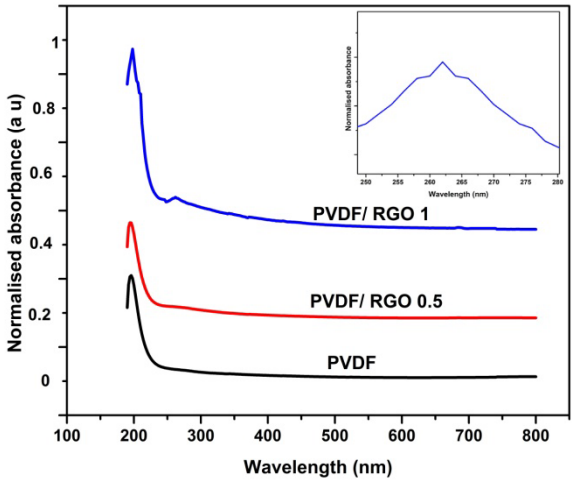

Fig. (4): UV visible absorption spectra of PVDF and PVDF/RGO films

5.3.2.2. Raman spectroscopic studies

The Raman spectrum of RGO is shown in figure (5a). The D band, G band and 2D band are observed at 1352 cm^{-1}, 1570 cm^{-1} and 2700 cm^{-1} respectively. From figure (5a), the ratio I_D/I_G is found to be nearly 1,which also confirms the reduction of graphene oxide to yield RGO [17,18]. In the Raman spectrum of PVDF/RGO film shown in figure (5b), in addition to the RGO peaks, the polymer peaks are also seen at 510 cm^{-1} and 840 cm^{-1}corresponding to the β phase of PVDF. The dispersion of RGO in PVDF matrix and the resulting enhancement in the β phase of PVDF is once again confirmed by this study.

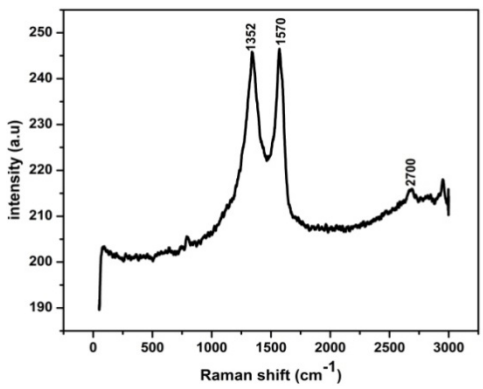

Fig. (5a) Raman spectrum of RGO

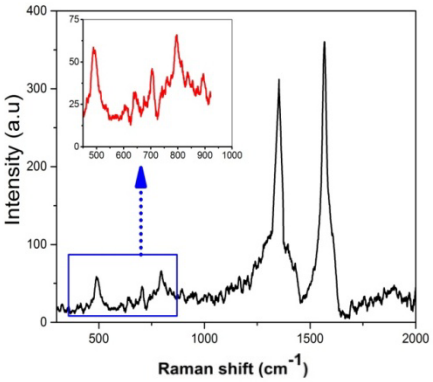

Fig. (5b) Raman spectrum of PVDF/ RGO film

5.3.3. Nonlinear optical studies

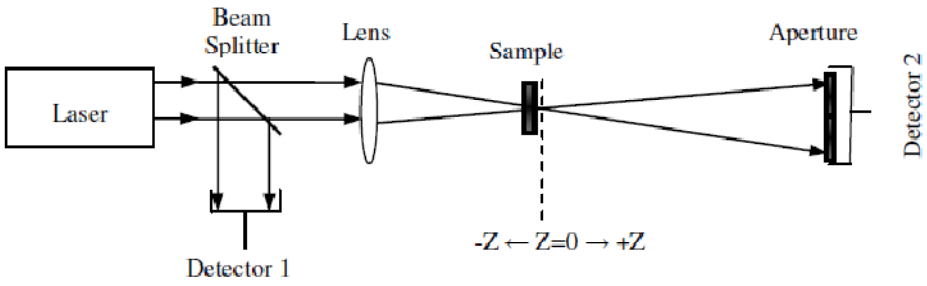

Fig. (6): Experimental setup for Z-scan studies

The Z-scan method introduced in 1989 by Sheik-Bahae and later developed by Eric Van Stryland, is a very simple technique for investigating the phenomena like nonlinear absorption (NLA) and nonlinear refraction (NLR) of materials [21,22]. The experimental set up for the Z-scan studies is shown in figure (6).

The Z-scan technique is carried out by translating the sample along the focus of a tightly focused laser beam. By measuring the

transmittance as a function of Z-position of the sample, information about the light-matter interaction can be extracted. The two measurable quantities connected with "open aperture" and "closed aperture" Z-scan technique are nonlinear absorption coefficient β' and nonlinear refractive index n_2 respectively. Here β' is associated with the imaginary part and n_2 with the real part of the third-order nonlinear susceptibility $\chi^{(3)}$ and provide important information about the nonlinear optical properties of the material.

For the Z-scan studies, a *Q*-switched Nd:YAG nanosecond laser output with nearly Gaussian intensity profile, having a pulse width of 7 ns at 532 nm and a pulse repetition rate of 10 Hz was used as the source of light and was focused using a lens of focal length 15 cm. Pure PVDF film was found to show neither nonlinear refraction nor nonlinear absorption. For the PVDF/RGO nanocomposite films, the observed nonlinearity is found to be of the third order, as the data fits to a two photon absorption (TPA) [23,24].

The corresponding net transmission is given by

$$T(z) = \frac{c}{q_o\sqrt{\pi}} \int_{-\infty}^{\infty} \ln\left(1 + q_o e^{-t^2}\right) dt \qquad (1)$$

Where

$$q_o = \beta' I_0(t) L_{eff} \qquad (2)$$

Here, L_{eff} = $1-e^{-\alpha L}/\alpha$, is the effective thickness with linear absorption coefficient α and nonlinear absorption coefficient β', L is the sample length and I_0 is the irradiance at focus [25-29]. Using the experimental data, values of nonlinear absorption coefficient β' at a pulse energy of 5 μJ for the 4 samples are calculated.

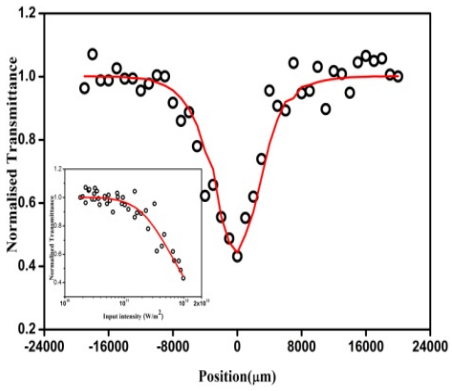

Fig. (7a) (O.A)Z-scan trace of PVDF/ RGO film

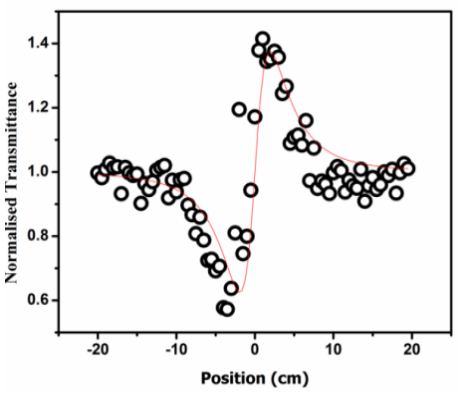

Fig. (7b) (C.A)Z-scan trace of PVDF/ RGO film

The open aperture (O.A) and the closed aperture (C.A) Z-scan traces of the PVDF/RGO (1%) film at 5 μJ energy, are shown in figures (7a) and (7b) respectively. The red solid curve is the theoretical curve to the experimental data shown as black circles. Optical limiters are devices that transmit light at low input intensities and the transmitted light intensity decreases at high input intensity. The optical limiting property is due to absorptive nonlinearity which is proportional to the imaginary part of $\chi^{(3)}$. In general, optical limiting property is facilitated by the presence of strong nonlinear absorption. All films show a decrease in

transmission with increase in the input laser intensity, as illustrated in the inset of figure (7a), which shows that the samples are suitable for optical limiting applications [27,30,31] . The magnitude of nonlinear absorption coefficient β' is calculated from the open aperture Z-scan data. Closed aperture Z-scan was carried out to determine the sign and magnitude of nonlinear refraction coefficient (n_2). The observation of a pre-focal transmittance minimum (valley), followed by a post-focal transmittance maximum (peak) for the studied films, indicates a positive lensing or a positive nonlinear refractive index (figure 7b). The cause of origin of on axis phase shift at the focus in closed aperture Z-scan analysis can be described as the change in transmittance about the focus , attributed by the special distribution of energy facilitated by high repetition rate of focused laser beam on the sample [32 – 36].

The nonlinear refractive index n_2, is related to the linear refractive index n_0 as

$$n_2 = \frac{cn_0\lambda\Delta\phi_0}{80\pi^2 I_0 L_{eff}}\ (esu) \qquad (3)$$

where

$$\Delta\phi_0 = \frac{\Delta T_{p-v}}{0.406(1-s)^{0.25}}$$

for $|\Delta\phi_0| \leq \pi$ (4)

Here, $\Delta Tp - v$, is the difference between peak and valley in the closed aperture Z-scan, S is the linear transmittance of the far field aperture

and λ is the excitation wavelength. The nonlinear refractive index n_2 is related to the real part of nonlinear susceptibility, Re $\chi^{(3)}$ by the relation

$$\text{Re } \chi^{(3)} = (n_0 n_2 / 3\pi) \ (esu) \quad (5)$$

where n_0 is the linear refractive index, which was determined using Abbe's refractometer as 1.42. The imaginary part of third order susceptibility, Im $\chi^{(3)}$determines the strength of the nonlinear absorption, which is given below.

$$\text{Im } \chi^{(3)} = n_0^2 c^2 \beta' / 240\pi^2 \omega \quad (esu) \quad (6)$$

where, c is the velocity of light in vacuum and ω, the angular frequency of the laser pulse. From the real and imaginary parts of $\chi^{(3)}$, the modulus of third order nonlinear susceptibility can be found out [24-28][31].

$$\chi^{(3)} = [(\text{Re } \chi^{(3)})^2 + (\text{Im } \chi^{(3)})^2]^{1/2} \quad (7)$$

The magnitude of $\chi^{(3)}$ determines the strength of nonlinear response of the material.

There are many mechanisms responsible for NLA in different types of materials. Still, the normalized transmittance valley in graphene and graphene nanocomposites can be mainly due to two mechanisms, reverse saturable absorption (RSA) and two photon absorption (TPA) [37].

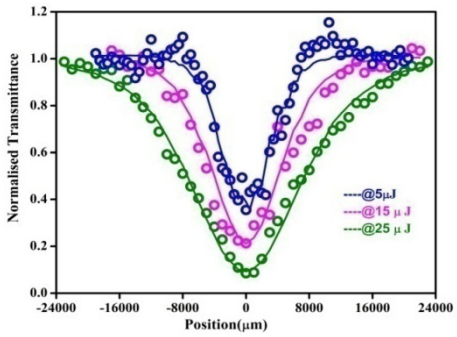

Fig. (8a) (O.A).Z-scan curves at different energies

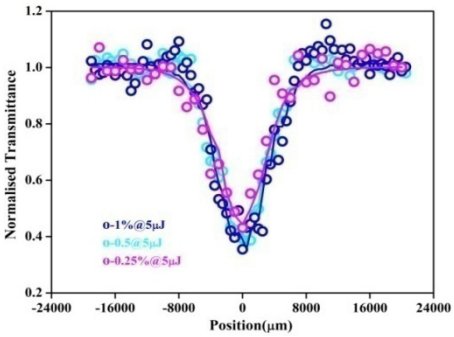

Fig. (8b) (O.A).Z-scan curves for different RGO concentrations

The open aperture Z-scan curves of PVDF/RGO (0.25%) film, corresponding to pulse energy 5 μJ, 15 μJ and 25 μJ are shown in figure (8a).This film is chosen for the above studies because, the O.A Z-scan traces of this film are showing the best fit with theoretical values and this is the sample with average RGO concentration. The beam intensities at the focus, corresponding to energies of 5 μJ, 15 μJ and 25 μJ are 0.13864 GW/cm^2, 0.416 GW/cm^2 and 0.6932 GW/cm^2 respectively. The minimum transmittance obtained is 0.1(10%) for the laser pulse energy of 25 μJ, and this is the lowest transmittance ever reported for free standing polymer nanocomposite films. By changing the pulse energy from 5 μJ to 25 μJ, the minimum transmittance can be tuned from 0.4 (40%) to 0.1(10%). These lowest transmittance values and high values of β' (nonlinear absorption co-efficient), combined with the flexibility and freestanding nature of the PVDF/RGO nanocomposite films offer ample scope for designing highly efficient optical limiting devices of any size or shape for protecting eyes or light sensitive devices such as

CCD cameras from possible damage caused by intense light exposure [9,12,23]. The transmittance minimum varies with variation in the concentration of RGO in the nanocomposite. When the concentration of RGO in the composite is increased, the transmittance decreases and β' increases as shown in figure (8b). On comparison with recently reported values, the β' values of the PVDF/RGO nanocomposite films are much higher. These nanocomposite films also show excellent optical limiting properties. Optical limiting capability of a material is usually evaluated by measuring the optical limiting threshold power (P_{th}). It is the minimum input intensity of the laser source at which the onset of optical limiting starts. It is evident that, lower the optical limiting threshold power, better is the nonlinear optical response of the material. Optical limiting (O.L) plots for various concentrations of RGO in the nanocomposite films are shown in figure (9a) and one typical plot with P_{th} marked is shown in figure (9b).

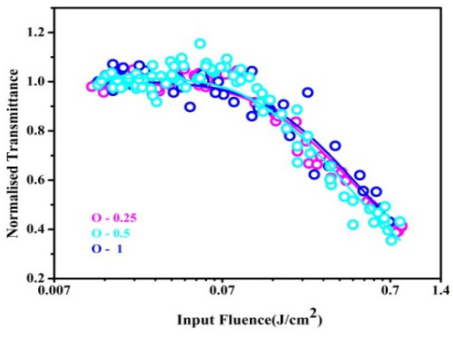

Fig. (9a) Optical limiting graphs for different concentrations of RGO

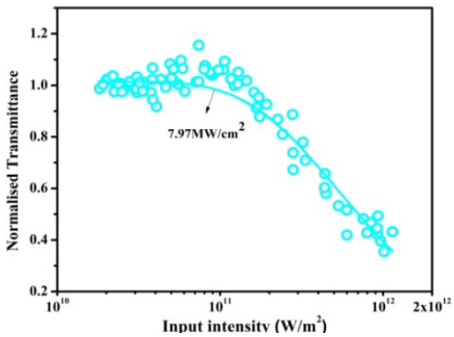

Fig. (9b) Optical limiting curve with P_{th} marked

From Table (1), the minimum P_{th} obtained for our nanocomposite film sample is 7.84 MW/cm^2 which is much lower compared to the values reported earlier [19]. It is seen that the P_{th} decreases, when the concentration of RGO in the nanocomposite increases. The values of P_{th} for various concentrations of RGO are noted and given in Table (1).

From the results of the open aperture Z-scan studies, it can be inferred that the inherent nonlinear optical properties of RGO, coupled with the order associated with its high extent of dispersion in the PVDF matrix are contributing towards the impressive nonlinear characteristics of the PVDF /RGO nanocomposite films. The increased crystallinity and electronic conjugation of RGO compared to graphene oxide (GO) and the increase in the β phase of PVDF are the main factors responsible for the excellent nonlinear response and optical limiting properties of the PVDF/RGO films of the present study [37].

The experimentally determined values of β', n_2, Im $\chi^{(3)}$, $\chi^{(3)}$ and P_{th} of the nanocomposite films are given in Table 1.

Table. (1) Variation of the nonlinear optical parameters with the concentration of RGO in the PVDF/RGO nanocomposite films

Concentration of RGO	n_2 (10^{-10}esu)	β' (cm/GW)	Im $\chi^{(3)}$ (10^{-11}esu)	$\chi^{(3)}$ (10^{-11}esu)	P_{th} (MW/cm^2) Our work	P_{th} (MW/cm^2) (Ref 19)
0.1%	3.41	195	6.19	6.20	8.4	100
0.25%	4.67	275	8.91	8.92	8.24	90
0.5%	5.14	340	11.04	11.05	7.97	70
1%	6.27	400	12.95	12.96	7.84	------

It is observed that the values of third order susceptibility $\chi^{(3)}$, nonlinear absorption coefficient β' and nonlinear refractive index n_2 increase with the increase in the concentration of RGO in the nanocomposite. But the value of P_{th} decreases with the increase in RGO concentration. The P_{th} values, obtained for 532 nm laser pulses of energy 5 μJ and pulse width 7 ns with on axis intensity I_0 = 138 MW/cm^2 shown in Table (1) are quite impressive and even superior to the values previously reported for polymer nanocomposite films [19].

5.4. Conclusions

The present work is focused on studying the nonlinear optical response of PVDF/RGO nanocomposite films which are quite flexible and freestanding. The addition of RGO to PVDF results in the enhancement of the β phase of PVDF and this has been confirmed by XRD and FTIR spectroscopic studies. The single beam Z-scan experimental results of PVDF/RGO nanocomposite films provide high values of the nonlinear absorption coefficient (β'), which is one of the prime requirements for efficient optical limiting applications. The high values of the various nonlinear coefficients and low values of optical limiting threshold power as evidenced from Table(1), offer ample scope for the use of PVDF/RGO films in the design of nonlinear optical devices. The highlight of the present work is the observation of normalized transmittance as low as 10% and low optical threshold power around 7.84 MW/cm^2 for the flexible and freestanding films of

PVDF/RGO nanocomposite. The above impressive results of the present study are being reported for the first time in free standing and flexible films of polymer nanocomposites. These highly stable, flexible and freestanding films of PVDF/RGO nanocomposite of thickness around 10 μm are quite suitable for the development of efficient optical limiting devices of any shape or size.

References

[1] K. S. Tan, W. C. Gan, T. S. Velayutham, and W. H. A. Majid, Pyroelectricity enhancement of PVDF nanocomposite thin films doped with ZnO nanoparticles, *Smart Mater. Struct.* **23**, 125006 (2014). doi:10.1088/0964-1726/23/12/125006

[2] J. Wang, J. Wu, W. Xu, Q. Zhang, and Q. Fu, Preparation of poly(vinylidene fluoride) films with excellent electric property, improved dielectric property and dominant polar crystalline forms by adding a quaternary phosphorus salt functionalized graphene, *Compos. Sci. Technol.* **91**, 1 (2014). http://dx.doi.org/10.1016/ j.compscitech.2013.11.002

[3] A. P. Indolia and M. S. Gaur, Investigation of structural and thermal characteristics of PVDF/ZnO nanocomposites, *J. Therm. Anal. Calorim.* **113**, 821 -830 (2012). doi 10.1007/s 10973-012-2834-0

[4] B. Jaleh and A. Jabbari, Evaluation of reduced graphene oxide/ZnO effect on properties of PVDF nanocomposite films, *Appl. Surf. Sci.* **320**, 339 (2014). http://dx.doi.org/10.1016/ j.apsusc.2014.09.030 0

[5] P. Indra Devi and K. Ramachandran, Dielectric studies on hybridised PVDF–ZnO nanocomposites, *J. Exp. Nanosci.* vol.6,no.3,June2011. doi:10.1080/17458080.2010.497947.

[6] H. M. Shanshool, M. Yahaya, W. M. M. Yunus, and I. Y. Abdullah, Measurements of Nonlinear Optical Properties of PVDF/ZnO Using Z-Scan Technique, *Brazilian J. Phys*. **45**, 538 (2015). doi:10.1007/s 13538-015-0345-8.

[7] L. Chu, Q. Xue, J. Sun, F. Xia, W. Xing, D. Xia, and M. Dong, Porous graphene sandwich/poly(vinylidene fluoride) composites with high dielectric properties, *Compos. Sci. Technol.* **86**, 70 (2013). http://dx.doi.org/10.1016/ j.compscitech. 2013.07.001

[8] Z. Y. Jiang, G. P. Zheng, Z. Han, Y. Z. Liu, and J. H. Yang, Enhanced ferroelectric and pyroelectric properties of poly(vinylidene fluoride) with addition of graphene oxides, *J. Appl. Phys*. **115**, (2014);); doi: 10.1063/1.4878935

[9] W. Song, C. He, W. Zhang, Y. Gao, Y. Yang, Y. Wu, Z. Chen, X. Li, and Y. Dong, Synthesis and nonlinear optical properties of reduced graphene oxide hybrid material covalently functionalized with zinc phthalocyanine, *Carbon* **77**, 1020 (2014); http://dx.doi.org/10.1016/ j.carbon.2014.06. 018

[10] K. Naseema, M. Shyma, K. B. Manjunatha, A. Muralidharan, G. Umesh, and V. Rao, χ (3) Measurement and Optical Limiting Studies of Urea Picrate, *Opt. Laser Technol*. **43**, 1286 (2011) doi:10.1016/ j.optlastec.2011.03.025

[11] K. Naseema, V.Rao, K. B. Manjunatha, G. Umesh, K.Sujith and B. Kalluraya , Synthesis, characterization and studies on nonlinear optical parameters of 4-amino-5-(4-nitrophenyl)-1, 2, 4-triazole-3-thione , *J .Opt* . 39:143–148 (2010).

[12] X. Zhao, X. Q. Yan, Q. Ma, J. Yao, X. L. Zhang, Z. B. Liu, and J. G. Tian, Nonlinear optical and optical limiting properties of graphene hybrids covalently functionalized by phthalocyanine, *Chem. Phys. Lett.* **577**, 62 (2013) http://dx.doi.org/10.1016/ j.cplett.2013.04.023

[13] Liu ZhiBo, Zhang XiaoLiang, Yan XiaoQing, Chen YongSheng & Tian JianGuo; Nonlinear optical properties of graphene-based materials; *Chinese science bulletin*, August 2012 Vol.57 No.23: 2971 -2982

[14] W. S. Hummers and R. E. Offeman, Preparation of Graphitic Oxide, *J. Am. Chem. Soc*. **80**, 1339 (1958).

[15] J. Shang, Y. Zhang, L. Yu, B. Shen, F. Lv, and P. K. Chu,. Fabrication and dielectric properties of oriented polyvinylidene fluoride nanocomposites incorporated with graphene nanosheets; *Mater Chem. Phys.* **134**, 867 (2012). doi:10.1016/ j.matchemphys.2012.03.082

[16] P. Martins, A. C. Lopes, and S. Lanceros-Mendez, Electroactive phases of poly(vinylidene fluoride): Determination, processing and applications, *Prog. Polym. Sci*. **39**, 683 (2014). http://dx.doi.org/ 10.1016/j.progpolymsci. 2013.07.006

[17] K. Krishnamoorthy , M. Veerapandian , R. Mohan and S.J. Kim, Investigation of Raman and photoluminescence studies of reduced graphene oxide sheets, *Appl Phys A .,Mat.Sci.Proc* 106:501–506 (2012).

[18] J. Sun, L. H. He, Q. L. Zhao, L. F. Cai, R. Song, Y. M. Hao, Z. Ma, and W. Huang, A simple and controllable nanostructure comprising non-conductive poly(vinylidene fluoride) and graphene nanosheets for supercapacitor, *Front. Mater. Sci.* **6**, 149 (2012).

[19] M.N. Muralidharan, S. Mathew , A. Seema , P. Radhakrishnan, Thomas Kurian; Optical limiting properties of in situ reduced graphene oxide/polymer nanocomposites, *Materials Chemistry and Physics,* 171 (2016) 367-373; http://dx.doi.org/ 10.1016/ j.matchemphys.2016.01.030

[20] Hongfei Shi, Can Wang, Zhipei Sun, Yueliang Zhou, Kuijuan Jin, Simon A. T. Redfern, and Guozhen Yang; Tuning the nonlinear optical absorption ofreduced graphene oxide by chemical reduction**,** *Optics Express* Vol. 22,11 August 2014, No. 16

[21] S. M. G. Rabbani, S. M. Sharif, Y. Haque, S. K. Das, and N. Chawdhury, Measurement of the Nonlinear Refractive Index of LiNb0 3 by Z-scan Technique, *SUST Journal of Science and Technology,* **16**, 22 (2012).

[22] K. Senthil, S. Kalainathan, A. R. Kumar and P. G. Aravindan, Investigation of synthesis, crystal structure and third-order NLO properties of a new stilbazolium derivative crystal: a promising material for nonlinear optical devices, *RSC Adv.* **4**, 56112 (2014); doi: 10.1039/c4ra09112d

[23] Z. Liu, Y. Wang, X. Zhang, Y. Xu, Y. Chen, and J. Tian, Nonlinear optical properties of graphene oxide in nanosecond and picosecond regimes, *Appl. Phys. Lett*. **94**, (2009); doi: 10.1063/1.3068498

[24] Z. Liu, X. Zhang, X. Yan, Y. Chen, and J. Tian, Nonlinear optical properties of graphene-based materials, *Chinese Sci. Bull.* **57**, 2971 (2012).

[25] M. Sheik-Bahae, A. A. Said, T. H. Wei, D. J. Hagan, and E. W. Van Stryland, Sensitive Measurement of Optical Nonlinearities Using a Single Beam, *IEEE J. Quantum Electron*. **26**, 760 (1990).

[26] P. P. Jeeju, S. Jayalekshmi, K. Chandrasekharan, and P. Sudheesh, Enhanced linear and nonlinear optical properties of thermally stable ZnO/poly(styrene)-poly(methyl methacrylate) nanocomposite films, *Thin Solid Films* **531**, 378 (2013). http://dx.doi.org/10.1016/ j.tsf.2012.12.043

[27] P. P. Jeeju, S. Jayalekshmi, K. Chandrasekharan, and P. Sudheesh, Size dependent nonlinear optical properties of spin coated zinc oxide-polystyrene nanocomposite films, *Opt. Commun.* **285**, 5433 (2012). http://dx.doi.org/10.1016/ j.optcom.2012.07.078

[28] R. Sreeja, J. John, P. M. Aneesh, and M. K. Jayaraj, Linear and nonlinear optical properties of luminescent ZnO nanoparticles embedded in PMMA matrix, *Opt. Commun*. **283**, 2908 (2010). doi:10.1016/j.optcom.2010.02.044

[29] E. W. Van Stryland and M. Sheik-Bahae, Z-Scan Measurements of Optical Nonlinearities, *Charact. Tech. Tabul. Org. Nonlinear Mater*. 655 (1998).

[30] N. K. Siji Narendran, R. Soman, P. Sankar, C. Arunkumar, and K. Chandrasekharan, Ultrafast and short pulse optical nonlinearities of meso-tetrakis-(2,3,5,6-tetrafluoro-N,N,N-trimethyl-4-aniliniumyl) porphyrin and its metal complexes, *Opt. Mater*. (Amst). **49**, 59 (2015).http://dx.doi.org/10.1016/ j.optmat.2015.08.018 0925-3467/

[31] P. Sudheesh, N. K. Siji Narendran, and K. Chandrasekharan, Third-order nonlinear optical responses in derivatives of phenylhydrazone by Z-scan and optical limiting studies-influence of noble metal nanoparticles, *Opt. Mater*. (Amst). **36**, 304 (2013). http://dx.doi.org/ 10.1016/j.optmat.2013. 09.014

[32] Bing Gu, Hui Tan Wang and Wei Ji; Z-scan technique for investigation of the non instantaneous optical Kerr non-linearity; *Optics Letters* 34 (2009) 2769-277

[33] Mohd Anis , Gajanan.G. Muley;Bulk growth of undoped and Nd^{3+} doped zinc thiourea chloride (ZTC) monocrystal: Exploring the remarkably enhanced structural, optical, electrical and mechanical performance of Nd^{3+} doped ZTC crystal for NLO device applications; *Optics and Laser Technology* 90 (2017) 190-196; http://dx.doi.org/ 10.1016/ j.optlastec.2016.11.020

[34] Mohd Anis, D.A. Hakeem , G.G. Muley ; Optical and dielectric studies of KH_2PO_4 crystal influenced by organic ligand of citric acid and L-valine: A single crystal growth and comparative study; *Results in Physics* 6 (2016) 645-650; http://dx.doi.org/ 10.1016/j.rinp.2016.09.001 2211

[35] S.M. Azhar , Mohd Anis , S.S. Hussaini , S. Kalainathan , M.D. Shirsat , G. Rabbani ; Doping effect of L-cystine on structural, UV–visible, SHG efficiency, third order nonlinear optical, laser damage threshold and surface properties of cadmium thiourea acetate single crystal; *Optics and Laser Technology* 87 (2017) 11-16; http://dx.doi.org/10.1016/ j.optlastec.2016.07.007

[36] Mohd Anis , G.G. Muley, A. Hakeem, M.D. Shirsat, S.S. Hussaini ; Exploring the influence of carboxylic acids on nonlinear optical (NLO) and dielectric properties of KDP crystal for applications of NLO facilitated photonic devices; *Optical Materials* 46 (2015) 517-521; http://dx.doi.org/10.1016/j.optmat.2015.04.064 ;

[37] I.Sebastian, S.Mathew, V.P.N.Nampoori, P. Radhakrishnan and S.Thomas, Concentration tuned bandgap and corresponding nonlinear refractive index dispersion in Ga-Ge-Se nanocolloids, *J. Appl. Phys.* **114**, (2013). doi: 10.1063/1.4817176

[38] M. Feng, H. Zhan, and Y. Chen, Nonlinear optical and optical limiting properties of graphene families, *Appl. Phys. Lett.* **96**, 2008 (2010) doi: 10.1063/1.3279148

Chapter 6

On the absorption dominated EMI shielding effects in freestanding and flexible films of PVDF/graphene nanocomposite

Contents

This chapter begins with the introductory ideas on the polluting effects of electromagnetic interference (EMI) due to the proliferation of electronic devices and the urgent necessity of developing suitable shielding materials against these interferences. The merits of the shielding materials based on polymer nanocomposites compared to conventional metallic shields are emphasized and the discussion proceeds to the focal theme of the present chapter. The work presented in this chapter highlights the remarkably high electro-magnetic interference (EMI) shielding effectiveness of about 47dB, exhibited by highly conducting and ordered poly(vinylidene fluoride) (PVDF)/graphene nanocomposite films of thickness around 20 microns, in the microwave frequency range 8–12 GHz, obtained by solution casting method. The high electrical conductivity of the composite films around 16 S/cm promotes shielding by absorption losses which is of ample significance in stealth applications. The present results identify the PVDF/graphene nanocomposite film as an effective, lightweight, flexible and mechanically and thermally stable, absorption dominated EMI shielding material with application prospects in a broad range of the electromagnetic spectrum. The freestanding and flexible nature of these films facilitates EMI shielding applications without the geometrical constraints of the shape or size of the object.

6.1. Introduction

The unprecedented technological developments during the last few decades in the field of electronics and communication and the subsequent proliferation of devices like mobile phones, laptop computers, Wi-Fi devices, modern radar systems and high speed communication systems in academic, military, industrial, healthcare and business sectors have resulted in the need for identifying suitable materials to handle the polluting effects of electromagnetic interference (EMI). This silent pollution of EMI is the undesirable and hysterical outcome of the explosive growth of electronic devices and the widespread use of transient power sources. Most common example of EMI is the cross communication of our laptop computers or radio speakers with mobile signals resulting in picture flicker or buzzing sounds. As the use of electronic gadgets has increased manifold these days, it is possible that the smooth functioning of electronic circuits gets disrupted in the vicinity of electromagnetic fields emitted by other electronic devices. Electromagnetic interference (EMI) usually occurs in the frequency range of 10^4 to 10^{12} Hz of the electromagnetic spectrum and can be both natural and man-made [1-5].

Recent studies have revealed that exposure to electromagnetic radiation for a prolonged period of time may cause health hazards to human life. The solution to these concerns is to minimize the effects of the interfering electromagnetic radiations by absorption and/or reflection

of the radiations using proper shielding materials. Limiting the transmission of electromagnetic radiation by reflection and/or absorption of the radiation by a material is termed as electromagnetic interference (EMI) shielding and the material does the job of a shield to inhibit the penetration of the radiation through it [6-9].

Considerable research efforts have been focused on developing cost effective and lightweight EMI shielding materials during the past two decades to address the adverse effects of EMI. When metals are used as EMI shields, their shortcomings like heavy weight, physical rigidity, susceptibility to corrosion and poor and complex processability pose challenges. There is hence a greater demand for light-weight, flexible, non-corrosive and processable EMI shielding materials [10-15]. Compared with conventional metals, polymer nanocomposites represent a novel class of materials that possess an exclusive combination of electrical, thermal, magnetic and mechanical properties which are helpful for the suppression of electromagnetic noises [16-20]. The EMI shielding effectiveness (SE) of a nanocomposite material mainly depends on the intrinsic conductivity, dielectric constant and the aspect ratio of the filler material. Compounding of polymers with conducting fillers is an effective technique to improve the electrical conductivity of polymers and to shield the E.M.I [17,18,21].

Poly (vinylidene fluoride) (PVDF) is a semi-crystalline fluoro polymer with a repeat unit of CH_2-CF_2, well-known for its excellent

ferroelectric, pyroelectric and piezoelectric properties and is known to possess good acid and solvent resistance properties, high thermal and mechanical stability and can be used in polymer sensors, actuators and transducers [22-25]. Graphene has been preferred over other conventional nanofillers, owing to its remarkable properties like high surface area, high aspect ratio, good tensile strength, quite high thermal and electrical conductivity, good flexibility and transparency. It has been reported that the improvement in mechanical and electrical properties of graphene based polymer nanocomposites is much better compared to that of clay, carbon nanotubes or other carbon filler based polymer nanocomposites. Since graphene has negligible mass and is ultrathin, transparent and flexible, it will be an excellent choice for making nanocomposites for light weight EMI shielding applications for portable electronic devices and in transparent electronics. [14],[26-31].

Previous studies have shown that incorporating carbonyl group containing fillers into the PVDF matrix results in their homogenous dispersion or distribution because of the strong and specific interaction between the fluorine group of PVDF and the carbonyl group at the filler's surface.

There is electrostatic interaction between the functional groups at the surface of graphene and the CH_2-CF_2 dipole of PVDF which leads to the transformation from the helix TGTG conformation of the α phase to the zigzag TTTT conformation of the β phase. This results in the

formation of a β polymorph structure of PVDF as well as in the improvement of the electrical, thermal and mechanical properties of such nanocomposites [32,33]. Graphene is not generally dispersible in polymers and it can be made dispersible by means of acid purification. The electrical conductivity of acid purified graphene is found to be comparatively higher.

When EMI shielding effectiveness increases, transmittance through the shielding material decreases. When an EM wave is incident on a shield, reflection takes place at its surface followed by some extent of absorption and transmission. This idea is used in the development of effective EMI shielding materials [9,10,17,34]. Polymer composites containing carbon-based fillers like graphite, carbon black, carbon fibers, carbon nanofibers, carbon nanotubes and graphene have extended excellent scope in microwave absorption applications owing to their high electrical conductivity, polymeric flexibility, light weight, low cost and easy processability [2,9,13,17].The present study is focused on developing a low cost, light weight and flexible EMI shielding material using purified graphene reinforced PVDF composite. The highlight of the present work is the observation of remarkably high values of EMI SE around 47dB over a broad range of microwave frequencies (8-12GHz), in highly ordered and conducting films of PVDF/graphene nanocomposite, having micrometer thickness.

6.2. Experimental Details

6.2.1. Materials and methods

Poly(vinylidene fluoride) granules (product code RM 4439) for the present work were obtained from Hi-Media Laboratories Private Limited, Mumbai and dimethyl formamide (DMF) and hydrochloric acid (HCl),from Spectrochem Private Limited, Mumbai. High pure graphene was purchased from Graphene super market, U.S.A. The purchased graphene was purified by treating with concentrated HCl in a conical flask and stirring vigorously for 5 hours. It was then washed well with de-ionized water and filtered .The filtrate was dried in a hot air oven overnight.

For making the PVDF/graphene nanocomposite films, the purified graphene flakes were initially dispersed in DMF solvent by ultrasonication for 24 hours. In a typical procedure, 1 gm of PVDF was dispersed in 10 ml of DMF under magnetic stirring at 60 ° C for 2 hours. The graphene / DMF dispersion was added to the solution of PVDF in DMF and the mixed solution was again sonicated for 2 hours. The resulting nanocomposite solution was poured into a petri-dish and kept in a vacuum oven at 60 °C for 2 hours. Flexible and free standing films of the PVDF/graphene nanocomposite could be peeled off the petri-dish after drying. The synthesis procedure adopted is represented in Scheme 1given below.

The experiment was repeated for 2, 5,10 and 15 weight percentages of graphene in the nanocomposite samples. The nanocomposite film samples were cut into the required dimensions for the EMI shielding measurements.

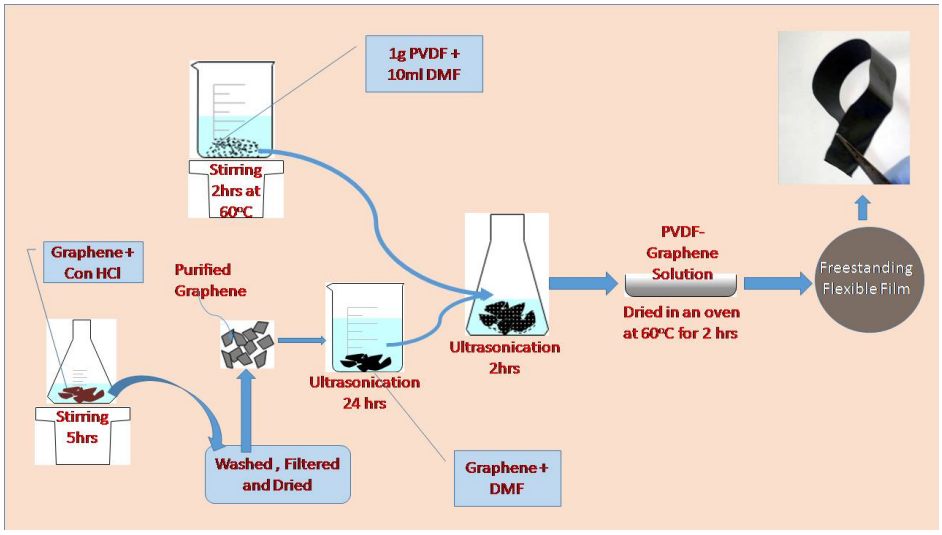

Scheme 1: Schematic representation of the growth of PVDF/graphene nanocomposite films

6.2.2. Characterization of the film samples

The X- ray diffraction (XRD) patterns of the nanocomposite films were obtained using a Rigaku X-ray diffractometer. The Fourier transform infrared (FTIR) spectra of the samples were recorded using a Shimadzu spectrophotometer in the wave number range 400–2500 cm^{-1} with a resolution of $4cm^{-1}$. Thermo gravimetric analysis (TGA) of the nanocomposite films was carried out on a Perkin Elmer, Diamond TG/DTA instrument and the mechanical stability of the films was tested with the Universal Testing Machine, Tinius Olesan, ASTM-D-638. Raman spectra were recorded using high resolution Raman spectrometer (Horiba JY) and FESEM images, using ZEISS Sigma field emission scanning electron microscope and TEM images using model JEM 2100

of JEOL Ltd, Japan. The electrical characterization of the film samples was carried out at room temperature using the Hall measurement unit Ecopia HMS-5300. The EMI shielding measurements of the films were done using wave guide transmission line technique in the Vector Network Analyser (Agilent-model PNA E8362B; 10 MHz to 20 GHz).

6.3. Results and Discussion

6. 3.1. X-Ray Diffraction (XRD) analysis

The XRD patterns of PVDF film and PVDF/graphene composite films are shown in figure (1).

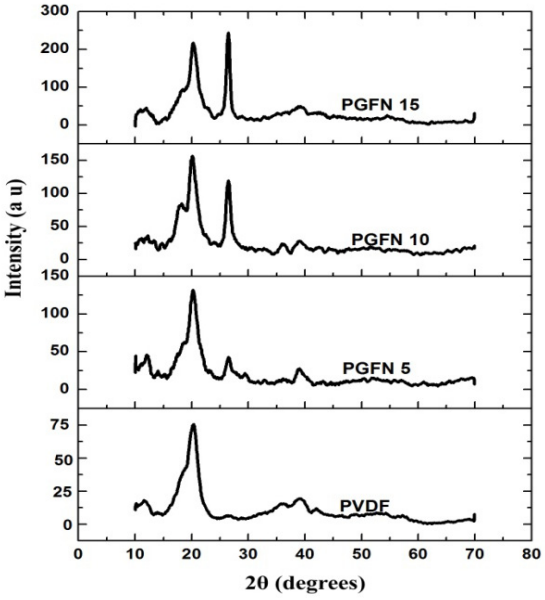

Fig. (1) XRD patterns of PVDF and PVDF/graphene films

In the figure, the symbols, PGFN 5, PGFN 10 and PGFN 15 refer to nanocomposite films with graphene concentrations of 5%, 10% and 15% respectively. There are peaks observed at 20.2° and 26° for the PVDF/graphene film samples. The peak at 20.2° corresponds to reflections from the β form of PVDF planes and that at 26° to graphene planes respectively. The increase in the intensity of the peak at 20.2°, with increasing graphene concentration, is a clear indication of the enhancement in the β phase of PVDF with the addition of graphene [32,35]

6.3.2. Raman spectral analysis

Raman spectra were recorded in the range 300 – 3000 cm^{-1}, using He-Ne laser as the source, having a wavelength of 633 nm, and using a CCD detector.

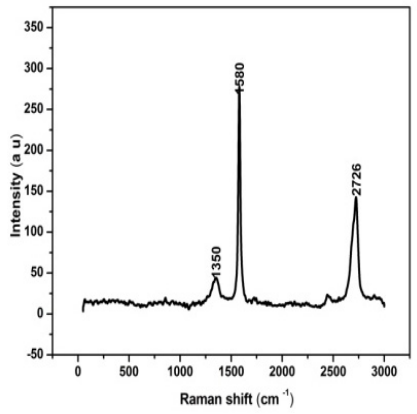

Fig. (2a) Raman spectrum of graphene

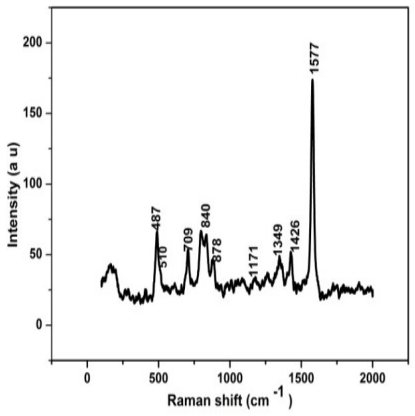

Fig. (2b) Raman spectrum of PVDF/ graphene film

In the Raman spectrum of graphene, shown in figure (2a), the D-mode appears at 1350 cm^{-1}, G-mode at 1580 cm^{-1} and 2D mode at 2726 cm^{-1}respectively. In the spectrum of PVDF/graphene composite film, shown in figure (2b), the peaks at 510 cm^{-1} corresponding to CF_2 bending and at 840 cm^{-1}, attributed to CH_2 rocking again confirm the enhancement in the β phase of PVDF with the addition of graphene [36]. The peaks at 878, 1171 and 1426 cm^{-1} can be assigned to C-C bond vibration, the stretching mode of CF_2 bond and the CH_2 deformation mode respectively of PVDF. The peaks at 487, 709 and 1349 cm^{-1} can be assigned to the α phase of PVDF.

6.3.3. Fourier Transform Infrared (FTIR) spectroscopic analysis

The FTIR spectra in the ATR mode for PVDF film and PVDF/ graphene film are shown in figure (3a) and figure (3b) respectively. The peaks at 766 and 976 cm^{-1} are typical of the α phase of PVDF. The important peaks of PVDF found in all polymorphs are the ones at 878 and 1170 cm^{-1}, corresponding to C-C bond vibrations and the stretching vibrations of CF_2 bond respectively. The intensity of the characteristic absorption peak at 840 cm^{-1} corresponding to CH_2 rocking, and at 1226 cm^{-1} due to CF_2 bending modes of the β phase of PVDF is found to be enhanced in the spectrum of PVDF/ graphene film.

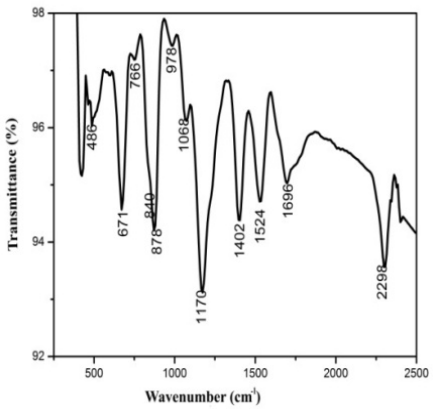

Fig. (3a) FTIR spectrum of PVDF film

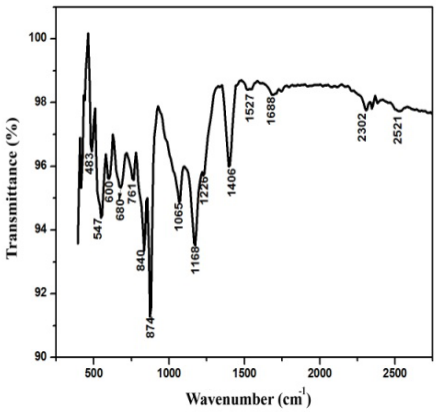

Fig. (3b) FTIR spectrum of PVDF/ graphene film

The peak at 976 cm^{-1}, attributed to the α phase of PVDF is clearly seen in the spectrum of the pristine PVDF film, but is absent in the spectrum of the PVDF/graphene nanocomposite film. These observations provide conclusive evidence for the enhancement of the β phase of PVDF on the addition of graphene [36].

6.3.4. Morphological studies

The field emission scanning electron microscopy image (FESEM) of the graphene nanoflakes is shown in figure (4a) and that of PVDF/graphene hybrid film in figure (4b). The dense dispersion of graphene within the PVDF matrix and the interconnectivity between graphene flakes are illustrated in the FESEM image of the PVDF/graphene composite film shown in figure 4(b). The selected area electron diffraction

(SAED) pattern and the TEM image of PVDF/graphene film are shown in figure (5a) and figure (5b) respectively.

From the SAED pattern shown in figure (5a), the crystalline nature of the PVDF/graphene film can be confirmed. Eventhough PVDF is a semi-crystalline polymer, PVDF/graphene film shows higher extent of crystallinity. This is because of the increase in the highly ordered β phase of PVDF, in the PVDF/graphene film samples. The TEM image of PVDF/graphene film ensures the dispersion of graphene in the PVDF matrix and graphene is seen like a transparent coating on the polymer matrix.

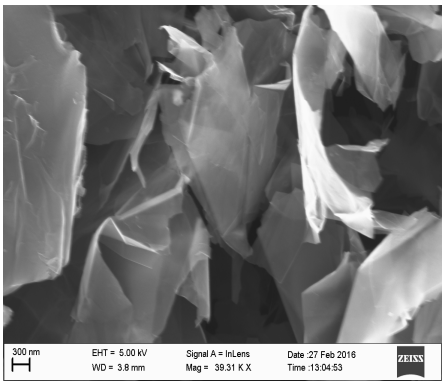

Fig. (4a) FESEM image of graphene

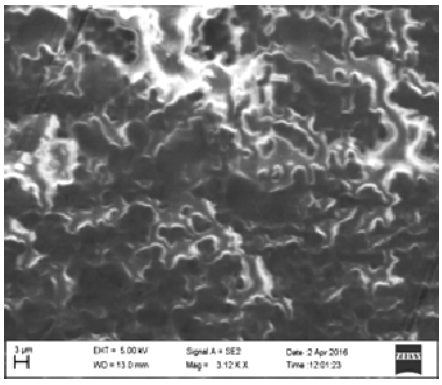

Fig. (4b) FESEM image of PVDF/ graphene film

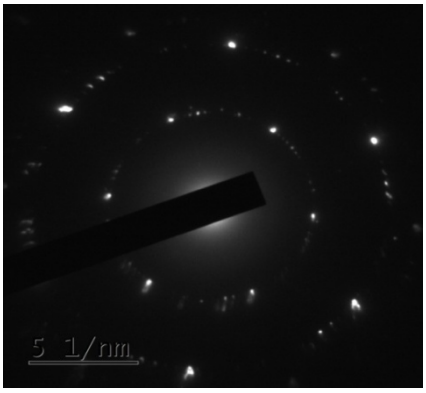

Fig. (5a) SAED pattern of PVDF /graphene film

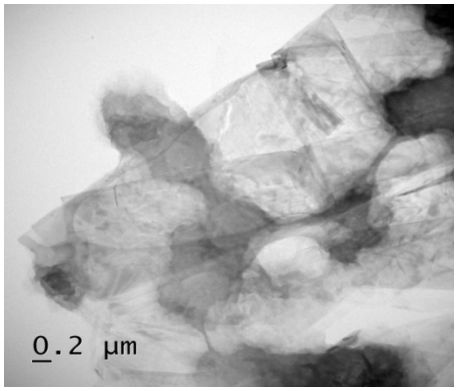

Fig. (5b) TEM image of PVDF/ graphene film

6.3.5. Measurement of thermal and mechanical stability

(a) Thermal studies

The thermal stability of the nanocomposite film was studied using thermo gravimetric analysis (TGA). In figures (6a) and (6b), curve (1) refers to PVDF film and curve (2) to PVDF/graphene nanocomposite film.

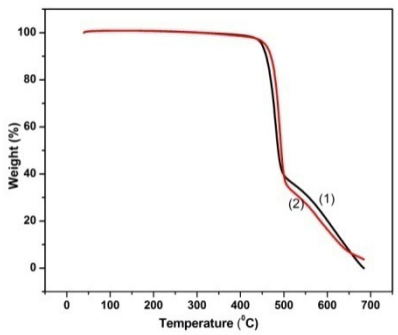

Fig. (6a) TGA plots of PVDF and PVDF/graphene films

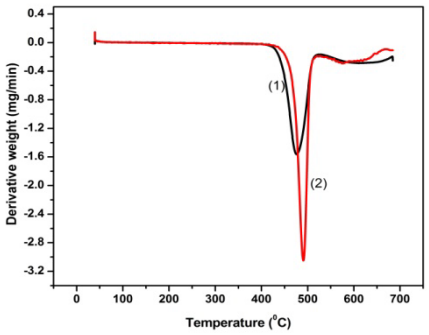

Fig. (6b) DTG curves of PVDF and PVDF/graphene films

The film samples were heated to 700 °C at a scan rate of 10 °C per minute in nitrogen atmosphere. It can be observed that pure PVDF decomposes at temperature of 440 °C whereas for PVDF/graphene film samples, the decomposition temperature is increased by about 15 °C. In order to increase the resolution of TGA analysis, the first derivative of the mass loss versus the temperature (DTG) was plotted and the plot is shown in figure (6b). It is noticed that the temperature at which the mass loss rate is maximum (inflection temperature T_i) shifts to higher temperatures in the nanocomposite sample, as a result of the addition of graphene. The high temperature shift of T_i demonstrates the enhancement of the thermal stability of the composite film. The higher thermal stability of the nanocomposite sample makes it suitable for high temperature EMI shielding applications.

(b) Mechanical studies

The mechanical studies were carried out using Universal Testing Machine, Tinius Olesan (ASTM-D-638). The samples were cut into pieces of dimensions 10 cmx1cm, and a force of 500N was applied at a crosshead speed of 10 mm/min. The stress Vs strain curve is shown in figure (7).

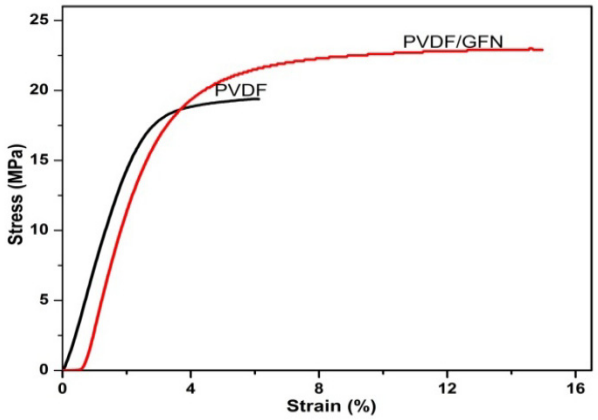

Fig. (7) Stress-Strain curve

The Young's modulus and tensile strength of PVDF are found to increase, by the addition of graphene as evidenced from the Table (1).

Table (1) Mechanical parameters

Sample name	Tensile strength (MPa)	Elongation at break	Young's modulus (MPa)
PVDF film	19.4	6.53 %	806
PVDF/graphene film	23	14.35 %	909

6.3.6. Measurement of electrical transport parameters

The dc electrical conductivity, resistivity, charge carrier concentration and the mobility of the majority charge carriers of the nanocomposite films were evaluated using the Hall measurement technique and the data is given in Table (2). It is observed that the dc electrical conductivity increases with increase in graphene concentration in the nanocomposite. Higher electrical conductivity is expected to

enhance the shielding effectiveness. In Table (2), the symbols, PGFN 2, PGFN 5, PGFN 10 and PGFN 15 refer to nanocomposite films with graphene concentrations of 2%, 5%, 10% and 15% respectively. The maximum electrical conductivity of the PVDF/ graphene film is around 16 S/cm, which is about 10^9 times higher than that of PVDF film. The continuous ultrasonication of the graphene flakes in DMF and that of PVDF/DMF solution with graphene/DMF solution for many hours can result in a homogenous dispersion of graphene within the PVDF host matrix with good extent of connectivity among the dispersed graphene flakes as evidenced from the FESEM images. The connectivity among the graphene flakes combined with the high carrier concentration and carrier mobility give rise to the observed high electrical conductivity of the PVDF/graphene nanocomposite films, which is quite significant for effective EMI shielding action [9,17].

Table. (2) Hall measurement data of PVDF/graphene film

Sample	Conductivity S/cm	Resistivity Ω cm	Mobility cm^2/Vs	Carrier Concentration $/cm^3$
PGFN 2	2.085	0.4796	0.1476	8.82 E19
PGFN 5	5.11	0.1957	0.1877	16.99 E19
PGFN 10	10.33	0.09682	0.7136	9.035 E19
PGFN15	16.03	0.06238	0.5421	18.46 E19

6.3.7. Measurement of EMI Shielding Effectiveness

The experimental setup for the measurement of EMI shielding effectiveness is shown in figure (6a). The schematic representation of the setup is shown in figure (6b) and the sample holder and the PVDF/graphene composite sample in the form of a free standing flexible film are shown in figure (6c). Free standing PVDF/graphene nanocomposite films of 20 micrometer thickness were inserted between standard C and X band rectangular waveguide adapter of the network analyser. The scattering parameters (S-parameters) corresponding to the transmission (S_{12}/S_{21}) and reflection (S_{11}/S_{22}) of the electromagnetic waves from the film samples were recorded over the C band and X band of the microwave radiation in the 4-8 GHz and 8-12 GHz frequency ranges respectively. The dimensions of the waveguides used were 34.8 x 15.7 mm^2 for the C-band and 22.8 x10.1 mm^2 for the X-band. The film samples were cut into the required dimensions and separate experiments were conducted for each band. The propagation of electromagnetic waves through a shielding material results in the attenuation of the incident radiation. The EMI shielding effectiveness gives a measure of this attenuation. The characteristic of a good shielding material is that it should cause maximum attenuation of the EM wave by reflection or absorption with negligible transmission. The commercially fixed standard for typical EMI shielding materials corresponds to shielding effectiveness value of 20 dB, which is equivalent to an attenuation of 99 % of the total incident energy [10].

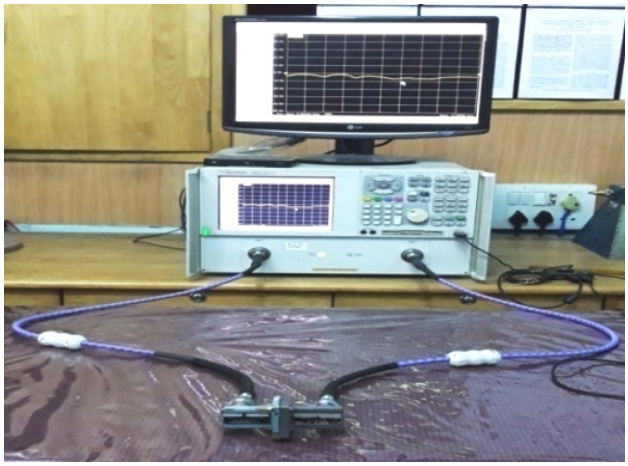

Fig. (8a) Experimental setup for SE measurement

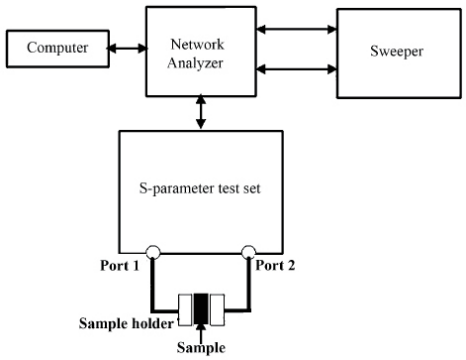

Fig. (8b) Schematic diagram of the set-up

Fig. (8c) Sample holder and sample

The EMI SE of a material is defined by the following equation

$$SE \text{ (in decibel)} = 10 \log_{10} (P_i/P_t) \quad (1)$$

where P_i and P_t refer to the incident power and transmitted power of electro-magnetic waves respectively. When electromagnetic radiation is incident on a shielding material, phenomena such as reflection,

absorption and transmission take place. The total EMI SE (SE_{tot}) is the sum of the SE due to absorption (SE_A), reflection (SE_R) and multiple reflections (SE_M).

$$SE_{tot} = SE_A + SE_R + SE_M \quad (2)$$

When SE_A is greater than 10dB, SE_M becomes negligible and can be safely neglected.

The S-parameters S_{11} (or S_{22}) and S_{12} (or S_{21}), which can be correlated with the reflectance R and transmittance T are given by the following equations,

$R = |S_{11}|^2 = |S_{22}|^2$; $T = |S_{12}|^2 = |S_{21}|^2$; giving absorbance as, $A = (1-R-T)$.

The experimental reflection and absorption losses can be expressed as [9,10,17,37,38]

$$SE_R = -10 \log_{10} (1-R) \quad (3)$$

$$SE_A = -10 \log_{10} [T/(1-R)] \quad (4)$$

The novelty of the present work is that, quite high values of SE around 47 dB are obtained in the X-band frequency range, for micrometer thick, free standing and flexible films of PVDF/graphene nanocomposite with 15% graphene loading, without adding foaming agents or surfactants. Moreover, the graphene used is rather pristine graphene without any functional groups attached. The synthesis method adopted in the present work is quite simple and cost effective. The observed, high value of the shielding effectiveness of the present work

can be attributed to the high electrical conductivity of the PVDF/graphene film. The EMI SE values of PVDF/graphene films in the C band and X band frequency range of the electromagnetic spectrum are shown in figures (9a) and (9b) respectively. Graphs (1), (2), (3) and (4) correspond to 2%, 5%, 10% and 15% of graphene loading in the PVDF/graphene film.

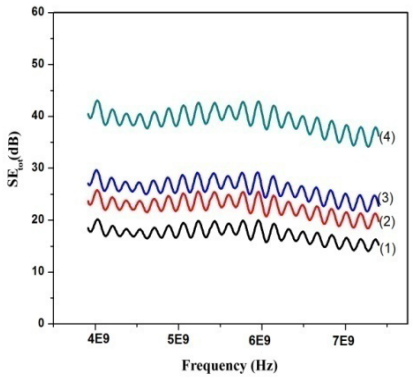

Fig. (9a) SE_{tot} as a function of frequency in C- band

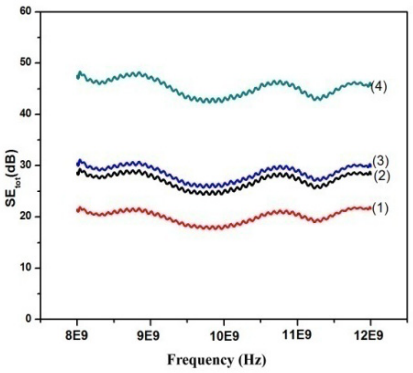

Fig. (9b) SE_{tot} as a function of frequency in X- band

The total shielding effectiveness comes to around 42 dB in the C band (4-8 GHz) and 47dB in the X band (8-12 GHz) respectively. The increase in EMI SE with increasing frequency is due to the decrease in skin depth of the material with increasing frequency [14]. The EMI shielding effectiveness of nanocomposite films depends on many factors like the electrical conductivity of the composite film, the size and shape of the nanostructured filler materials in the matrix and the extent of their dispersion in the host matrix. The high electrical conductivity of the

PVDF/graphene nanocomposite films and the homogenous dispersion of graphene in the PVDF matrix are the prime factors responsible for the impressive EMI shielding behaviour of these nanocomposite films.

The shielding effectiveness increases with the increase in the concentration of graphene in the nanocomposite as shown in the table (3) and the shielding due to absorption losses predominates over that due to reflection losses. As evident from table (3), the primary contribution to total EMI SE is due to absorption rather than reflection in the frequency range studied. On the basis of the above results, it can be inferred that the major shielding mechanism of PVDF/graphene composite is absorption mediated with a small contribution from reflection effects. This suggests that the PVDF/graphene nanocomposite films of the present work are good EM absorbers and may be used as radar absorbing materials.

Table (3) Variation of shielding effectiveness with graphene concentration at 8GHz

SAMPLE	SE Absorption	SE Reflection	SE Total
PGFN 2	20.75	0.698	21.45
PGFN 5	27.50	1.162	28.67
PGFN 10	29.18	1.302	30.48
PGFN 15	45.36	2.170	47.53

The SE_R and SE_A are related to the electrical conductivity of composite as given in the following equations [9]

$$SE_R = -10 \log\left(\frac{\sigma}{16\varepsilon\omega\mu}\right) \quad (5)$$

$$SE_A = -8.68\, t\left(\sqrt{\frac{\sigma\omega\mu}{2}}\right) \quad (6)$$

Here σ is the electrical conductivity, ε the permittivity, μ the magnetic permeability and t the thickness of the shielding material and ω, the angular frequency of the electromagnetic radiation. It can be inferred from equation (6) that changes in the absorption losses will be more pronounced than those in the reflection losses, by changes in electrical conductivity, assuming the other parameters to be invariant. This aspect is especially valid in the present studies. The samples which exhibit higher electrical conductivity show higher absorption losses as well. Because of the high EM absorption properties, these PVDF/graphene nanocomposite films have high application prospects in stealth technology as well.

To conclude the discussion, we have compared our results with those reported in the literature and the data are comprehensively presented in Table 4. It can be seen that the EMI shielding characteristics obtained in the present study are superior to those reported in the studies mentioned in Table 4, except in the work reported by Sudheer Kumar et al (ref.9). However, in this work, the thickness of the films used is more than ten times the thickness our films and the films are grown by melt mixing rather than the simple method of solution casting adopted in our work.

Table. (4). Comparison of EMI shielding characteristics obtained in the present study with those of the various PVDF composites reported in the literature

Polymer Matrix	Filler	Concentration of the filler	Thickness	Frequency (GHz)	Max.SE (dB)	Method	Reference
PVDF foam	f- .graphene	5 wt%	------	8-12	20	Solution cast	13
PVDF	CNT	3 wt%	1 mm	8-18	31	Solution cast	41
PVDF	CNT/BT.GO	3wt% / 5 vol%	1 mm	8-18	31	Solution cast	41
PVDF	CNT/Co NWs	3 wt% / 2.2 vol%	1 mm	8-18	35	Solution cast	41
PVDF	$BaTiO_3$/Ag	20 vol% / 10vol%	1.2 mm	8-12	26	Solution cast	40
PVDF	Carbonyl Fe powder	50 vol%	1.2 mm	8-12	20	Solution cast	42
PVDF	f-MWNT	4 wt%	0.3 mm	8-12	58	Melt mixing	9
PVDF	f-MWNTs	0.5 wt%	0.3 mm	8-12	47	Melt mixing	9
PVDF	MWCNTs	3 wt%	0.5 mm	8-12	21.6	Solution cast	19
PVDF	MWCNTs/Au Nps	3 wt% / 3 wt%	0.5 mm	8-12	26.71	Solution cast	19
PVDF	Graphene / RGO/ CuS	5 wt%	2.5 mm	2-18	32.7	Solution cast	43
PVDF	Nickel	40 vol%	1.95 mm	8-12	20-26	Blending and Hot moulding	39
PVDF	MnO_2 nanotubes/ f-MWCNTs	5 wt% MNTs/ 2 wt% f-MWNTs	----------	8-12	20	Solution cast	1
PVDF	Acid treated graphene	15 wt%	20 μm	8-12	47	Solution cast	Our work

6.4 Conclusions

The present work highlights the development of free-standing, flexible, thermally and mechanically stable films of PVDF/ graphene nanocomposite of about 20 microns thickness, showing quite remarkable, absorption dominated EMI shielding properties, with prospective applications as efficient and light weight shielding materials. The synthesis method adopted in the present work is quite simple and cost effective. On the addition of graphene, there is an enhancement in the highly ordered β phase of PVDF, which is one of the prime reasons for the enormous increase in the electrical conductivity and the high EMI shielding effectiveness of the composite material. The EMI SE value of 47dB observed in the present work for the PVDF/graphene nanocomposite film samples is so far the highest value reported in the X-band frequency region in these types of nanocomposite, free standing films of micrometer thickness. These highly conducting films having remarkable EMI shielding effectiveness are ideal as excellent shielding materials and the absorption dominated shielding properties of these films are quite suitable for stealth applications. Since these films are free standing and flexible, they are suitable for EMI shielding applications without the geometrical constraints of the shape or size of the object.

References

[1] Varrla Eswaraiah, Venkataraman Sankaranarayanan, Sundara Ramaprabhu; "Inorganic nanotubes reinforced polyvinylidene fluoride composites as low-cost electromagnetic interference shielding materials" ; Nanoscale Res. Lett. (2011) 6:137; doi: 10.1186/1556-276x-6-137.

[2] Parveen Saini, Veena Choudhary; "Enhanced electromagnetic interference shielding effectiveness of polyaniline functionalized carbon nanotubes filled polystyrene composites" J . Nanopart. Res. (2013) 15:1415; doi 10.1007/s11051-012-1415-2.

[3] Weiwei Liu, Hua Li, Qingping Zeng, Huanan Duan, Yiping Guo, Xuefa Liu, "Fabrication of ultralight three-dimensional graphene networks with strong electromagnetic wave absorption properties"; J. Mater. Chem. A, 2015, 3, 3739; doi: 10.1039/ c4ta06091a .

[4] Pradeep Sambyal, Avanish Pratap Singh, Meenakshi Verma, M. Farukh, Bhanu Pratap Singh and S. K. Dhawan; "Tailored polyaniline/ barium strontium titanate/ expanded graphite multiphase composite for efficient radar absorption" RSC Adv., (2014) 4, 12614; doi: 10.1039/c3ra46479b

[5] D. Micheli, C. Apollo, R. Pastore, M. Marchetti; "X-Band microwave characterization of carbon-based nanocomposite material, absorption capability comparison and RAS design simulation", Compos. Sci. Tech. (2009) doi:10.1016/ j.compscitech.2009.11.015

[6] S. Geetha, K. K. Satheesh Kumar and C. R. K. Rao; "EMI shielding: methods and materials-a review"; J. Appl. Polym. Sci.; Vol. 112, 2073–2086 (2009); doi. 10.1002/app.29812

[7] Vaibhav Kasar, Aditya Pawar; "A Novel Approach to Electromagnetic Interference Shielding for Cell Phones"; Int. Jou. Science and Research (IJSR) (2014) Volume 3, Issue 11 ISSN (Online): 2319-7064 .

[8] K.Jagadeesan, A.Ramasamy, A.Das, A.Basu; "Electromagnetic shielding behaviour of conductive filler composites and conductive fabrics – A review "; Indian Journal of Fibre and Textile Research. (2014) Vol.39, pp 329-342.

[9] G. Sudheer Kumar, D. Vishnupriya, Anupama Joshi, Suwarna Datar and T. Umasankar Patro; "Electromagnetic interference shielding in 1–18 GHz frequency and electrical property correlations in poly(vinylidene fluoride)/ multi-walled carbon nanotube composites"; Phys.Chem. Chem.Phys. (2015) 17, 20347; doi: 10.1039/c5cp02585k

[10] Ranjini R. Mohan, Sreekanth J. Varma, Muhammad Faisal and Jayalekshmi S; "Polyaniline /graphene hybrid film as an effective broadband electromagnetic shield" RSC Adv.; (2015) 5, 5917; doi: 10.1039/c4ra13704c.

[11] Wei-Li Song, Mao-Sheng Cao, Ming-Ming Lu, Song Bi, Chan-Yuan Wang, Jia Liu, "Flexible graphene/polymer composite films in sandwich structures for effective EMI Shielding"; Carbon 2013; http://dx.doi.org/10.1016/j.carbon. 2013.08.043;

[12] Yonglai Yang, Mool C Gupta and Kenneth L Dudley ; "Towards cost-efficient EMI shielding materials using carbon nanostructure-based nanocomposites"; Nanotechnology.**18** (2007) 345701 (4pp) ; doi:10.1088/0957-4484/18/34/345701

[13] Varrla Eswaraiah, Venkataraman Sankaranarayanan, Sundara Ramaprabhu; "Functionalized Graphene–PVDF Foam Composites for EMI Shielding"; Macromol. Mater. Eng. (2011) 296, 894–898 ; doi: 10.1002/mame.201100035

[14] Prerana Modak, Subhash B. Kondawar, D.V. Nandanwar*; "*Synthesis and characterization of conducting polyaniline/ graphene nanocomposites for electromagnetic interference shielding"; Procedia Materials Science. 10 (2015) 588 – 594; doi: 10.1016/j.mspro. 2015.06.010

[15] Ranjini R. Mohan, Sreekanth J. Varma, and Jayalekshmi Sankaran; "Impressive electromagnetic shielding effects exhibited by highly ordered, micrometer thick polyaniline films" Appl. Phys. Lett. 108, 154101 (2016); doi: 10.1063/ 1.4945791.

[16] Ranjana Singh, Suresh G. Kulkarni; "Nanocomposites based on transition metal oxides in polyvinyl alcohol for EMI shielding application"; Polym. Bull. (2014) 71:497–513; doi 10.1007/s00289-013-1073-2

[17] Shailaja Pande , B. P. Singh, R. B. Mathur , T. L. Dhami, P. Saini and S. K. Dhawan "Improved EMI Shielding Properties of MWCNT–PMMA Composites Using Layered Structures"; Nanoscale. Res. Lett. (2009) 4:327–334; doi 10.1007/s11671-008-9246-x.

[18] Jiajie Liang, Yan Wang, Yi Huang, Yanfeng Ma, Zunfeng Liu, Jinming Cai, Chendong Zhang, Hongjun Gao, Yongsheng Chen; "EMI shielding of graphene/epoxy Composites"; Carbon .47 (2009) 922-925; doi:10.1016/j.carbon.2008.12. 038

[19] R Kumaran, S Dinesh kumar, N. Balasubramanian, M.Alagar, V.Subramanian, K. Dinakaran; " Enhanced EMI Shielding in a Au−MWCNT Composite Nanostructure Dispersed PVDF Thin Films"; J. Phys. Chem. C. 2016, 120, 13771−13778; doi: 10.1021/ acs.jpcc.6b01333

[20] Veena Choudhary, S.K. Dhawan and Parveen Saini; "Polymer based nanocomposites for electromagnetic interference (EMI) shielding"; https://www.researchgate.net/ publication/ 231336841; Sept 2012 ; ISBN: 978-81-308-0499-6.

[21] Tae Wook Yoo , Yun Kyun Lee , Seung Joon Lim , Ho Gyu Yoon , Woo Nyon Kim; "Effects of hybrid fillers on the EMI shielding effectiveness of polyamide 6/conductive filler composites"; J. Mater. Sci. (2014) 49:1701–1708; doi 10.1007/s10853-013-7855-y

[22] Jin Woo Jang, Byung Gil Min, Jeong Hyun Yeum, and Young Gyu Jeong; "Structures and Physical Properties of Graphene/PVDF Nanocomposite Films Prepared by Solution-mixing and Melt-compression"; Fibers and Polymers. 2013, Vol.14, No.8, 1332-1338

[23] P. Indra Devi , K. Ramachandran ; "Dielectric studies on hybridised PVDF–ZnO nanocomposites"; Journal of Experimental Nanoscience. Vol. 6, No. 3, June 2011, 281–293. doi:10.1080/17458080. 2010.497947

[24] Ajay Pal Indolia , M. S. Gaur; "Investigation of structural and thermal characteristics of PVDF/ZnO nanocomposite", J. Therm Anal Calorim. (2013) 113:821–830 ; doi 10.1007/s 10973-012-2834-0

[25] J.Wang, J.Wu, W.Xu, Q. Zhang, Q. Fu; "Preparation of poly(vinylidene fluoride) films with excellent electric property, improved dielectric property and dominant polar crystalline forms by adding a quaternary phosphorus salt functionalized graphene" ; Compos. Sci. Tech. 91 (2014) 1–7; doi.10.1016/ j.compscitech. 2013.11.002.

[26] Wei-Li Song, Mao-Sheng Cao, Li-Zhen Fan , Ming-Ming Lu, Yong Li, Chan-Yuan Wang, Hong-Fei Ju; "Strong and thermostable polymeric graphene/silica textile for Lightweight practical microwave absorption composites"; Carbon .100 (2016) 109-117 doi.org/10.1016/ j.carbon.2016.01.002

[27] Weiwei Liu, Hua Li, Qingping Zeng, Huanan Duan, Yiping Guo, Xuefa Liu,C.Y.Sun and Hezhou Liu; "Fabrication of ultralight three-dimensional graphene networks with strong electromagnetic wave absorption properties" J. Mater. Chem. A., 2015, 3, 3739 doi: 10.1039/c4ta06091a;

[28] Mao-Sheng Cao, Xi-Xi Wang, Wen-Qiang Cao and Jie Yuan "Ultrathin graphene: electrical properties and highly efficient electromagnetic interference shielding" J. Mater. Chem. C **,** 2015, 3, 6589 ; doi: 10.1039/c5tc01354b

[29] Dilini Galpaya, Mingchao Wang, Meinan Liu, Nunzio Motta, Eric Waclawik, Cheng Yan; "Recent Advances in Fabrication and Characterization of Graphene-Polymer Nanocomposites" Graphene, 2012, 1, 30-49; http://dx.doi.org/10.4236/ graphene. 2012.12005

[30] Tapan K. Das and Smita Prusty; "Graphene-Based Polymer Composites and Their Applications"; Polymer-Plastics Technology and Engineering, 52: 319–331, 2013; doi: 10.1080/03602559.2012. 751410

[31] Vivek Dhand, Kyong Yop Rhee, Hyun Ju Kim, and Dong Ho Jung; "A Comprehensive Review of Graphene Nanocomposites: Research Status and Trends"; J. Nanomater. Volume 2013 (2013), http://dx.doi.org/10.1155/ 2013/763953

[32] M. El Achaby, F.Z. Arrakhiz, S. Vaudreuil, E.M. Essassi, A. Qaiss; "Piezoelectric β polymorph formation and properties enhancement in graphene oxide / PVDF nanocomposite films"; Appl. Surf. Sci. 258 (2012) 7668– 7677

[33] Jiwu Shang, Yihe Zhang, Li Yu, Bo Shen, Fengzhu Lv, Paul K. Chu; "Fabrication and dielectric properties of oriented polyvinylidene fluoride nanocomposites incorporated with graphene nanosheets"; Mater. Chem. Phys. 134 (2012) 867-874; doi:10.1016/ j.matchemphys. 2012.03.082

[34] Parveen Saini, Veena Choudhary, B.P. Singh, R.B. Mathur, S.K. Dhawan; "Polyaniline–MWCNT nanocomposites for microwave absorption and EMI shielding"; Mater. Chem. Phys. 113 (2009) 919–926; doi:10.1016/j.matchemphys.2008. 08.065

[35] B. Jaleh, A. Jabbari ; "Evaluation of reduced graphene oxide/ZnO effect on properties of PVDF nanocomposite films"; Appl. Surf. Sci. 320 (2014) 339–347; http://dx.doi.org/ 10.1016/ j.apsusc.2014.09.030

[36] P. Martins, A. C. Lopes, and S. Lanceros-Mendez, "Electroactive phases of poly (vinylidene fluoride): Determination, processing and applications", Prog. Polym. Sci. **39**, 683 (2014) http://dx.doi.org/ 10.1016/j.progpolymsci. 2013.07.006

[37] Wei-Li Song , Mao-Sheng Cao , Li-Zhen Fan , Ming-Ming Lu, Yong Li ,Chan-Yuan Wang , Hong-Fei Ju; Highly ordered porous carbon/wax composites for effective electromagnetic attenuation and shielding"; Carbon.7 7 (2 0 1 4) 1 3 0 –1 4 2 ; doi.org/10.1016/j.carbon. 2014.05.014

[38] K. Lakshmi, Honey John, K.T. Mathew, Rani Joseph , K.E. George; "Microwave absorption, reflection and EMI shielding of PU–PANI composite"; Acta Mater. 57 (2009) 371–375; doi:10.1016/j.actamat. 2008.09.018.

[39] H. Gargama, A. K. Thakur and S. K. Chaturvedi; "Polyvinylidene fluoride/nickel composite materials for charge storing, electromagnetic interference absorption, and shielding applications"; Journal of Applied Physics 117, 224903 (2015); doi: 10.1063/1.4922411

[40] N. Joseph, S. K. Singh, R. K. Sirugudu, V. R. K. Murthy, S. Ananthakumar, and M. T. Sebastian; " Effect of silver incorporation into PVDF barium titanate composites for EMI shielding applications"; Mater. Res. Bull. 48, 1681 (2013); http://dx.doi.org/ 10.1016/j.materresbull.2012.11.115.

[41] M. Sharma, M. P. Singh, C. Srivastava, G. Madras and S. Bose; "Poly (vinylidene fluoride)-Based Flexible and Lightweight Materials for Attenuating Microwave Radiations"; ACS Appl. Mater. Interfaces, 2014, 6(23), 21151–21160. doi. 10.1021/am 506042a

[42] N. Joseph and M. T. Sebastian; "Electromagnetic interference shielding nature of PVDF-carbonyl iron composites"; Mater. Lett. 2013, 90, 64–67.

[43] X.J. Zhang, G.S. Wang, Y.Z. Wei, L. Guo and M.S. Cao; "Polymer composites with enhanced wave absorption properties based on modified graphite and polyvinylidene fluoride" ; J. Mater. Chem. A 1 (24), 7031-7036 (2013); doi 10.1039/c3ta11170a.

Chapter 7

Summary and Future Prospects

Contents

The conclusions drawn from the present investigations are summarized in this chapter. The significant outcomes of the present study are highlighted. The future prospects of the present investigations are also addressed.

7.1. Summary and Conclusions

The focal theme of the work presented in the thesis is centered around realizing polymer nanocomposites in the form of flexible films with application prospects in technological areas of contemporary relevance, utilizing the laudable characteristics of the highly sought after polymer, poly(vinylidene fluoride) (PVDF) as the host polymer matrix. Polymer nanocomposites are composed of polymers as host materials and nanostructured, conducting or semiconducting additives as fillers. They find fabulous applications in various technological fields ranging from optoelectronics, magneto-optics, energy harvesting and storage to nanophotonics, bio-imaging, bio-sensing and drug delivery. The nanostructured filler materials used in the present work are zinc oxide (ZnO), zinc sulphide (ZnS), reduced graphene oxide (RGO) and graphene.

Depending upon the versatility of the filler materials used, these PVDF based nanocomposites are found to function as excellent UV shielding materials, light emitting (both white light and coloured light) films, optical limiters and EMI shielding films.

As the first phase of the work, the renowned semiconducting materials ZnS and ZnO are used as the nanostructured filler materials for making nanocomposites with the host polymer, PVDF. The semiconductor, ZnS has been extensively investigated for its versatile applications in cathode-ray tubes (CRT), field emission display (FED) devices, electroluminescent devices, photodiodes and sensors. In the present work, nanostructured ZnS, doped with manganese (ZnS:Mn) and copper (ZnS:Cu) are used for making nanocomposites with PVDF and flexible, free standing films of PVDF/ZnS:Mn and PVDF/ZnS:Cu are grown using the simple method of solution casting. The ZnS:Mn and ZnS:Cu based nanocomposite films are found to show intense yellow orange emission at 598 nm and blue emission at 432 nm respectively and offer ample scope for applications in flexible, luminescent devices. The photoluminescence quantum yields of these nanocomposite films are estimated using spectrofluorimeter in combination with integrating sphere, coated with $BaSO_4$ and the data is consistent with the photoluminescence spectral data. By optimizing the doping concentrations of Mn and Cu, the intensities of the yellow and blue emissions can be tuned to generate white light emission from these nanocomposite films, by mixing the complementary emission colours, yellow and blue.

The nanocomposite films of the well-known transparent conducting oxide ZnO, with PVDF, obtained as flexible and free standing films of thickness around 20 micrometers, by solution casting technique are found to have fascinating UV absorption properties, in addition to the intense photoluminescence emission all through the visible region, culminating in appealing white light emission. The PVDF/ZnO nanocomposite films exhibit excellent UV absorption in the wavelength range 370 – 200 nm and the UV transmission is almost close to zero in this range. This range covers most of the unhealthy UV-B radiation, the exposure to which causes a number of skin related diseases and long term exposure to UV-B radiation might cause even skin cancer. These nanocomposite films hence offer excellent application prospects as flexible UV shielding materials. The simultaneous observation of excellent UV shielding and white light emission in these films is the novelty of the work on PVDF/ZnO nanocomposite films.The present work also offers scope for developing white light emitting flexible films, in a cost effective way.

The second phase of the work deals with the studies on the nanocomposite films of PVDF with the carbon based filler materials, reduced graphene oxide (RGO) and graphene.The filler material, RGO is synthesized from graphite by modified Hummer's method using hydrazine hydrate as the reducing agent and the PVDF/RGO nanocomposite films are grown by solution casting method. The addition of RGO is found to bring about good extent of enhancement in the β

phase of PVDF, which is the most ordered polymorph form of PVDF and this has been confirmed from the structural studies using XRD, FTIR and Raman spectroscopic techniques. The focal theme of the investigations is related to assessing the nonlinear optical response of these nanocomposite films using open aperture and closed aperture Z scan technique, using Nd:YAG laser of 7 ns pulses and 532 nm wavelength, as the source. From the single beam Z-scan experimental results of PVDF/RGO nanocomposite films, it is seen that the nonlinear absorption coefficient is quite high for these films, which is one of the prime requirements for efficient optical limiting applications. The high values of the various nonlinear coefficients and the low values of optical limiting threshold power, offer ample scope for the use of PVDF/RGO films in the design of nonlinear optical devices. The highlight of the present work is the observation of normalized transmittance as low as 10% and low optical threshold power around 7.84 MW/cm^2 for the flexible and free-standing films of PVDF/RGO nanocomposite. These highly stable, flexible films of PVDF/RGO nanocomposite of thickness around 10 microns are quite suitable for the development of efficient optical limiting devices of any shape or size.

The last part of the work is focused on investigating the electro-magnetic interference (EMI) shielding properties of the PVDF/graphene nanocomposite films. The films are obtained by solution casting method using commercially purchased graphene. The film samples are cut into the required dimensions for the EMI shielding measurements in the

frequency range, 4-12 GHz and the measurements are done using wave guide transmission line technique in a Vector Network Analyser. The structural characterization using XRD, Raman and FTIR spectroscopic techniques, provide conclusive evidence for the increase in the β phase of PVDF with the addition of graphene, similar to the enhancement observed upon the addition of RGO to PVDF. The higher thermal stability and mechanical strength of the nanocomposite film samples compared to pure PVDF films have been established from the thermal studies and the mechanical strength measurements. The dense dispersion of graphene within the PVDF matrix and the interconnectivity between graphene flakes can be confirmed from the FESEM studies and the crystalline nature of the PVDF/graphene films, from the SAED pattern. The dc electrical conductivity, carrier concentration and the mobility of the majority charge carriers are evaluated using the Hall effect measurement technique. The connectivity among the graphene flakes, combined with the high carrier concentration and carrier mobility observed in these nanocomposite films result in the observed high electrical conductivity of the nanocomposite films around 16 S/cm, which is quite significant for effective EMI shielding action. The highlight of the present work is the observation of remarkably high electro-magnetic interference (EMI) shielding effectiveness of about 47 dB, exhibited by the highly conducting and ordered PVDF / graphene nanocomposite films of thickness around 20 microns, in the microwave frequency range. The EMI shielding effectiveness of around 47dB has

been observed in the X-band frequency range, for micrometer thick, flexible films of PVDF/graphene nanocomposite with 15% graphene loading, without adding foaming agents or surfactants. Since these films are free standing and flexible, they are ideal for EMI shielding applications, without the geometrical constraints of the shape or size of the object. The shielding properties of these nanocomposite films are found to be absorption dominated and are hence quite suitable for stealth applications as well.

7.2. Future Prospects

The present work offers ample scope for further investigations, based on the results of the present studies and the conclusions drawn there from.

1. By combining manganese doped and copper doped ZnS in suitable concentrations and dispersing them in PVDF matrix, it should be possible to realize flexible and free standing white light emitting films, by mixing the emissions of the complementary colours, yellow and blue. They can be of applications in solid state light emitting technology.
2. The nonlinear optical response of the PVDF/RGO films can be studied using femto second laser pulses and it might be possible to observe the effects of higher order nonlinearity.
3. The viscous nature of PVDF solution can be utilized for electro-spinning the PVDF based nanocomposite solutions for making

nano-fibers. By electro-spinning PVDF/graphene solution, nano-fibers can be formed and these fiber mats can be used for EMI shielding applications with much enhanced shielding effectiveness in a much broader range of microwave radiation.

The present studies identify PVDF as an exotic host matrix for realizing various types of stable nanocomposite films with high application prospects in different technological fields. The full potential of PVDF can be tapped only by enhancing the β form to a large extent by stretching and poling the PVDF films. The stretched and poled PVDF nanocomposites are expected to offer many novel and exciting phenomena to watch, understand and explore.